Interpretation of Sensory Information From Skeletal Muscle Receptors For External Control

Milan Djilas

UNIVERSITE MONTPELLIER II
SCIENCES ET TECHNIQUES DU LANGUEDOC

T H E S E

pour obtenir le grade de

DOCTEUR DE L'UNIVERSITE MONTPELLIER II

Formation doctorale: SYSTEMES AUTOMATIQUES ET MICROELECTRONIQUES
Ecole Doctorale: INFORMATION, STRUCTURES ET SYSTEMES

présentée et soutenue publiquement

par

Milan DJILAS

le 13 octobre 2008

Titre:

INTERPRETATION DES INFORMATIONS SENSORIELLES DES RECEPTEURS DU MUSCLE SQUELETTIQUE POUR LE CONTROLE EXTERNE

INTERPRETATION OF SENSORY INFORMATION FROM SKELETAL MUSCLE RECEPTORS FOR EXTERNAL CONTROL

JURY

Jacques LEVY VEHEL	Directeur de Recherches, INRIA	Rapporteur
Xavier NAVARRO	Professeur, Université Autonome de Barcelone	Rapporteur
André CROSNIER	Professeur, Université Montpellier II	Examinateur
Régis GUILLEMAUD	Ingénieur, CEA Léti / Minatec	Examinateur
Serge PICAUD	Directeur de Recherches, INSERM	Examinateur
Guy CATHEBRAS	Professeur, Université Montpellier II	Directeur de Thèse
Christine AZEVEDO-COSTE	Chargé de Recherches, INRIA	Co-encadrante
Ken YOSHIDA	Associate Professor, IUPUI / Aalborg University	Co-encadrant

Preface

This manuscript has been written to document my research work as a doctoral candidate in the DEMAR team at the Laboratory of Computer Science, Microelectronics and Control in Montpellier (LIRMM), during the period from October 2005 to October 2008.

DEMAR (Démbulation et Mouvement Artificiel) is a joint project between the French National Institute in Computer Science and Control (INRIA), the French National Center for Scientific Research (CNRS), and Universities of Montpellier I and II. The team's research activities are modeling and controlling the human sensory motor system, and implanted neuroprosthetic devices.

International collaboration between DEMAR and the Center for Sensory-Motor Interaction (SMI) at the University of Aalborg in Denmark exists since 2003, and the research proposal for this thesis is the result of this collaboration. The proposal concerns the rehabilitation of movement of paralyzed limbs through functional electrical stimulation (FES), an interdisciplinary field that requires joint efforts of scientists with backgrounds in neurophysiology, robotics, and microelectronics. The objective of the project is to explore the possibility of using information from sensory nerve fibers of muscle receptors as feedback in closed-loop FES systems. Challenges involve theoretical, experimental, and technical aspects.

Financial support for the duration of the thesis was insured by INRIA on the basis of funding provided by the European Aeronautic Defense and Space (EADS) corporate foundation.

Acknowledgements

I would like to express my gratitude to everyone at the Laboratory of Computer Science, Robotics and Microelectronics in Montpellier (LIRMM) and its director, Michel Robert, for welcoming me and having me here for the last three years. I am also grateful to the European Aeronautic Defense and Space company (EADS) and their foundation for the funding provided for this thesis. Without their financial support, this thesis would have not been possible.

I wish to express my deepest and sincere gratitude to my supervisors Christine Azevedo-Coste, permanent research scientist in the DEMAR project team, part of the French National Institute for Research in Computer Science and Control (INRIA), Guy Cathébras, professor at the University of Montpellier II, and Ken Yoshida, associate professor at the Department of Biomedical Engineering at Indiana University - Purdue University Indianapolis (IUPUI), and also Associate Professor at the Center for Sensory-Motor Interaction at the Department of Health Science and Technology at Aalborg University, for their never failing interest in discussing and commenting on research directions and manuscript drafts, and also for helping out with the animal experiments. Special thanks goes to David Guiraud, project leader of the DEMAR team, for his invaluable advise and support throughout the thesis. I would like to thank and Jérôme Bourien, at the Institute of Neurosciences in Montpellier, for his valuable advise.

I sincerely thank Xavier Navarro, professor at the Autonomous University of Barcelona, Jacques Lévy Véhel, permanent research scientist in the APIS project team at INRIA, Régis Guillemaud, head of the Laboratory of Microelectronics for Health (LE2S) at the French Atomic Energy Commission in Grenoble (CEA-LETI), André Crosnier, professor at the University of Montpellier II, and Serge Picaud, director of research at the French National Institute for Health and Medical Research (INSERM), for kindly accepting to be jury members at my thesis defense.

I wish to thank the staff at the two locations where animal experiments took place, for their technical assistance: Ole Sørensen, Torben Madsen, Jens Sørensen and Henrik

Barlebo from the Department of Pathology at Aarhus University Hospital in Aalborg; and Hubert Taillades from the Laboratory of Experimental Surgery at the Institute of Biology in Montpellier. Additional thanks goes to Mathijs Kurstjens for helping out with experiments and giving me a crash course in how to make nerve cuff electrodes, at the Bioelectronics Laboratory at the Center for Sensory-Motor Interaction at Aalborg University in Denmark. I also thank Thierry Duquesne and Olivier Tempier, for providing me with access to the robotics and microelectronics workshops, and for their technical assistance. Special thanks also to Annie Aliaga and Elisabeth Greverie, for their help with solving the maze of French administration.

I thank my colleagues and friends at the lab, for providing a positive and stimulating work environment: Carla Aguiar, Andreea-Elena Ancuta, Yousra Ben Zaida, Mourad Benoussaad, Antonio Bo, Vincent Bonnet, Floor Campfens, Lotfi Chikh, David Corbel, Michel Dominici, Lionel Gouyet, Mitsuhiro Hayashibe, Jérémy Laforet, Chao Liu, José-Marconi Rodrigues, Sebastien Lengagne, Kevin Loquin, Baptiste Magnier, Ionut Olaru, Rogério Richa, Ashvin Sobhee, Guillaume Souquet, Jean-Mathias Spiewak, Walid Zarrad, and Dingguo Zhang. Thank you all again. It has been a pleasure.

A big thanks to a few very special people outside the lab: Maria Papaiordanidou, Szymon Stoma, and Karine Dennis. Thank you for your friendship.

Lastly, and most importantly, I would like to thank my family, brother Marko and parents Slavko and Dana, for their support and encouragement throughout my graduate studies. To them I dedicate this thesis.

Abstract

The topic of this thesis was the rehabilitation of movement of paralyzed limbs through functional electrical stimulation (FES). The objective of the project was to explore the possibility of using information from sensory nerve fibers of muscle receptors as feedback of the closed-loop control of FES systems using intrafascicular peripheral nerve electrodes.

Acute animal experiments were performed to record afferent muscle spindle responses to passive stretch. The recordings were performed using the new thin-film Longitudinal Intra-Fascicular Electrode (tfLIFE), developed by Dr. Ken Yoshida at Aalborg University in Denmark. A first-order model of muscle spindle response to passive muscle stretch was proposed that manages to capture the non-linear properties of the afferent neural activity. Moreover, estimation of muscle state from the recorded multi-channel ENG provided more robust results compared to using single-channel recordings.

For the abovementioned model to be usable in a estimator of muscle state, the rate of change of muscle length during movement must have negligible effect on model parameters. A neural spike detection and classification scheme was developed for the purpose of isolating sensory neural activity of muscle receptors having minimal sensitivity to the velocity of muscle motion. The algorithm was based on the multi-scale continuous wavelet transform using complex wavelets. The detection scheme outperformes the commonly used simple threshold detection, especially with recordings having low SNR. Results of classification of units indicate that the developed classifier is able to isolate activity having linear relationship with muscle length, which is a step towards on-line model-based estimation of muscle length that can be used in a closed-loop FES system with natural sensory feedback.

One of the main issues limiting the interpretation of ENG data is the low level of the neural signal compared to the level of noise in the recordings. Our hypothesis was that shielding the implant site would help improve signal-to-noise level. Experimental results from a preliminary study we had performed indicate that placing a standard cuff electrode around the tfLIFE active sites increases the level of ENG signal in the recordings.

Key words: Neural Engineering, Neural Prostheses, Biomedical Signal Processing, Functional Electrical Stimulation, Natural Sensory Feedback, Control Strategies.

Contents

Chapter 1

Introduction

Injuries to both central and peripheral nervous system can seriously disrupt normal movements. Stroke can destroy neurons in cortical and subcortical areas. Multiple sclerosis or spinal cord injury can block transmission of signals to motor neurons. Clearly, a "cure" in the form of complete repair of the damaged neural structures with restoration of normal bodily functions would be the ideal, but it is not achievable at this time.

Much interest and optimism was generated in the 1980s when it was shown that portions of peripheral nerves could be used as tissue grafts with the potential to "bridge the gap" of a complete spinal transection [Richardson et al., 1980]. Stem cells transplant therapy is another approach [Zigova et al., 2002]. In the last decade there have been several reports of successful regeneration of certain spinal pathways in rats, apparently resulting in improvements of motor function after partial or even complete spinal transections [Bregman et al., 1995], [Cheng et al., 1996], [Olson, 1997], [Kim et al., 1999], [Brosamle et al., 2000], [Ramon-Cueto et al., 2000]. However, though neural regeneration using tissue bridges can certainly be achieved, it is far from clear whether functional connections are made between descending axons and neurones below the level of lesion. Restored function, when it occurs, may result from a facilitated recovery of local neuronal circuits rather than a restored flow of commands in descending pathways [Jones et al., 2001], [Pearson, 2001].

Taking the optimistic view that some combination of tissue bridging, stem-cell implants [Ribotta et al., 2000], [Slawinska et al., 2000] and growth factors and molecules that block factors inhibitory to regeneration [Marcoux and Rossignol, 2000] will become a clinical reality in the future, it remains almost certain that the functions of daily life will only be partially restored. In the light of this, there is clearly a continuing need for assisting technologies [Prochazka et al., 2001], which should be seen as complementary rather than concurrent research areas.

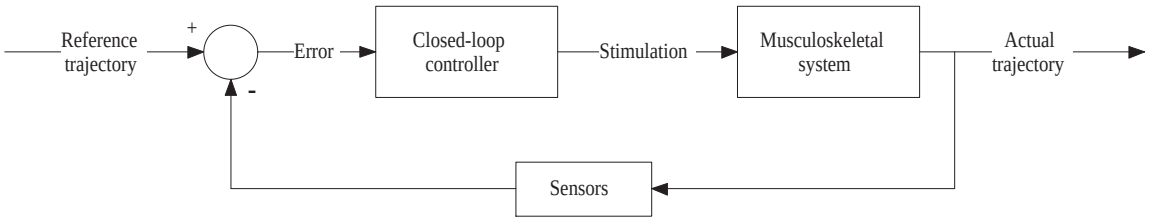

Figure 1.1: Organization of a classical closed-loop control functional electrical stimulation system. From Popović and Sinkjær [2000].

1.1 Restoring Movement with Functional Electrical Stimulation

The 1960s saw the birth of functional electrical stimulation (FES) for the restoration of movement in partially paralyzed people [Vodovnik et al., 1965], [Vodovnik et al., 1967]. FES is a technique for restoring function of paralyzed muscles by applying electrical stimulation pulses to sensory-motor systems via electrodes which are placed on the skin, or implanted. Forces generated in muscles activated by FES can be graded by varying parameters of stimulation pulses in order to restore function. Typical FES applications include correction of drop-foot [Haugland and Sinkjær, 1995], [Lyons et al., 2002], [Hansen et al., 2003], [Hansen et al., 2004], hand grasp in stroke and paraplegic patients [Haugland et al., 1999], [Popović and Sinkjær, 2000], [Inmann and Haugland, 2004], standing and walking in paraplegic patients [Guiraud et al., 2006], and bladder and bowel voiding [Jezernik and Sinkjær, 1998], [Johnston et al., 2005].

1.2 Closed-Loop FES using Natural Sensory Feedback

When FES is used for restoration of movement, closed-loop control is desirable, in order to correct for disturbances and unavoidable musculoskeletal modeling errors. Joint angle and force transducers provide signals from which the current state of the system can be estimated and fed back to the controller (Fig. 1.1). Closed-loop controllers are classically error driven, i.e. they respond to the trajectory error which is determined by comparing the actual and the reference trajectory.

In order to provide complex motor actions such as walking or grasping, closed-loop FES systems require feedback from many sensors. Artificial force and joint angle transducers are difficult to embbed and are insufficiently biocompatible and reliable for implementation [Zou et al., 2003], [Roetenberg et al., 2007]. They can be used as a source of

information during the stimulation of the neuromuscular system but they present problems such as the need for frequent calibration, difficulties to position, and cosmetic unacceptability due to sensor dimensions and appearance. The latter can be solved by making the sensors fully implanted [Loeb et al., 2000], [Loeb et al., 2003], [Guiraud et al., 2006]. This is particularly suitable when the stimulator and electrodes are implanted.

With the advent of advanced implanted prosthetic interfaces, natural sensors are being explored as an alternative source for feedback information. By directly interfacing the peripheral nerves, it is possible to record signals from natural sensors distributed throughout the body [Haugland and Hoffer, 1994], [Hoffer et al., 1996], [Strange and Hoffer, 1999], [Sinkjær, 2000]. Muscle spindles are one type of natural sensor. Their main function is to signal changes in the length of the muscle within which they reside [Kandel et al., 2000]. Changes in the muscle length are associated with changes in the angles of the joints that the muscles cross. Therefore, their activity could be used to provide feedback information about muscle state in a closed-loop FES system [Yoshida and Horch, 1996].

1.3 Problem Statement

One of the main challenges in systems using natural sensory feedback is the lack of a fully reliable and sufficiently selective neural interface for recording of natural sensors activity. The neuroelectric activity recorded with state-of-the-art neural interfaces is a mixture of signals from several adjacent neurons and noise. To improve selectivity, electrode active sites size must be reduced, which unfortunately implies the increase of background noise in the recordings. Consequently, the nerve signal level is in the order of a magnitude of the background noise, leading to low signal-to-noise ratio (SNR). This, in turn, impedes the performance of closed-loop FES systems where muscle spindle nerve activity is used as feedback. Due to the lack of recording selectivity and low SNR, state of the art systems are still unable to access information from individual sensory fibers, but only their aggregate activity [Yoshida and Horch, 1996]. This leads to limited applicability of such systems (limited motion speed and range).

Moreover, state of the art closed-loop systems using muscle receptor neural activity for feedback, such as the system of Yoshida and Horch [1996], are based on PID controllers. PID gains are especially difficult to tune when dealing with muscle and do not allow for coping with complex muscle behaviour and properties, including fatigue. Model-based closed-loop control would allow for having more advanced control laws designed that could eventually provide more robust control to face perturbations and fatigue.

1.4 Contribution

In this thesis we use a promising new multi-electrode structure for FES: the microfabricated multi-site thin-film Longitudinal Intra-Fascicular Electrode (tfLIFE) array that is realized as a patterned thin film on polyimide structure [Yoshida et al., 2000]. The electrode had not yet been fully tested in experimental conditions and it was the first objective of our work to test the new electrode in vivo, in recordings of multi-channel ENG in acute animal preparations. Throughout the thesis more than 20 acute animal experiments have been performed, where in almost all the tfLIFE was successfully implanted and ENG data acquired.

The second objective was to improve the state of the art in closed-loop control of FES using muscle spindle activity as feedback. A model of muscle spindle neural response to passive muscle stretch was developed which, in combination with a developed novel spike sorting algorithm, provides a basis for an on-line estimator of muscle state in a closed-loop FES system, where the estimator would feed back to the controller the information about the length of the muscle in which the spindles reside in. The novel method for classification based on spike signatures in wavelet space performs equally well as the best state of the art methods, but, unlike other methods, requires no additional computation time because it uses data obtained directly from the detection step of the algorithm. Classification of muscle receptor action potentials manages to produce classes having firing rates that are less dependant on muscle motion velocity compared to the case where aggregate firing of all fibers is used. This should provide a larger range of muscle motion in which the developed model could be used as a basis for a future on-line estimator of muscle state in a closed-loop FES system. We have also shown that using multiple channels of ENG, now available with the tfLIFE, provides a more robust estimation of muscle length compared to estimation based on a single channel of ENG.

A novel shielding technique was also proposed for improving SNR in signal acquisition. Several recording configurations were experimentally evaluated and the results indicate that placing a cuff electrode around the tfLIFE implant site improves the SNR in recordings made using intraneural longitudinally placed electrodes.

During the course of the work, three papers have been accepted and presented at international conferences, and one journal paper has been submitted. Work on two more journal papers is underway and will be submitted as soon as possible.

1.5 Thesis Outline

Chapter 2 starts with a brief overview of the neuroanatomical basis and sensory-motor systems relevant for natural control of movement. Pathology of these systems is given for

the most common injuries of the central nervous system. Eventually, the chapter concludes with an introduction to neuroprostheses for the restoration of movement and an overview of principles and instrumentation for recording of activity from the peripheral nervous system.

Chapter 3 introduces the FES control scheme adopted in this thesis and reports the work on modeling the muscle spindle nerve response to passive muscle stretch, required for eventually building the a model-based estimator of muscle state. Acute animal experiments are described first, followed by the modeling part. Model evaluation and discussion of results are presented last.

Chapter 4 reports the work on an algorithm for decomposing the mixture of signals from multiple nerve fibers into separate sources. The algorithm is divided into two parts: 1) neural spike detection and 2) classification of detected action potentials. The developed method was evaluated on synthesized data and its performance compared to existing methods. Eventually, the algorithm was evaluated on experimentally recorded data. The chapter concludes with the discussion of results.

Chapter 5 reports the work on a shielding technique for improving the signal-to-noise ratio in recording neural activity using intra-neural longitudinal electrodes. The method is described and evaluated in experimental conditions. Results are discussed and the chapter concludes with suggestions of how the shielding structure could be improved.

Chapter 6 gives the global final remarks and suggests possible directions for future work. The final chapter gives the summary of the thesis in French.

Chapter 2

Control of Movement

2.1 Neuroanatomical Basis for Control of Movement

In this section we recall the principles and mechanisms of human motor control that are necessary for understanding the following chapters. This thesis is on the border between engineering and biology worlds and some readers may not be familiar with physiology. Most of the background presented in this chapter are extracts from Popović and Sinkjær [2000] and Kandel et al. [2000].

2.1.1 The Central Nervous System

The central nervous system consists of the brain and the spinal cord. The spinal cord receives information from receptors in the skin, joints and muscles from the trunk and limbs, and it is the final station of issuing commands for movement. In the spinal cord there is an orderly arrangement of motor and sensory nuclei, controlling the limbs and trunk. In addition to nuclei, the spinal cord is connected to the peripheral nervous system through *afferent* pathways for sensory information to flow from the body to the brain and *efferent* pathways for commands necessary for motor control to descend from the brain to the body. Thus, afferent nerve fibers carry information to the central nervous system and efferent nerve fibers carry command out of the central nervous system.

A transverse section of the spinal cord shows that it is organized in a butterfly-shaped centralized gray area, where the cell bodies of the centralized neurons are located, and a surrounding region of the white matter that contains afferent and efferent axons (Fig. 2.1). The gray matter is divided into the dorsal horn and the ventral horn. This is where the cell bodies of motor neurons that innervate the skeletal muscles are located. Sensory fibers carrying information about perception enter the spinal cord at the dorsal side. The cell

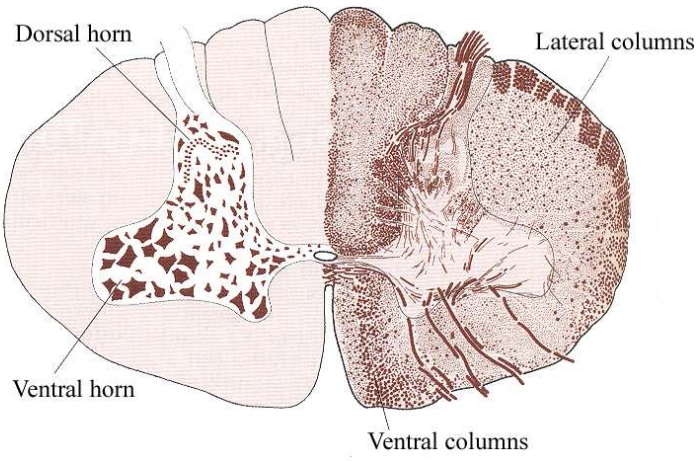

Figure 2.1: Major anatomical features of the spinal cord. The left side depicts a cell stain of the gray matter and the right side a fiber stained section. The ventral horn contains motor neurons whereas the dorsal horn contains sensory neurons. From Kandel et al. [2000].

bodies of these fibers are in the dorsal root ganglia, located just outside the spinal cord. The information from these fibers is projected into the cerebral cortex, where it is used for the perception of limb position.

Large regions of the cerebral cortex are committed to movement and sensation (Fig. 2.2). The primary motor cortex has neurons that project directly to the spinal cord. The primary sensory cortex receive information from peripheral receptors with only a few synapses interposed. Surrounding the primary areas are the higher order sensory and motor areas. These areas process more complex aspects of a sensory modality or motor function. The purpose of the higher order sensory areas is to achieve greater analysis and integration of information coming from the primary sensory areas. In contrast, the flow of information from the motor areas is in the opposite direction. Higher order motor areas distill complex information about a potential motor action and relay it to the primary motor cortex, which is the site from which voluntary movement is initiated [Kandel et al., 2000], [Popović and Sinkjær, 2000]. Damage to any of these areas can leed to sensory-motor deficiencies and disruption of the normal control of movement.

2.1.2 The Neuron

The nervous system is composed of two major types of cells: neurons and glia. Neurons integrate and convey information and glia provide support for the neurons. A generic neural cell or neuron consists of four morphologically and physiologically distinct parts: a

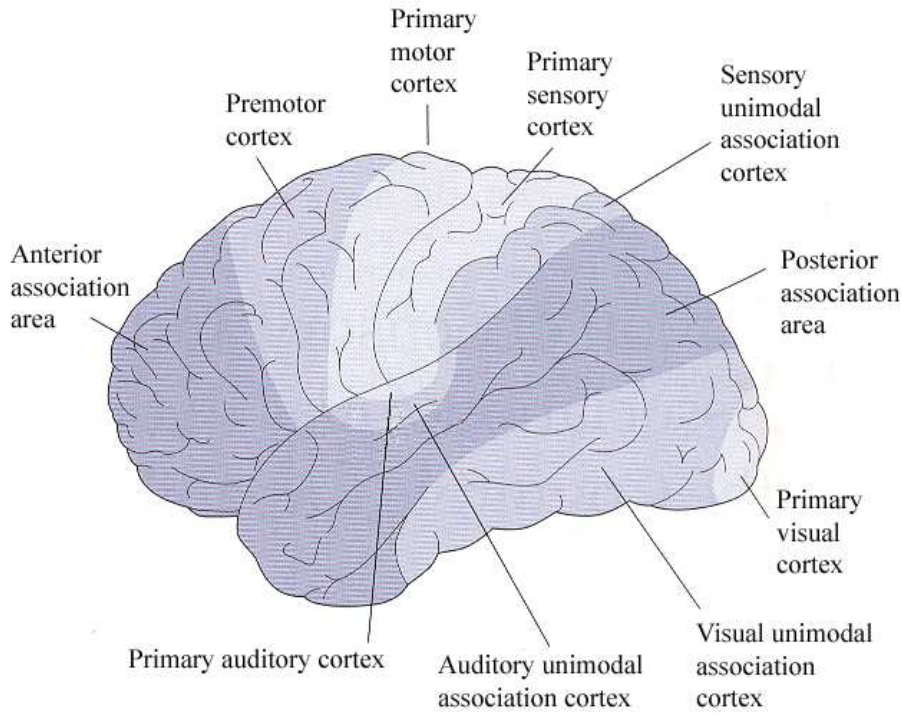

Figure 2.2: The lateral surface of the human brain shows the regions of the primary sensory and motor cortices, and the higher-order motor and sensory cortices. From Kandel et al. [2000].

receiving pole, a terminal transmitting pole, an intervening conducting segment, and a cell body or soma (Fig. 2.3). The neuron possess two types of protoplasmic processes extending outward from the soma: dentrites and axons. The processes vary in length and in the amount and extent of their branching. The dendrites are usually multiple, short and highly branched. They constitute the receiving pole of the cell. The axons are usually single, long, and although one or more collateral branches may occur, relatively unbranched except at their ends. The axon is responsible for both conduction of excitation and its transmission to other cells.

An axon generates action potentials (nerve impulses) and conducts them from the receiving part of the cell to the transmitting region. It is a delicate cylinder of neural cytoplasm with a limitting membrane, the axolemma. It varies in length and in diameter in different types of neurons. Axons are enclosed in a cellular sheath of lipid material, the myelin sheath, which serves to electrically insulate individual axons from one another. Small axons, which are invested by only a single layer of sheath cell process, are called “unmyelinated” fibers. Large axons are enclosed with more numerous sheathing layers

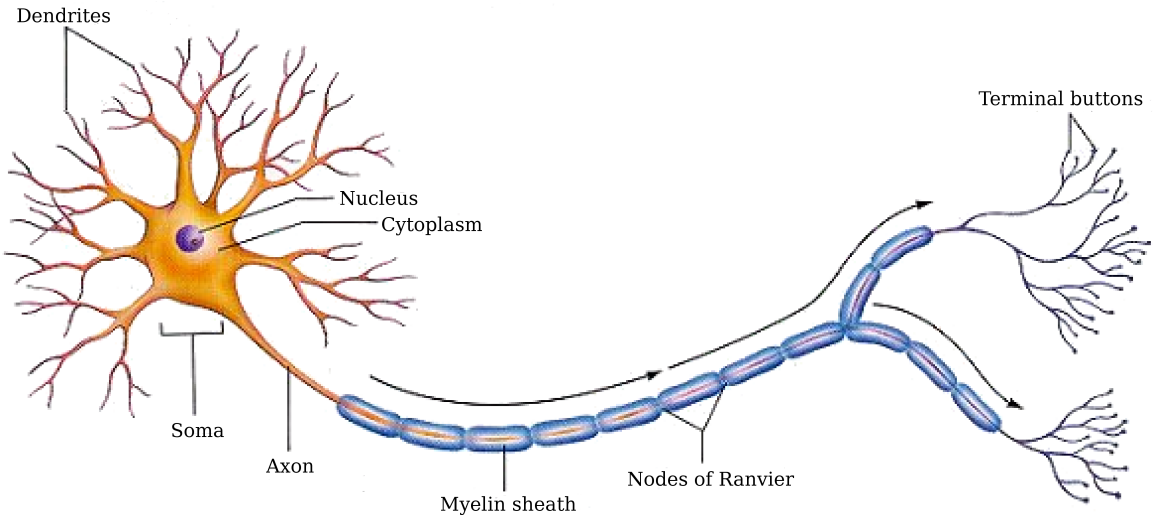

Figure 2.3: Structure of a neuron. From Martini [2005].

formed by one or more windings of the sheath cell process. The myelin sheath of larger axons is segmented, rather than continuous, and a single sheath cell encloses each segment. The length of the segments and the thickness of the myelin are quite consistent for neurons of a given diameter. Large axons have longer segments (1 to 2 mm long) and thicker sheaths. The segments are separated by short unmyelinated gaps, called Ranvier nodes. Neurons can have axon diameters ranging from 0.5 μm in small unmyelinated fibers to about 20 μm in the largest myelinated fibers.

The cell body of the neuron is the metabolic center of the cell. If severed from the cell body, a neuronal axon soon degenerates because these metabolic processes are interrupted.

Neurons can be classified as either receptor neurons or synaptic neurons, based on the type of input they receive. Receptor neurons are specialized to react to specific types of stimuli, and their dendritic parts are appropriately adapted in structure. Synaptic neurons receive information from other neurons by means of synaptic transmission.

A number of different kinds of stimuli may excite neurons. The normal stimulus for synaptic neurons is the action upon their membranes of chemical transmitters released by other neurons. Stimulation of receptor neurons is normally provided by chemical, thermal, mechanical, and electromagnetic stimuli.

2.1.3 Membrane Excitation and the Action Potential

Inside the cell membrane of a neuron, there is a slight negative charge with respect to the outside. The cause is a slight excess of positive ions outside the cell membrane and a

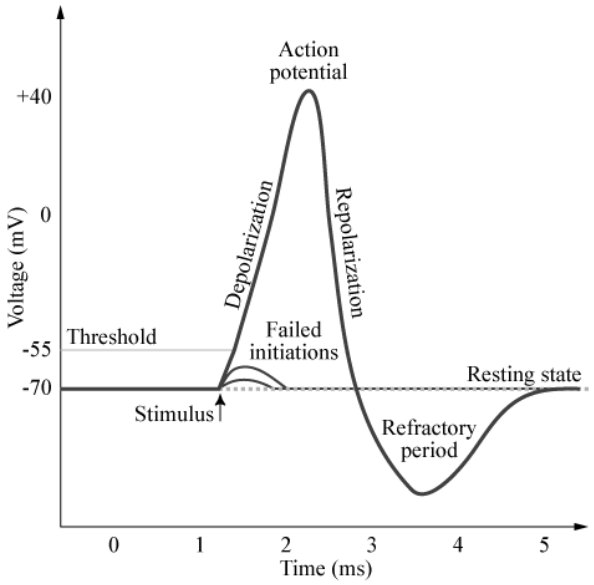

Figure 2.4: Phases of the action potential: depolarization, repolarization and hyperpolarization. From Martini [2005].

slight excess of negative ions inside the cell membrane. This unequal charge distribution is created by differences in the permeability of the membrane to various ions as well as by active mechanisms that transport ions accross the membrane. The resulting potential across the cell membrane is referred as the transmembrane potential or resting potential when the cell is undisturbed.

All neural activity begins with a change in the resting potential. A stimulus produces a localized temporary change in the transmembrane potential, which decreases with distance. It is called a graded potential. If the graded potential is sufficiently large it produces an action potential in the membrane of the axon. An action potential is an electrical impulse that is propagated across the surface of the membrane and that does not diminish as it moves away from its source.

When a biological cell or patch of membrane undergoes an action potential, or electrical excitation, the polarity of the transmembrane voltage swings rapidly from negative to positive and back. An action potential involves a depolarization, a re-polarization and finally a hyperpolarization (or ”undershoot”). The period of membrane hyperpolarization is called the refractory period of the nerve fiber (to be explained in the next section). The different phases of the action potential can be seen on Fig. 2.4.

The action potential spreads actively across the neuron, with an ”all-or-none” response. In this response, the action potential is activated to depolarization, or not at all.

The transmembrane voltage changes that take place during an action potential result from changes in the permeability of the membrane to specific ions, the internal and external concentrations of which cells maintain in an imbalance. In the axon fibers of nerves, depolarization results from the inward rush of sodium ions, while repolarization and hyperpolarization arise from an outward rush of potassium ions. Calcium ions make up most or all of the depolarizing currents at an axon's presynaptic terminus, in muscle cells and in some dendrites.

Changes in membrane permeability and the onset and cessation of ionic currents reflect the opening and closing of voltage-gated ion channels, which provide portals through the membrane for ions. Residing in and spanning the membrane, these proteins sense and respond to changes in transmembrane potential.

The depolarization phase of an action potential is due to the opening of voltage-gated ion channels, either sodium channels or calcium channels or a combination of both, depending on the particular membrane. Sodium ions and calcium ions are positively charged. Cells use chemical energy to pump sodium and calcium ions out across the cell surface membrane. When a voltage-gated sodium channel or calcium channel opens, positively charged ions move into the cell. Voltage-gated sodium channels automatically gate shut after about a millisecond. Calcium-mediated action potentials can be much longer in duration. The re-polarization phase of an action potential is due to the opening of voltage-gated potassium channels. Cells normally keep the concentration of potassium ions high inside cells. When voltage-gated potassium channels open, positively charged potassium ions move out of the cell, causing the membrane potential to return to a negative inside potential.

In myelinated fibers the action potential travels from one location in the cell to another, but ion flow occurs only at the nodes of Ranvier. As a result, the action potential signal jumps along the axon, from node to node, rather than propagating smoothly, as they do in unmyelinated axons. The clustering of voltage-gated sodium and potassium ion channels at the nodes permit this behavior, called saltatory conduction.

2.1.4 Some Characteristics of Nerve Conduction

Refractory Periods

As the action potential travels along the fiber surface, it consists of a wave of negativity followed by an area of gradually recovering positivity. While an area is in its reverse (active) state, it is absolutely refractory and cannot be restimulated. During recovery, the membrane is relatively refractory. During this period, intense or sustained stimuli can restimulate the original site.

Frequency of Impulses

Neurons normally carry trains of impulses. In general, natural stimuli are of sufficient duration to reactivate the membrane after the absolute refractory period. A single electric shock may produce a single action potential, but only because its duration does not outlast the absolute refractory period of the fiber. The stronger the stimulus, the the earlier will it re-excite, the shorter will be the time between impulses, hence, the greater the frequency.

Velocity of Conduction

Velocity of conduction depends not only on the myelination but also on the diameter of the fiber. It can be fairly accurately said that the conduction velocity is proportional to the diameter of the axon. The largest motor and sensory nerve fibers, with diameters near 20 μm, have conduction velocities up to 120 m/s. In small unmyelinated fibers, the velocities range from 0.7 to 2 m/s. Large fibers not only conduct more rapidly than small fibers, but characteristically have lower stimulus thresholds and larger spikes with shorter duration.

Classification of Nerve Fibers

Efferent nerve fibers are classified into three major groups, A, B, and C, on the basis of their conduction velocity. Group C contains the unmyelinated postganglionic fibers and group B the small myelinated fibers. Group A includes the large, rapidly conducting myelinated fibers. Group A has been further divided into four subgroups: alpha (α), beta (β), gamma (γ), and delta (δ), based on the velocity and diameter. Sensory nerve fibers have been separately classified according to diameter into groups I, II, III, and IV, with corresponding velocities. In order to avoid confusion, use of alphabetical designations is restricted to efferent fibers and the numerical designations to afferent fibers.

Neural Adaptation

Neural adaptation, or sensory adaptation, is a change over time in the responsiveness of the sensory system to a constant stimulus. It results in a decrease of neural firing rate over time.

2.2 Skeletal Muscles as Actuators of Movement

The human motor system comprises three interrelated anatomical systems: the muscle system, which supplies the power to move the skeleton; the nervous system, which directs and regulates the activity of the muscles. Muscle pairs are situated across joints, being attached at two or more points to bones via tendons. Movement is produced by shortening of the muscle, which brings the muscle ends closer to each other, ultimately changing the joint across which it acts.

The most distinguishing characteristic of muscle is contractility. By contractility, reference is made to the capacity of the muscle to produce force between its ends. Relaxation is the opposite of contraction. It is entirely passive. Both relaxation and contraction progress from zero to maximal values over a finite time. Neither is instantaneous.

2.2.1 Muscle Length and Force

The most obvious property of the muscle is its capacity to develop force against resistance. The length of the muscle at the time of activation markedly affects its ability to develop force and to perform external work. When a muscle contracts, the contractile material itself shortens, but whether the muscle shortens or not depends on the relation of the internal force developed by the muscle to the external force exerted by the resistance or load.

Two general types of muscle contractions are distinguished according to the length change, induced by the relationship between internal and external forces: isometric and isotonic. If the internal force generated by the contractile components does not exceed the external force of the resistance and if no change of muscle length occurs during the contraction, the contraction is *isometric*. If the constant internal force produced by the muscle is maintained during the movement, the contraction is *isotonic*.

The initial length of the muscle, i.e. its length at the time of stimulation, influences the magnitude of its contractile response to a given stimulus. A stretched muscle contracts more forcefully than when it is unstretched at the time of activation. The force produced by skeletal muscle can be differentiated into 2 types, active and passive, their sum comprising the muscle total force. The relationship of force to length can be presented graphically in a form of a force-length curve, in which a force in an isolated muscle is plotted against a series of muscle lengths from less that to greater than the resting length. (Fig. 2.5).

Within physiological limits, the greater the initial length, the greater the passive elastic force of the muscle will be. Maximal active force is produced at the so called optimal length of the muscle. In general, optimal length is close to the maximal body length of the muscle, i.e. the greatest length the muscle can attain in the normal living body. It is about

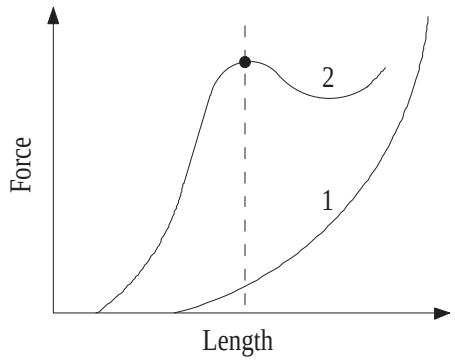

Figure 2.5: Illustration of what the force vs. length curve for isolated muscle looks like: 1) passive elastic tension; 2) total force. The dashed line marks the muscle length at which contraction force is maximal.

1.2 to 1.3 times the rest length of the muscle. Force capability is less at shorter and longer lengths.

2.2.2 Muscle Function

Motor skill and all forms of movement result from the interaction of muscular force, gravity and any other external forces that act upon skeletal levers. The muscles rarely act alone. Rather, groups of muscles interact in many ways so that the desired movement is accomplished. This interaction may take many different forms so that a muscle may serve in a number of different capacities, depending on the movement. Whenever a muscle causes movement by shortening, it is functioning as a mover or agonist. The muscles whose action oppose that of the agonists, are called antagonists.

2.3 Sensory Systems for Control of Movement

Sensory receptors are highly specialized neural structures that receive information about the external world. Various external stimuli that impinge upon our bodies are transformed into neural signals at these neural structures. Sensory information is coming from the environment and from within our bodies (e.g. blood vessels, the actions of skeletal muscles). To distinguish the systems that convey signals from these different sources, the sensory systems are divided into three categories: exteroceptive, proprioceptive, and interoceptive. Exteroceptive sensors are sensitive to external stimuli and include vision, audition, skin sensation, and some chemical senses. Proprioceptive sensors provide information about

the relative position of the body in space. Interoceptive sensors are concerned with internal bodily events such as blood pressure and the concentration of glucose in the blood. In the following we will limit ourselves to proprioceptive sensors. Muscle receptors in particular.

Muscles and joints contain a variety of receptors. Some inform the central nervous system about the length of the muscle, others detect its tension, and still other respond to pressure and noxious stimuli. Among these receptors, two have been most thoroughly studied: muscle spindles and Golgi tendon organs. Although both of these receptors discharge when the muscle is stretched, differences in their anatomical arrangement within the muscle are reflected in the differences in information they convey to the central nervous system. Muscle spindles, arranged in parallel to the muscle fibers, provide information about the length of the muscle. Golgi tendon organs are arranged in series with the muscle fibers and inform the nervous system of the tension exerted by the muscle on its tendon insertion to the bone.

2.3.1 Muscle Spindles

Mammalian muscle spindles are receptors that are distributed throughout the fleshy parts of skeletal muscles. Each spindle, which consists of an encapsulated group of specialized muscle fibers, is tapered at each end and expanded at its center in a fluid-filled capsule. Within this capsule the terminal branches of afferent nerve fibers entwine the muscular elements (Fig. 2.6).

The small muscle fibers within the spindle are called intrafusal fibers. They do not contribute to the overall tension of the muscle, but regulate the excitability of the spindle afferents by mechanically deforming the receptors. Intrafusal fibers are innervated by small motor cells of the ventral horn called gamma motorneurons. The large skeletal muscle fibers that do develop substantial muscle tension are called extrafusal fibers and are innervated by large alpha motorneurons of the ventral horn of the spinal cord.

Muscle spindles contain two types of intrafusal muscle fibers called nuclear bag fibers and nuclear chain fibers after the arrangement of nuclei in their equatorial region. The bag fibers have nuclei clustered in groups of two and three. The nuclear chain fibers have nuclei in a single row. The bag and chain fibers also differ in the kind of contraction they exhibit. Bag fibers produce slow contractions, whereas chain fibers produce fast (twitch) contractions.

There are two types of afferent terminals in muscles spindles: primary and secondary. Primary endings innervate every single intrafusal fiber within a spindle, while secondary endings lie almost exclusively on nuclear chain fibers.

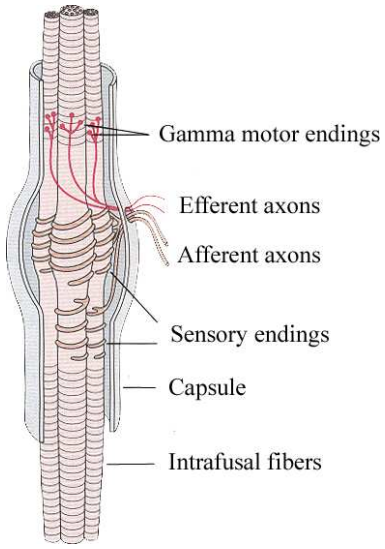

Figure 2.6: The main components of the muscle spindle are intrafusal muscle fibers, afferent sensory fiber endings, and efferent motor fiber endings. The sensory fiber endings spiral around the the central regions of the intrafusal fibers and are responsive to stretch of these fibers. From Kandel et al. [2000].

2.3.2 Golgi Tendon Organs

The Golgi tendon organ is a slender capsule approximately 1 mm long and 0.1 mm in diameter. Each organ is in series with about 15-20 extrafusal skeletal muscle fibers that enter the capsule through a tight fitting collar. The muscle fibers terminate in musculotendonious junctions after entering the capsule and give rise to collagen fiber bundles that become braided and run the length of the capsule (Fig. 2.7). An afferent nerve fiber enters the capsule in the middle and branches many times so that the axons of the afferent fiber become twisted within the braids of the collagen fiber bundles. When the skeletal muscle fibers contract, they cause the collagen fibers to contract, resulting in compression of the afferent nerve fibers and, thereby, their firing. Thus, the organization of the collagen fiber bundles makes them sensitive to small changes of muscle tension.

2.3.3 Muscle Receptors Information Encoding

Muscle stretch receptors encode information about muscle length, tension and velocity of stretch. Loading the muscle activates both the tendon organ and the muscle spindle receptors. Contraction further stretches the tendon organs. On the other hand, contraction of the extrafusal muscle fibers makes the intrafusal fibers go slack, unloading the spindle so it is

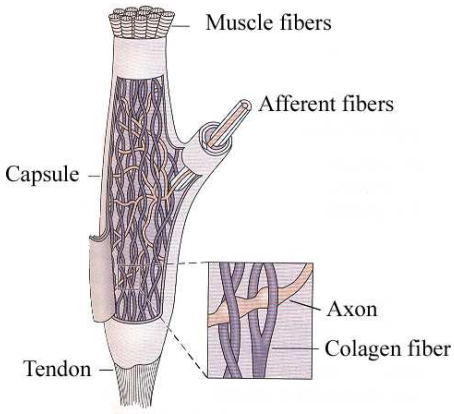

Figure 2.7: When a Golgi tendon organ is stretched, the afferent axon is compressed by collagen fibers and its rate of firing increases. From Kandel et al. [2000].

no longer stretched. As a result, when the muscle is passively stretched, the afferent fibers from either the tendon organ or the spindle would increase their rate of discharge. In contrast, when the muscle actively contracts, the tendon organ further increases its discharge, but the spindle decreases or ceases altogether.

The primary and secondary afferents in the muscle spindles respond quite differently to passive muscle stretch [Matthews and Stein, 1969a]. Both fiber types respond to static (steady-state) stretch, but they respond differently to the dynamic phase of stretch. Primary endings are very sensitive to the dynamic phase of stretch, whereas the secondary endings are not. The secondary endings mainly encode information about the length of the muscle, whereas the primary endings encode mainly information about the rate of change in length. The dynamic sensitivity of the primary endings is largely due to the mechanical properties of the nuclear bag fibers.

There are two type of gamma motorneurons. One type innervates nuclear bag fibers (gamma dynamic or γ_d) and the other type innervates nuclear chain fibers (gamma static or γ_s). The reason for the names dynamic and static is that these gamma motorneurons regulate the sensitivity of spindle afferents either to dynamic or static phases of stretch. An important role of the gamma system is to allow the spindle to maintain a high sensitivity over a wide range of muscle lengths during reflex and voluntary contractions [Barker et al., 1970].

Golgi tendon organs have a relatively high activation thresholds which is why it is believed that they, together with their inhibitory spinal connections, function as a safety device to prevent muscle damage during excessive strain [Houk and Simon, 1967]. For this reason muscle spindles are thought to have a more important role in proprioception, as

they are continuously operating transducers.

Muscle receptors show sensory adaptation. Afferent fiber firing rates drop to the value which is 40-70% of the initial firing rate. Moreover, the rate of adaptation seems to be indipendent from stimulus intensity [Adrian and Zotterman, 1926].

2.4 Injury to Sensory-Motor Systems

Injury to any part of the organs and tissues responsible for movement may have many, very different consequences. In the following we give a very short overview.

2.4.1 Cerebro-Vascular Infarction (Stroke)

The term stroke, or cerebro-vascular accident, refers to the neurological symptoms and signs, usually focal and acute, which result from diseases involving blood vessels. Strokes are either occlusive (due to closure of a blood vessel) or hemorrhagic (due to bleeding from a vessel). Insufficiency of blood supply is called ischemia. If it is temporary, symptoms and signs may clear with little or no pathological evidence of tissue damage. Ischemia reduces blood supply, thereby deprives tissue from oxygen, glucose, and prevents the removal of potentially toxic metabolites such as lactic acid. When ischemia is sufficiently severe and prolonged, neurons and other cellular elements die. Depending on which region of the central nervous system is affected, the consequences can be different: contralateral weakness, sensory loss, impaired spacial perception, and other not directly related to movement.

2.4.2 Spinal Cord Injuries

Spinal cord injuries or diseases are a frequent reason of disability and result in total and partial obstruction of flow of both sensory and motor information being instrumental for normal life. Spinal cord injuries are most often caused by trauma, especially following motor vehicle or sport accidents. The resulting syndrome depends on the extent of direct injury of the cord or compression of the cord by displaced vertebrae or blood clots. In extreme cases trauma may lead to complete or partial transsection of the spinal cord. Lesions of the spinal cord give rise to motor and sensory symptoms that are often related to a particular sensory or motor segmental level of the spinal cord (Fig. 2.8).

Tetraplegia refers to impairment or loss or motor and/or sensory function in the cervical segments of the spinal cord due to damage of neural elements within the spinal canal. It results in the impairment of function in the arms as well as in the trunk, legs and pelvic organs. Paraplegia is the impairment or loss of motor and/or sensory function in the thoracic,

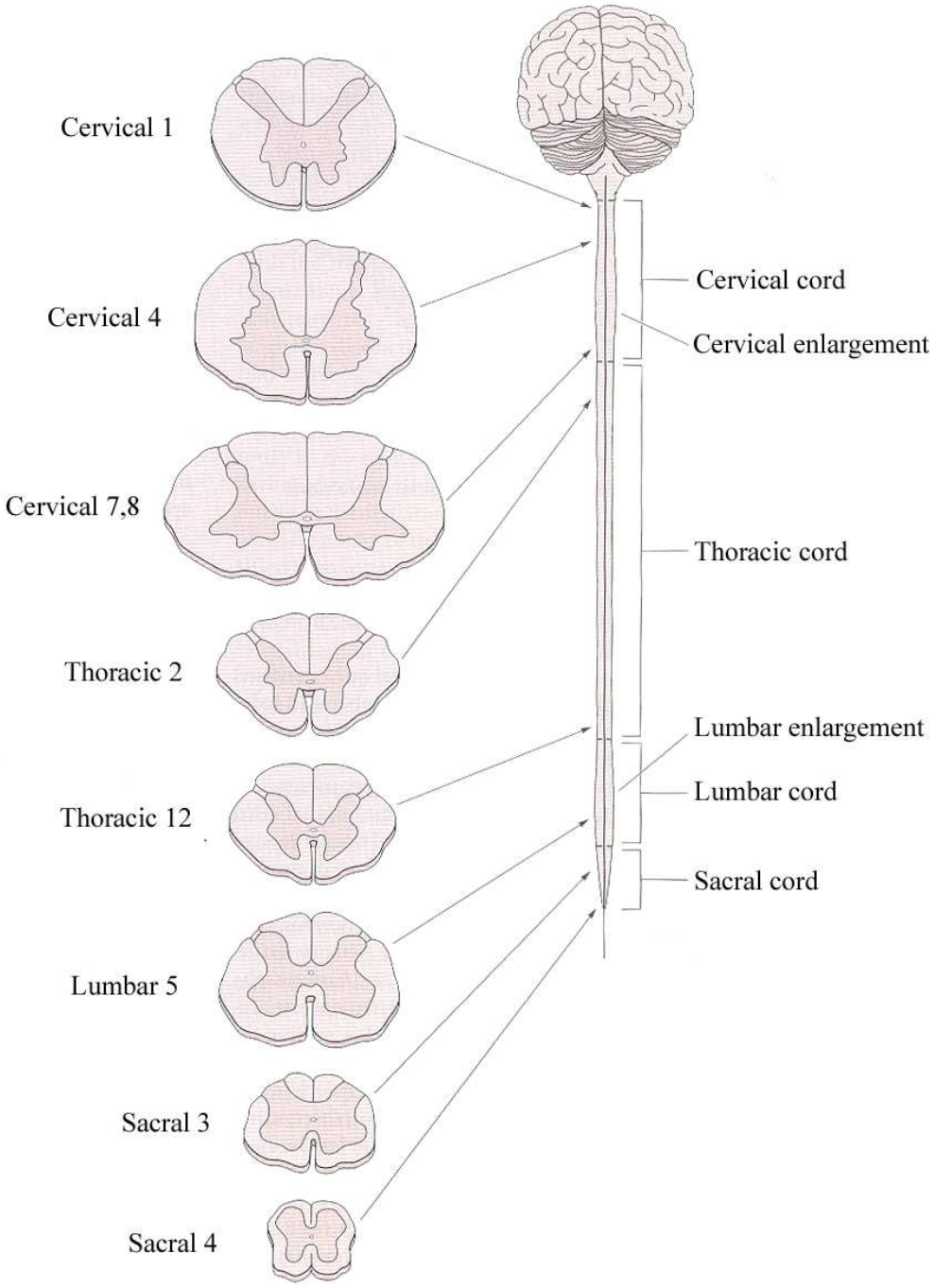

Figure 2.8: The spinal cord at different levels. It is divided in 4 major regions: cervical, thoracic, lumbar, and sacral. Spinal nerves at the cervical levels innervate the head, neck, and arms. Nerves at the thoracic level innervate the upper trunk, while lumbar and sacral spinal nerves innervate the lower trunk, back and legs. From Kandel et al. [2000].

lumbar or sacral (but not cervical) segments of the spinal cord. With paraplegia arm functioning is spared, but, depending on the level of injury, the trunk, legs, and pelvic organs may be involved. Terms quadriparesis and paraparesis describe incomplete lessions, where many functions are preserved.

2.4.3 Multiple Sclerosis

Multiple sclerosis (MS) is an autoimmune condition in which the immune system attacks the central nervous system, leading to demyelination. It affects the areas of the brain and spinal cord known as the white matter. More specifically, MS destroys oligodendrocytes which are the cells responsible for creating and maintaining a fatty layer, known as the myelin sheath, which helps the neurons carry electrical signals. MS results in a thinning or complete loss of myelin and, less frequently, the cutting (transection) of the neuron's extensions or axons. When the myelin is lost, the neurons can no longer effectively conduct their electrical signals. The name multiple sclerosis refers to the scars (scleroses - better known as plaques or lesions) in the white matter. Loss of myelin in these lesions causes some of the symptoms, which vary widely depending upon which signals are interrupted. Almost any neurological symptom can accompany the disease. Those related to movement include changes in sensation (hypoesthesia), muscle weakness, abnormal muscle spasms, and difficulties with coordination and balance.

2.5 Neuroprostheses for Restoration of Movement

A neuroprosthesis is a system for replacing or augmenting a function that is lost or diminished because of injury or disease of the nervous system. The basic principle for operation of a neuroprosthesis is the stimulation of neuro-muscular tissue, i.e. activation of sensory and/or motor system. Advanced neuroprosthesis are bidirectional, also capable of sensing neuroelectric activity either in the central either in the peripheral nervous system. Functional electrical stimulation (FES) is at this time the essence of neuroprosthesis. FES elicits controlled neural activation by delivering low level electrical currents.

Fig. 2.9 shows the principle of operation of a neuroprosthesis. After an injury or disease of the central nervous system, parts of the body remain functioning normally, but other parts of the body will be paralyzed. Many muscles will remain connected to the CNS below the level of injury. They are innervated, but not under volitional control. These muscles can be used for movement restoration. At the same time many sensory pathways remain intact below the level of injury. Neuroprostheses can be considered as a bypass of the damaged

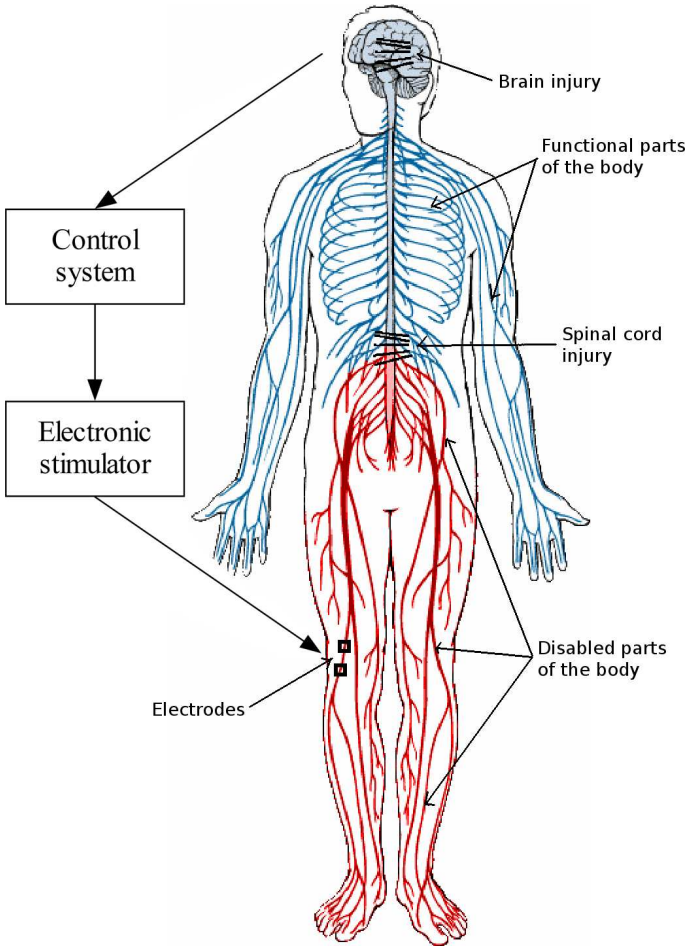

Figure 2.9: Principle of operation of neuroprostheses. Components of the system are the control system, stimulator, sensory feedback (not shown) and electrodes.

sensory-motor structure. Basically, the FES system consists of an interface to the sensory and motor systems of the body and a controlable stimulator.

2.5.1 Instrumentation for FES Systems

A functional diagram of the FES system (Fig. 2.10) shows the main components required for restoring motor function after injury of the central nervous system. The stimulator receives control signals, generates trains of pulses of electrical charge, and delivers those to the the excitable tissue via electrodes.

Each of the components has to be selected or built based on the specific application, e.g. lower extremities upper extremities, single-channel, multi-channel, transcutaneous,

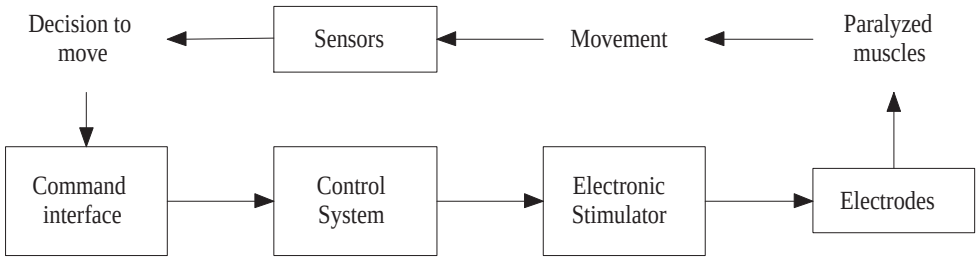

Figure 2.10: Instrumentation for FES: command interface, control system, electronic stimulator, electrodes and sensors. Decision to move is at the voluntary level of the user.

Figure 2.11: Organization of an open-loop control system. From Popović and Sinkjær [2000].

percutaneous, and fully implanted systems.

2.5.2 Control Systems for Movement

Open-loop controllers can be designed to function without knowledge of the actual plant trajectory as shown in Fig. 2.11. The open-loop controller delivers command signals based on precomputed sequences. If there is any perturbation in the trajectory, an error will occur, to which the system will not react. The precomputed sequences are patterns of stimulation for the appropriate muscles. Regardless of design method and implementation, the performance of any open-loop control system will probably be inadequate, since disturbances will cause performance to deviate significantly and lead to undesired behavior.

To correct for disturbances, a closed-loop controller with ongoing knowledge of the effects of the disturbance, or modification of muscle performance due to fatigue, must be designed. Joint angle and force transducers provide signals from which the current state of the system can be estimated and fed back to the controller (Fig. 2.12). Closed-loop controllers are classically error driven – they respond to the trajectory error which is determined by comparing the actual and the desired trajectories. PID controllers are not an entirely appropriate solution and it is difficult to tune the gain factors.

Model-based closed-loop controllers would be more robust. They require sensors and a dynamic model of the system to continuously recalculate the desired trajectory in order

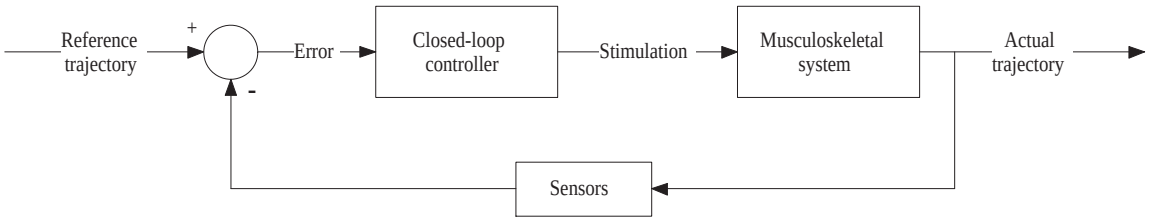

Figure 2.12: Organization of a closed-loop control system. From Popović and Sinkjær [2000].

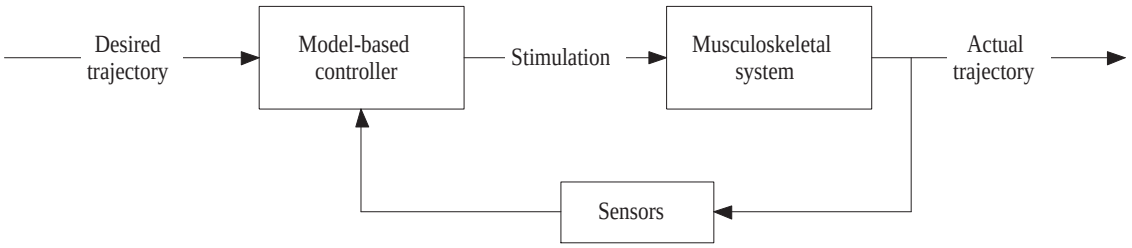

Figure 2.13: Organization of a model-based control system. From Popović and Sinkjær [2000].

to accomplish the task (Fig. 2.13). For example, during walking, if the body is following a desired path, the model-based controller uses the same muscle stimulation pattern as an open-loop controller. If the body deviates from the desires path, the model-based controller generates a new stimulation pattern which, according to the model, should maintain or restore stable walking. Accounting for change of muscle properties and fatigue would also be desirable.

2.5.3 Recording Nerve Activity

Advanced implanted neuroprostheses aim to take advantage of both recording and activating properties of the neural interface to restore sensory-motor functions. Measurement of nerve signals implies a recording chain that can be broken into three subsystems: biology, interface, and signal conditioning system. The biology system comprises the peripheral nervous system, responsible for driving information from/to the central nervous system to/from the periphery. The interface, i.e. the electrodes, senses and translates chemoelectric potentials, which result from electrical activity of cells. The signal conditioning system is the electronic apparatus that allows recording nerve signals as potentials. A classical signal conditioning scheme can be seen on Fig. 2.14.

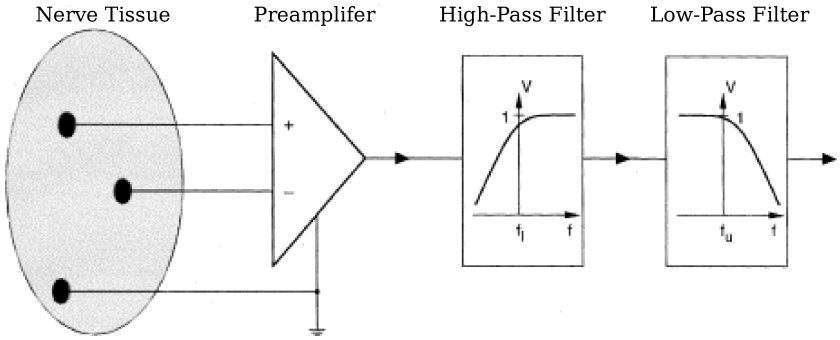

Figure 2.14: Basic configuration of a biopotential recording system. From Bronzino [2000].

The measurements involve voltages at very low levels, with high source impedances and superimposed high level interference signals and noise. The signals need to be amplified to be compatible with devices such as displays, recorders, or A/D converters for computerized equipment. Amplifiers adequate to measure these signals have to satisfy very specific requirements. They have to provide amplification selective to the physiological signal, reject superimposed noise and interference signals, and guarantee protection from damages through voltage and current surges for both patient and electronic equipment. Visual representation of recorded neuroelectric activity is called the electroneurogram (ENG).

2.5.4 Interfacing the Peripheral Nerve

A transverse section of a nerve is illustrated on Fig. 2.15. Nerve axons travel in bundles through the body. These bundles are encapsulated in fibroconnective tissue. Entire nerve bundles are surrounded by the epineurium, which bears most of the mechanical tension applied to the nerve. Branching from the epineurium and dividing the nerve bundle into fascicles is the perineurium, which bears the elongation load. Finally each individual axon is surrounded by the endoneurium. Each axon, or nerve fiber, can be seen as an individual information channel.

There are two basic designs of peripheral nerve recording electrodes: extraneural and intraneural electrodes. Extraneural electrodes are generally wrapped around the circumference of the nerve and commonly named cuff electrodes. Less invasive than intraneural electrodes, they permit recording from a whole nerve and do not provide access to information from a small group of neurons. Cuff electrodes come in a variety of configurations, but they all have a longitudinal opening to allow installation on the nerve without damaging it [Andreasen and Struijk, 2002], [Yoo and Durand, 2005], [Navarro et al., 2005].

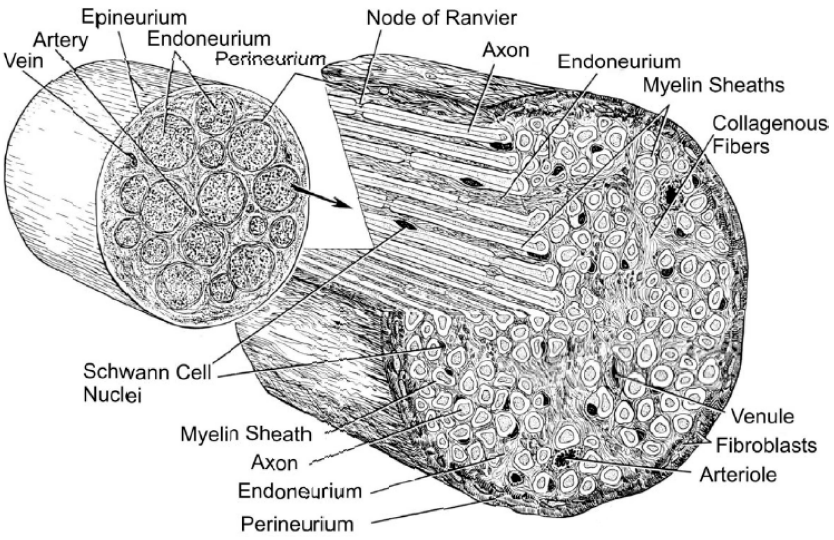

Figure 2.15: The structure of a peripheral nerve. From Horch and Dhillon [2004].

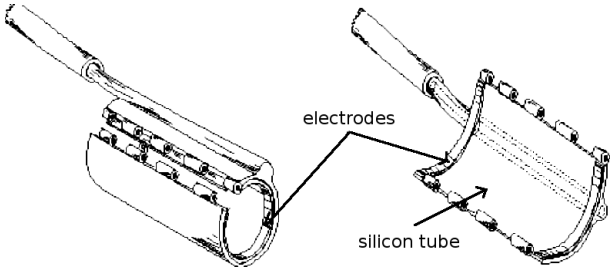

Figure 2.16: Cuff electrode. It is wrapped around the circumference of the nerve. The closed cuff is shown on the left, and the open on the right. From Hoffer and Kallesøe [1999].

They can also be in a form of a spiral [Naples et al., 1988] and have multiple contacts [Grill and Mortimer, 1996], [Stieglitz et al., 2003]. The standard cuff is made out a polymer and the electrodes within the cuff are made out of metal, usually being circumferential around the inner surface of the cuff (Fig. 2.16).

Cuff electrodes are a proved method for chronic recording from the peripheral nervous system. The first chronic studies were done in the 1970s by Hoffer [1975] and Stein et al. [1978]. For more than a decade now it has been used in many studies where information from whole-nerve recordings were extracted to provide event detection. A recent review has been published by Struijk et al. [1999]. One example is recording from cutaneous sensors for the detection of object slippage while being held [Hoffer et al., 1991] and obtaining skin contact force information [Hoffer et al., 1989]. Human trials have also also

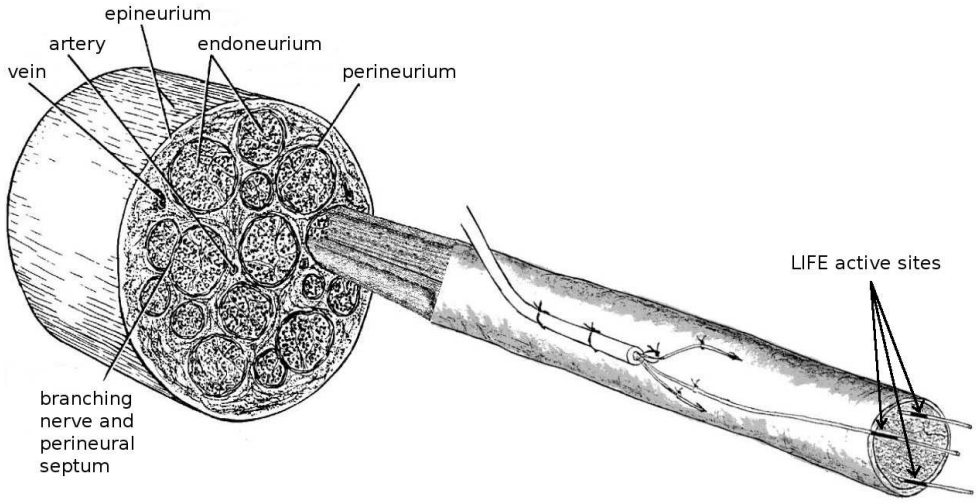

Figure 2.17: Longitudinal intrafascicular electrode. The electrode invades the epineurium and perineurium, and placed longitudinally inside a nerve fascicle. Courtesy of Dr. Ken Yoshida.

been conducted [Sinkjær et al., 1991]. Muscle spindle afferent activity was recorded to provide natural sensory feedback in studies by [Haugland and Hoffer, 1994], [Jensen et al., 2002b], [Micera et al., 2001], [Riso et al., 2000], [Strange and Hoffer, 1999]. Due to its poor selectivity and low signal-to-noise ratio, the digital signal processing algorithms used to decode afferent nerve activity fail to provide reliable information to be used for feedback [Upshaw and Sinkjær, 1998].

An alternative to the cuff is the longitudinal intrafascicular electrode (LIFE). It is designed to be implanted within the body of the peripheral nerve to ultimately serve as a neural interface for use in applications such as FES. They are placed in intimate contact with the nerve fibres to form a highly selective implanted neural interface (Fig. 2.17). When used for stimulation, they demonstrate topological selectivity in axonal recruitment, and when used for recording, they pick up neural activity from a relatively small population of fibres to enable the resolution of single fibres [Goodall and Horch, 1992], [Goodall et al., 1993], [Malmstorm et al., 1998], [Yoshida and Stein, 1999], [Chemineau et al., 2004].

The first LIFE was produced by Ken Horch and Andy Schoenberg of the University of Utah [Schoenberg et al., 1987]. Malagodi et al. [1989] did the first stimulation and recordings. Nannini and Horch [1991] did the first major work on electrical stimulation using LIFEs. The first work with recording in chronic animals was done by Lefurge et al. [1991] and Goodall et al. [1991]. Results from their six-month study showed that intrafascicular electrodes can be used on a chronic basis to acquire neural activity.

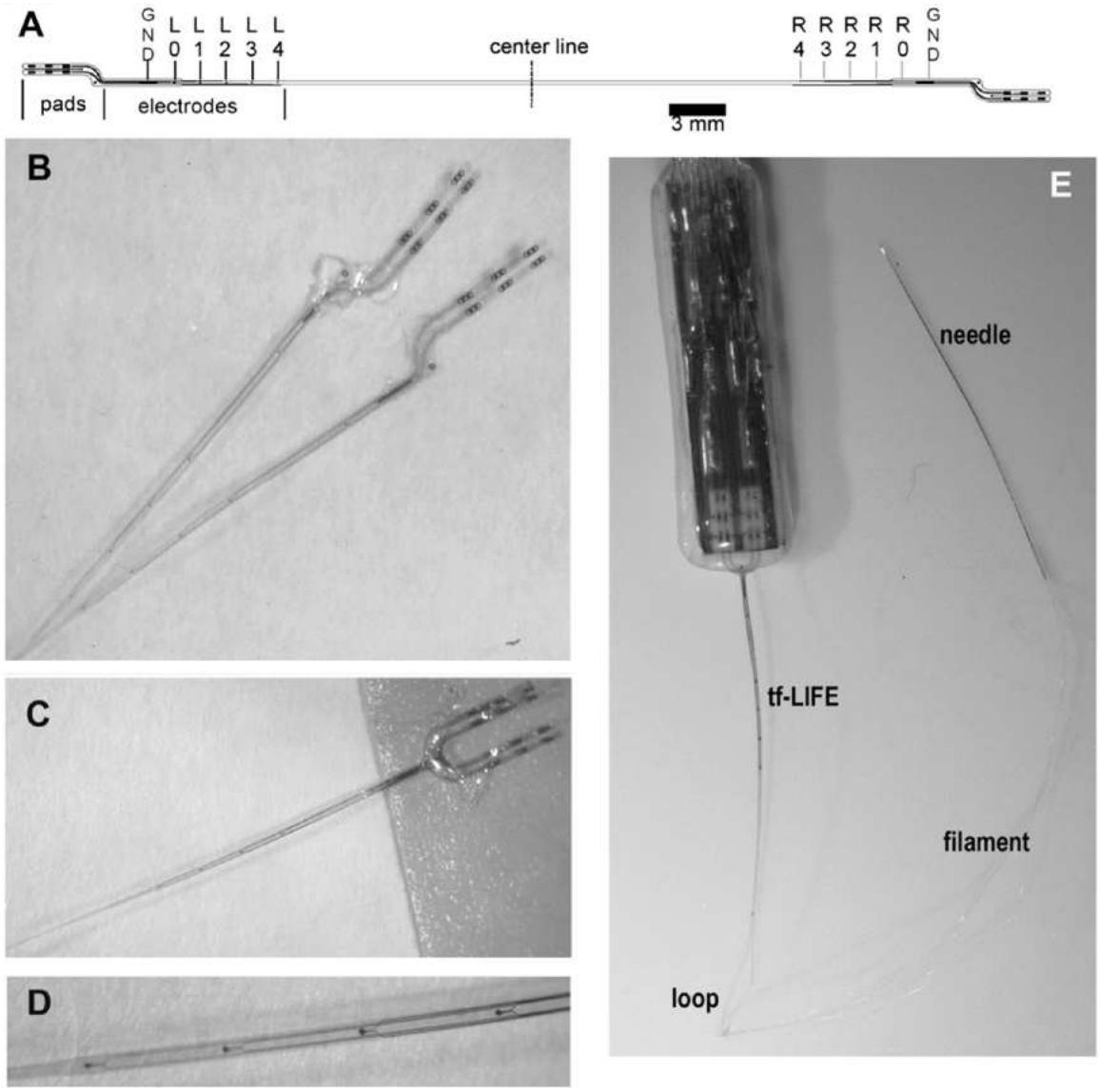

Figure 2.18: (A) Schematic of the tf-LIFE. Each half of the structure has a ground electrode (GND), an indifferent electrode (L0, R0) and four recording sites (L1-4, R1-4). (B) The tfLIFE is folded by the central line, so both branches can be closely apposed. (C) View of the proximal part of the electrode. (D) Higher magnication view showing the four active sites made by Pt sputtering. (E) Photograph of the whole system. The tf-LIFE is attached at the ending part to a ceramic connector for nerve recording/stimulation. The loop between the two branches of the tfLIFE is connected to a Kevlar lament that in turn is glued to a tungsten needle for insertion in the nerve. From Lago et al. [2007].

McNaughton and Horch [1992] developed the first dual channel recording with LIFEs. Yoshida and Horch [1993] did the first work with multichannel stimulation. It has been shown that stimulation through them can be used to selectively stimulate nerve fascicles as well as subfascicular regions within the nerve in the cat animal model. Yoshida and Horch [1996] followed up this work by closing the control loop.

In an effort to create LIFEs with smaller, more precise, and more reproducible active sites, a flexible micromachined polymer structure was designed to replace the key component of the electrode, the fine wire in contact with the endoneural tissue that forms the neural interface of the electrode. Yoshida et al. [2000] developed the first thin-film multichannel LIFE structure. The thin-film LIFE was later developed through work with the Fraunhofer IMBT in Ingbert, Germany. The latest version of the electrode is the microfabricated multi-site thin-film Longitudinal Intra-Fascicular Electrode (tfLIFE) array that is realized as a patterned thin film on polyimide structure [Hoffmann and Koch, 2005]. It allows recording up to 8 channels of ENG (Fig. 2.18).

In the meantime, the polyLIFE was being developed by Lawrence et al. [2003] and Lawrence et al. [2004], who did a series of experiments to show their acute and chronic feasibility in rabbits. Based on this work, Dhillon et al. [2004] and Dhillon and Horch [2005] implanted an advanced version of the polyLIFE in amputee human subjects for a short term trial. They showed the proof of concept of using LIFEs to elicit sensations and record volition from electrodes implanted semi-chronically in nerve stumps of human upper extremity amputee volunteers.

Chapter 3

Modeling the Afferent Nerve Activity to Estimate Muscle State

3.1 Introduction

Changes in muscle length are associated with changes in the angle of the joint that the muscle crosses. Thus, activity from muscle spindles can be used to sense relative positions of body segments. These sensors remain intact and active below the level of lesion in spinal cord injured patients. Therefore, their activity could be used to provide feedback information about muscle state in a closed-loop control FES system, if on-line extraction of reliable information from neural activity in a form usable by the controller is possible.

Recently, Stein et al. [2004] have shown how populations of sensory receptors could encode limb position and how the firing of a small number of neurons can be used to decode the position of the limb. In their study, microelectrode arrays have been used to record impulses simultaneously from individual nerve cells in the dorsal root ganglia (DRG) of the cat. They showed that a small number of informative neurons (68) could account for over 80% of the variance. The drawback of this technique is the risk associated to the surgery needed to place the electrodes at the DRG. Recording activity from peripheral nerves is less invasive; it is classically done using cuff electrodes which sense the aggregate activity of the whole nerve fibers. We propose to use intrafascicular electrodes which allow solving the lack of selectivity of the cuff electrodes.

Closed-loop control of joint movement using neuromuscular stimulation adopted in this thesis is based on the approach developed by Yoshida and Horch [1996], where a pair of single-channel LIFE's was implanted in the nerves innervating the joint agonist/antagonist muscle pair. The idea is to have the two electrodes working in opposite modes, e.g. while

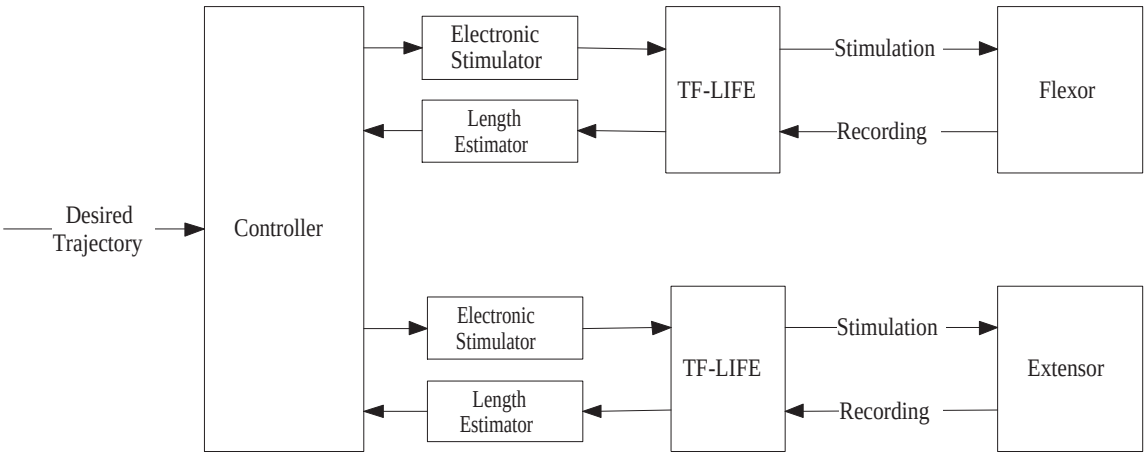

Figure 3.1: Scheme of FES closed-loop control of joint movement where a pair of tfLIFE electrodes is implanted in nerves innervating the the joint agonist/antagonist muscle pair.

one electrode is stimulating the agonist, the other is recording muscle spindle activity from the antagonist, and vice versa (Fig. 3.1). This way the recording electrode is always sensing neural activity from a passively stretched muscle.

For estimating muscle length from this activity the authors used a look-up table. Estimation of muscle length was fed back to the controller and used to modulate the stimulation pulse train parameters to minimize ankle position error. With such a control scheme, the need for simoultaneous recording and electrical stimulation of the same muscle is avoided. Electrical stimulation in close proximity of the recording electrode produce large stimulation artifacts which corrupt the recorded signals. The control scheme also allows using passive mechanical muscle models for estimating muscle state, instead of complex modeling of active muscle.

This approach proved to be applicable as feedback in on-line closed-loop control in restrictive conditions (limited motion speed and range), most probably due to the unaccounted variation of dynamic sensitivity of the sensory endings. The purpose of the study was to assess the feasibility of using muscle spindles as a sensor in a closed-loop FES system, rather than to build an optimized controller, per se, a simple PI (proportional-integral) controller was implemented to modulate the pulse width of a constant amplitude, fixed frequency stimulus pulse train.

If a valid analytical model, linking muscle spindle afferent nerve activity and muscle length, could be found for the locomotor range of ankle motion (in terms of both range of motion and motion speed), it would allow for having an on-line model-based estimator of muscle length and advanced control laws can be designed. Our aim is to develop a model,

as simple as possible, which can be implemented in a on-line estimator of muscle state in a closed-loop contol system.

In a recent study a simple linear model was adopted to express the relationship between length and neural firing rate [Azevedo and Yoshida, 2005]. The preliminary results from the study had indicated that a linear relationship between the neural firing rate and muscle length can be found for a limited range of motion. In the present thesis the first objective was to complete this study by verifying if the linear model is a good fit to experimental data on a sufficiently large statistical sample.

Just before beginning the work on this thesis, a new generation of the intrafascicular neural interface, the tfLIFE, had been fabricated [Hoffmann and Koch, 2005], but not yet fully tested in experimental conditions. The acute rabbit experiments, needed to be performed in order to acquire data for completeling the linear model study, were also a opportunity to test the new electrode in vivo. Implantation of intrafascicular electrodes is not a trivial task and requires surgical training. Even after successful implantation of the electrode, executing the experiments is difficult to achieve due to other issues, one of them being noise.

3.2 Acute Animal Experiments

Acute animal experiments were conducted to acquire experimental data with which proposed models of muscle spindle afferent nerve activity in response to passive muscle stretch would be validated. In this section of the report the procedures during animal preparation are given first, followed by the necessary steps in the preparation of the electrodes used in the experiments. The equipment used for data acquisition is also given, followed by the description of the experimental protocol.

3.2.1 Animal Preparation

Acute rabbit experiments were conducted on 10 New Zealand white rabbits, median weight 4 kg and standard deviation 0.24 kg. Anesthesia was induced and maintained throughout the experiments with periodic intramuscular doses of a cocktail of 0.15 mg/kg Midazolam (Dormicum, Alpharma A/S), 0.03 mg/kg Fetanyl and 1 mg/kg Fluranison (combined in Hypnorm®, Janssen Pharmaceutica). In order to immobilize the left leg of the rabbit, it was anchored at knee and ankle joints to a fixed mechanical frame using bone pins placed through the distal epiphyses of the femur and tibia. The common calceneon tendon was attached to the arm of a motorized lever system (Dual-mode system 310B Aurora Scientific Inc.) using a yarn of polyaramid fibres (Kevlar 49, Goodfellow Cambridge Ltd). Skeleton

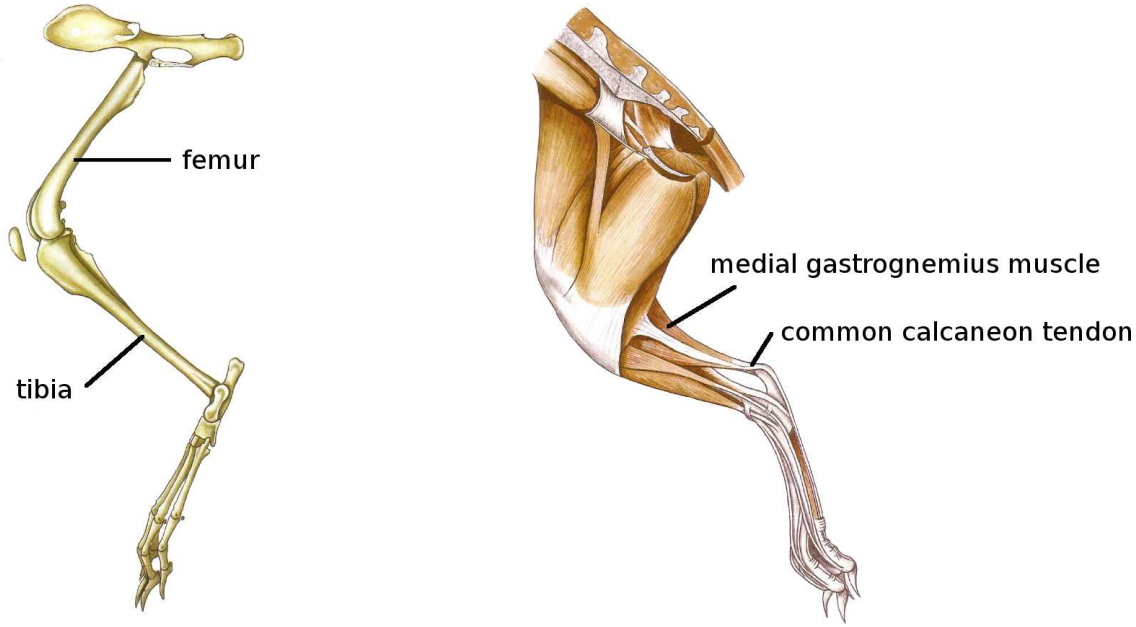

Figure 3.2: Skeleton of the rabbit's pelvic limb (on the left) and the medial muscles of the rabbit's thigh; superficial layer (on the right). Adapted from Popesko et al. [2002].

of the rabbit's leg and the medial muscles of rabbit's thigh are illustrated on Fig. 3.2 and a photograph of the setup is shown of Fig. 3.3. The motorized lever system provided both the actuation and measuring. Pulling the Kevlar fibers produced ankle extension and releasing tension on the Kevlar fibers resulted in ankle flexion (stretched muscle returning to its resting state due to its intrinsic elasticity). Fixation to the mechanical frame insured the elimination of mechanical vibration that might have resulted from a free swinging foot.

A tripolar cuff electrode was implanted around the sciatic nerve (Fig. 3.4, left). It was used to find the length-tension curve for the MG muscle (section 2.2.1). Electrical charge was delivered using a stimulation unit (Grass Technologies SD9), coupled with a photoelectric isolation unit (Grass Technologies PSIU6). The nerve was stimulated with 300 μs twitches and a pulse repetition frequency of 2 Hz. Stimulation intensity was set to the level that produced maximal nerve twitch respose (maximal amplitude of compound action potential). Keeping the stimulation level constant, muscle length was varied in small incremental steps. Isometric force produced by the stimulated muscle was simultaneously monitored.

A tfLIFE structure was implanted in the tibial branch of the sciatic nerve innervating the MG muscle of the rabbits left hind limb (Fig. 3.4, right). It was located 3 cm proximal to the tfLIFE implantation site. The electrode enabled the monitoring of multi-channel

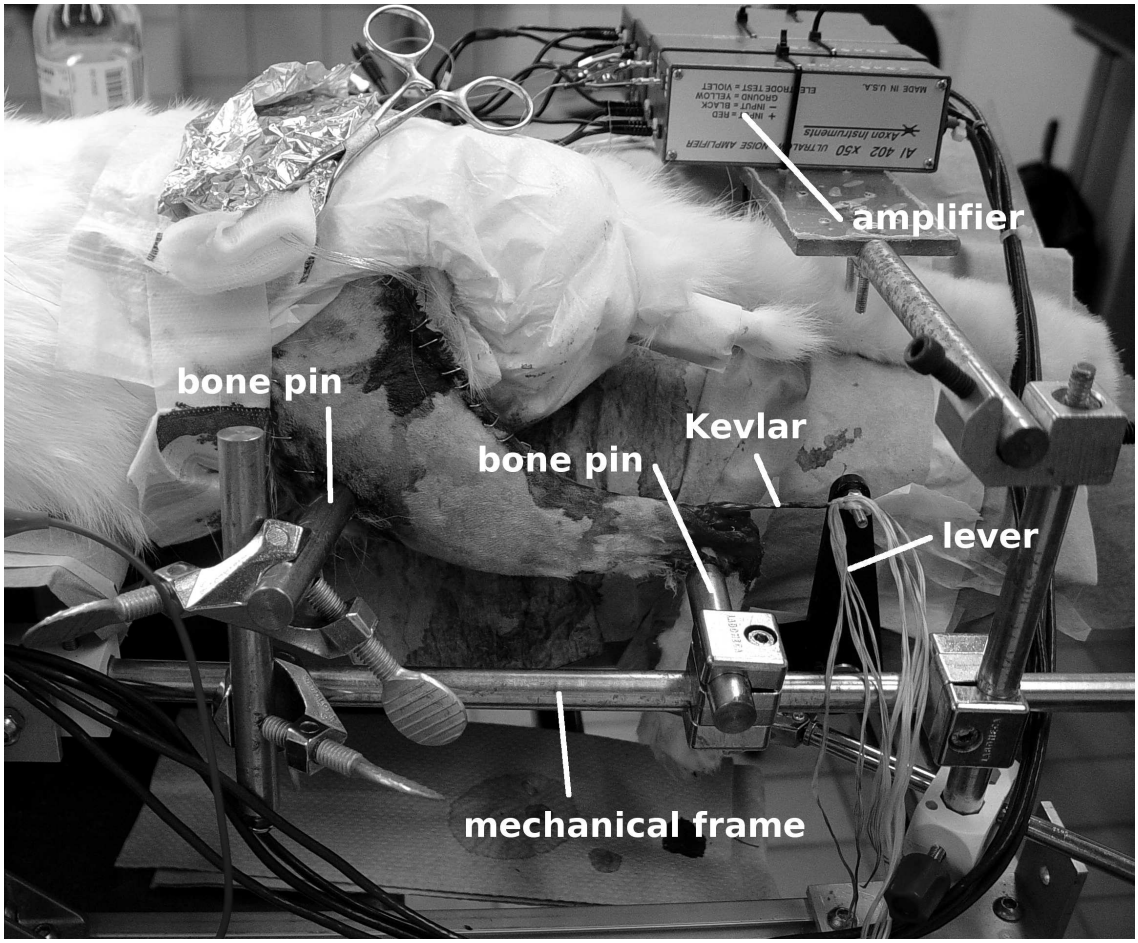

Figure 3.3: Experimental setup. The left leg of the rabbit was anchored at knee and ankle joints to a fixed mechanical frame using bone pins placed through the distal epiphyses of the femur and tibia. The common calceneon tendon was attached to the arm of a motorized lever system using a yarn of Kevlar fibres

ENG from the fascicle in which the structure was implanted. By having the electrode implanted very close to the muscle, chances of having anything except muscle spindle activity recorded are minimized. Moreover, in order to have purely muscle afferent activity in the recordings, the sciatic nerve was crushed proximally of the cuff and tfLIFE implantation sites using a pair of forceps. It should also be mentioned that with increasing levels of anesthesia, the effects of reflex mechanisms diminish, and decreased tonic stiffness of muscles is observed [Sherrington and Hering, 1897-1898], [Pagès and Proske, 1970]. As for Golgi tendon organ activity that encodes muscle force information, it accounts for only a small part of the muscle afferent signal under passive conditions. A histological study reports that

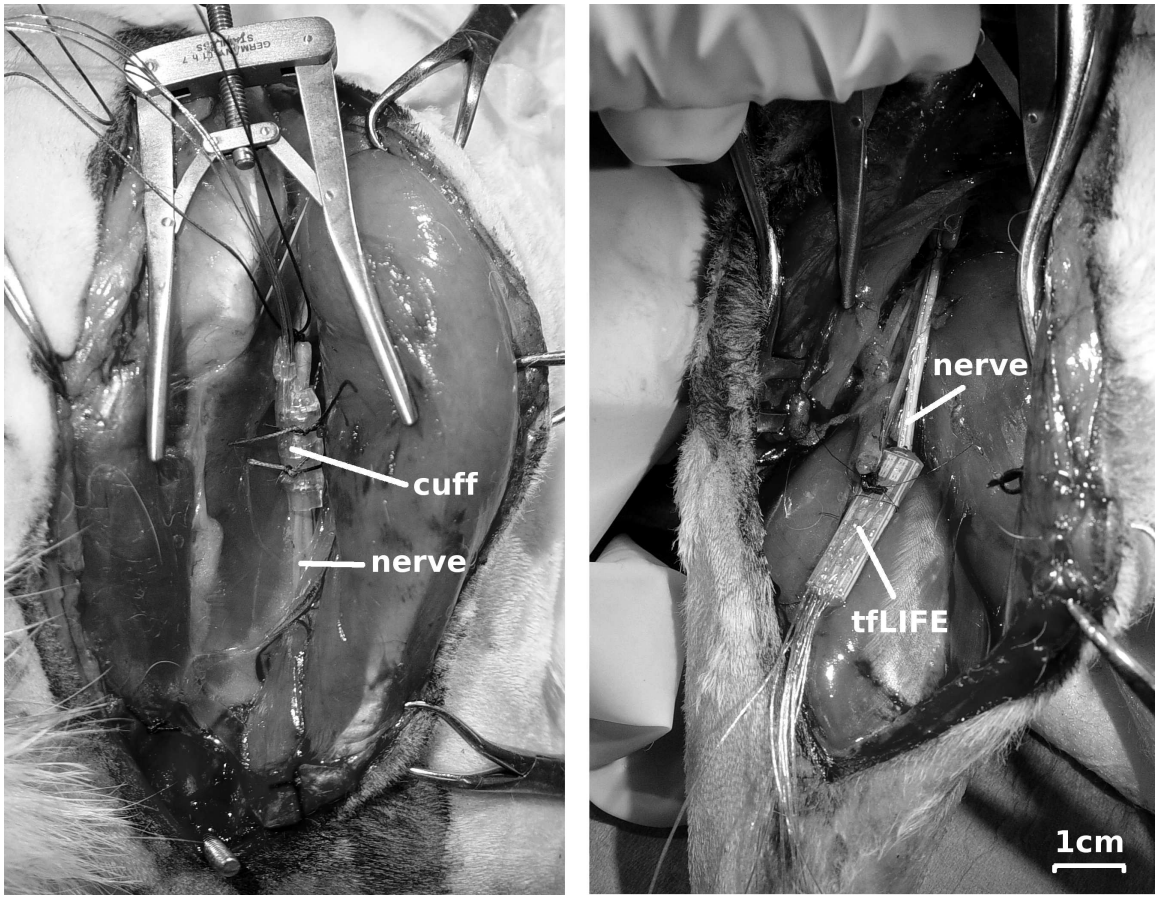

Figure 3.4: Electrodes used in the experiments. *Left:* tripolar cuff electrode implanted around the sciatic nerve. *Right:* tfLIFE implanted inside the fascicle of the sciatic nerve innervating the MG muscle. The thin-film structure is too small to be seen, only the electrode connector is visible. The scale for both images is the same. It is shown in the bottom right corner of the right image.

they account for less than 5% of the total number of receptors in tibialis anterior muscle [Wei et al., 1986].

Animals were euthanized at the end of the experiments. All procedures used in experiments were approved by the Danish Committee for the Ethical use of Animals in Research.

3.2.2 Electrode Preparation

The tripolar cuff electrode used in the experiments had been fabricated by using platinum foil electrodes fixed by rubber bands on a Teflon coated mandrel, that was then dip-coated

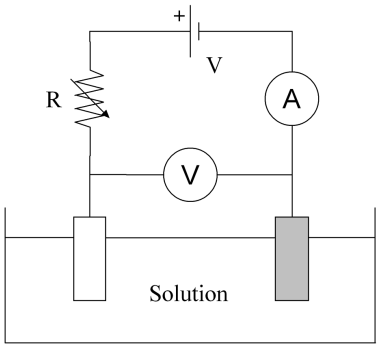

Figure 3.5: Schematic of the electrolytic cell used for electroplating the tfLIFE with Platinum in the process of electrode preparation. The white cathode on the left is the tfLIFE and the grey anode on the right is the Pt wire. The variable resistor is used to limit the current flowing throught the solution.

with silicone. The detailed procedure is described by Haugland [1996]. The electrode had an inner diameter of 2 mm and a 10 mm distance between its outer rings. We had fabricated the electrode ourselves in the clean room facilities at the Center for Sensory-Motor Interaction at Aalborg university, in Aalborg, Denmark.

The tfLIFE's were implanted into the target nerve fascicle using a 50 μm electrosharpened tungsten needle [Yoshida et al., 2007]. The needle was attached to the electrodes using 2 to 3 Kevlar threads (Fig. 2.18, panel E). In order to reduce the impedance of the electrode, its recording sites were electroplated with platinum in an electrolytic cell consiting of the tfLIFE, as the cathode, and a platinum wire, as the counter-electrode (VWR International). The working solution was made by mixing double deionized water and Dihydrogen hexachloroplatinate (IV) hexahydrate (VWR International). Details about the procedure can be found in literature [Whalen III et al., 2005]. The electrodeposition was performed under ultrasonic aggitation, which offers a level of control of the electrochemical deposition mechanism at the cathode. It insures firm attachment of platinum onto the electrodes and minimizes the deposition of platinum hydroxide, known as "burning" of the deposit [Jensen et al., 2002a]. The schematic of the electrolytic cell for tfLIFE preparation is illustrated on Fig 3.5. The white cathode on the left is the tfLIFE and the grey anode on the right is the Pt wire. The variable resistor is used to limit the current flowing throught the solution.

3.2.3 Data Acquisition System

The amplification system consisted of a low-noise preamplifier (AI402, Axon Instruments), followed by a gain-filter amplifier (Cyberamp 380, Axon Instruments). Signals were recorded using a custom modified multi-channel digital tape recorder (ADAT-XT, Alesis). ENG data were low-pass filtered (corner at 0.1 Hz), amplified (gain 5000) and acquired with a sampling rate of 48 kHz per channel. Out of the eight available electrode sites on the tfLIFE, only the four having the lowest background noise level were selected to be recorded from, due to the limited number of available channels on our recording system.

Signals for driving the motorized lever system were generated on a portable computer using Mathworks LabVIEW. Before feeding the analog signal into the lever system input, the signal passed through a low-pass filtering stage (corner at 100 Hz) in order to remove any quantization noise resulting from the D/A conversion. Quantization noise would translate into vibration of the lever arm which could have induced activity of muscle spindles [Jansen and Matthews, 1962], [Goodwin et al., 1972]. Measured length and force were attenuated by a factor of 10 to have the signals' amplitude dynamic ranges compatible with the input range of the recording system. Length and force signals were digitized using a sampling rate of 10 kHz.

3.2.4 Muscle Stretch Protocol

The recorded nerve activity is supposed to be a mixture of activity from two sensory fiber types. Activity from type I fibers should primarily encode information about muscle stretch velocity, and the activity from type IIb fibers should encode information about muscle length. A convenient and common way for studying muscle spindle afferent response is applying sinusoidal extensions to a muscle and simultaneously recording the muscle receptor afferent ENG [Jansen and Matthews, 1962], [Matthews and Stein, 1969a]. With recordings made with such a protocol, it is later possible to analyze the contributions of the two components to the aggregate recorded activity. In our experiments the MG muscle was passively stretched by rotating the ankle in the extension/flexion plane using the lever arm. The initial muscle length L_0 was set to the muscle length at which the produced isometric force was maximal. Ankle position was set so it was flexed 90° and then finely adjusted by experimentally finding the maximum of the length/tension curve. The muscle was presented with sinusoidal stretches of 2 frequencies: 10 mHz and 250 mHz. Both stretch profiles had a peak-to-peak amplitude of 4 mm. The durations of the recordings were 2 minutes for the slower stretch (to allow for one full cycle of the sine to complete), and just over 1 minute for the faster stretch (4 cycles of the sine). The 10 and 250 mHz frequencies were chosen to be able to evaluate models for different motion speeds. Simultaneous recordings

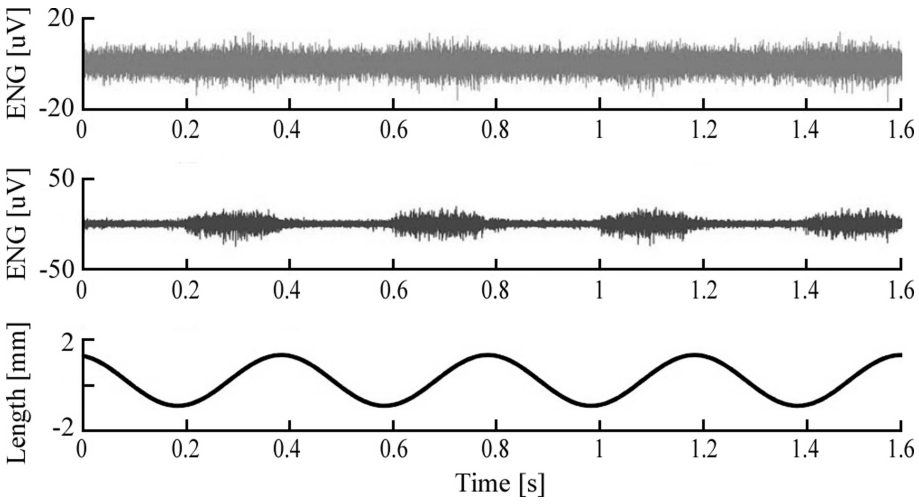

Figure 3.6: Recorded nerve response from the cuff electrode (top trace) and from the tfLIFE (middle trace) for a sinusiodal muscle stretch (bottom trace).

were made from the four intrafascicular electrode sites, together with force and position recordings from the muscle lever system.

An example of recorded ENG signals using the cuff and tfLIFE electrodes are shown on Fig. 3.6. The figure clearly illustrates the better signal to noise ratio obtained when recording with the intra-fascicular electrode.

3.3 Modeling the Nerve Response

3.3.1 Noise Processing

Noise artifacts from the recorded ENG were removed from the raw recorded signals using a 8th order high-pass Butterworth filter with a corner frequency at 500 Hz. The corner frequency is sufficiently high for removing low-frequency noise from the recording. Spectral peak power of the muscle artifact is around 250 Hz and spectral components of motion artifact are lower than muscle artifact. Spectral components of the neural signal are preserved as they fall above the corner frequency of the filter [Yoshida and Stein, 1999]. Powerline noise in the signal is a combination of the dominant (baseband) component of the noise and its harmonics. Spectral analysis of the recorded data showed peaks in the spectrum up to the seventh harmonic, which also puts them under the lower corner frequency of the filter.

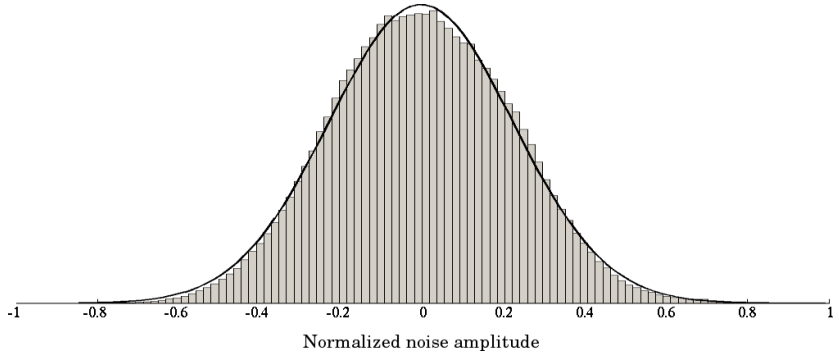

Figure 3.7: Normal distribution fit on the histogram of experimentally recorded background noise in the ENG. The histogram is the bar plot and the distribution fit is the full curve. The figure shows that a zero-mean normal distribution is a good model for the data. The noise signal was normalized to have a maximal absolute amplitude of 1.

3.3.2 Quantifying Neural Activity

For many neurons, the most prominent feature of the action potential is its amplitude, or the height of the spike. One of the simplest ways to measure the activity of a neuron is with a voltage threshold trigger. This method is by far the most common for measuring neural activity [Lewicki, 1998]. The obvious advantages of threshold detection are that it requires minimal computing power for signal processing. The disadvantage is that it is not always possible to achieve acceptable isolation between nerve and noise spikes. Because of this simplicity, this method was used in quantifying the neural activity in our recorded data. Analysis of the baseline (where the muscle was slack and only background noise was recorded) showed that the noise amplitude distribution is a good fit onto a normal distribution (spectral analysis of the noise showed that the noise can not be considered white, but the amplitude distribution is zero-mean Gaussian). This was true for baseline recordings of all experiments. An example of the noise histogram and the Gaussian zero-mean distribution fit to the data is shown on Fig. 3.7. Consequently, a threshold value was chosen to be equal to 3 standard deviations of the background noise. This value statistically accounts for 99.7% of the noise spikes, which in practice means almost all noise spikes are below the threshold.

After noise removal, the post-processed ENG signals were rectified and the aggregate afferent firing rates were computed by counting the number of peaks above threshold in a 100 ms moving time window with a 10% overlap between adjacent iterations. The choice of sliding window duration is a trade off between having a smaller percentage of noise peaks in the computation of firing rate (longer window duration required) and capability of tracking

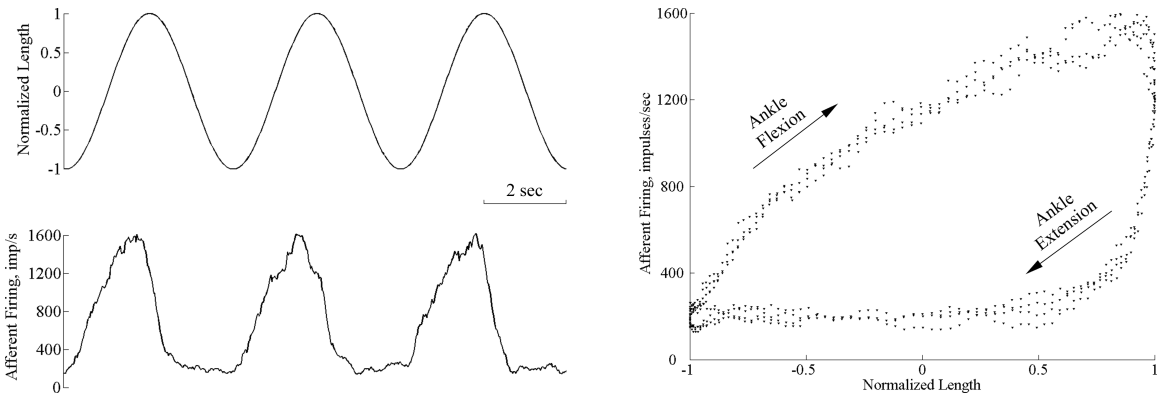

Figure 3.8: *Top left:* Three periods of a normalized sine wave used as the muscle passive stretch profile with amplitude 4 mm peak-to-peak and frequency 250 mHz. *Bottom left:* Aggregate firing rate computed using a 100 ms moving window on one channel of the post-processed ENG. *Right:* Relationship between firing rate and normalized muscle length for the 3 periods of the sine plotted superimposed. The muscle is being stretched during ankle flexion and shortened during ankle extension.

faster muscle motion (shorter duration required). Feasibility of implementation of closed-loop FES system also needs to be taken into account. Muscle fusion frequency is always above around 20 Hz so there is no need to perform control with an update of controller parameters with a clock period under 40 ms (including feedback delay). For relatively slow movements the frequency used to discretize the command is about 100 ms, which is the value we chose for the window duration. Values larger than this are not appropriate for accurate closed-loop control (such as trajectory control), but if the aim of the feedback if simple event detection (e.g. foot drop, detection of threshold ankle angle) or rough posture estimation, then larger values could be acceptable [Guiraud et al., 2006].

An example illustrating the zero-mean normalized muscle length and the simultaneously recorded ENG from one channel of the tfLIFE is shown on Fig. 3.8, on the left. The corresponding neural firing rate plotted against the normalized muscle length is shown on the same figure, on the right.

3.3.3 Linear Model Approximation

With the adopted FES control scheme (section 3.1), it is of interest to find a model between afferent nerve activity and muscle length only for the periods of ankle plantar flexion (muscle stretching), because muscle spindle afferents are silent during the dorsiflexion period (muscle spindles are unloaded when the muscle is slack). The objective was to find a model

that would be valid for the locomotor range of ankle joint motion and, at the same time, have the model as simple as possible, so an on-line muscle length estimator based on this model could be feasible. Being the simplest case, a linear model approximation was a logical starting point. It is formulated with the following equation:

$$s = K_p \cdot l + K_r$$

where s is the aggregate neural firing rate, l is the muscle length variation, K_p is the proportional gain, and K_r is the coefficient modeling the residual activity originating either from other (non-proprioceptive) nerve fibers in the fascicle and noise. Golgi tendon organ activity is considered to take a very small part in the aggregate firing rate (section 3.2.1), but even if picked up in the recordings, firing of Golgi tendon organ afferent fibers can roughly be considered to have a linear relation to length [Renkin and Vallbo, 1964]. Therefore, it is expected that their activity is also modeled by the coefficient K_p.

The muscle was stretched with a sine wave profile l:

$$l = A_0 \cdot sin(wt) + L_0$$

where A_0 is the sine amplitude, L_0 is the muscle initial length set during animal preparation (section 3.2.1), and w is the sine angle frequency. From the above two equations the following can be derived:

$$s = K_p \cdot A_0 \cdot sin(wt) + K_p \cdot L_0 + K_r$$

After writing the length in its zero-mean normalized form and substituting it in the above equation, we get:

$$s = P_1 \cdot l_n + R_1$$

where l_n is the zero-mean normalized length, and P_1 and R_1 are new coefficients:

$$l_n = \frac{l - L_0}{A_0}; \quad P_1 = K_p \cdot A_0; \quad R_1 = K_p \cdot L_0 + K_r$$

Linear regression analysis was performed using data from both slower and faster sine wave stretch profiles. Results showed that the model is a good fit to the experimental data only in a limited number of cases where the muscle is stretched using the slower sine wave. Stretching the muscle with the faster sine produces a nonlinear relationship between firing rate and muscle length due to the increased sensitivity of the primary muscle spindle afferents. The simple linear approximation is not a good model is this case, although it remains applicable in the linear part of the curves.

3.3.4 First-Order Model Approximation

In order to improve the model, it was necessary to introduce non-linearity into the relationship between afferent activity and length:

$$s = K_p \cdot l + K_v \cdot \frac{dl}{dt} + K_r \tag{3.1}$$

where s, l and K_r are the same as in the linear model, and K_p and K_v are now coefficients corresponding to the activity of different sensory fiber types. K_p models activity of position-sensitive (type II) fibers, and K_v models the activity of velocity-sensitive (type Ia) fibers. Following the same mathematical operations as above, we get the following:

$$s = K_p \cdot l + K_v \cdot A_0 \cdot w \cdot \sqrt{1 - (\frac{1 - L_0}{A_0})^2} + K_r \tag{3.2}$$

where the link between length and its derivative is found from Euler's formula:

$$e^{i(wt)} = cos(wt) + i \cdot sin(wt) \tag{3.3}$$

This way we avoid direct numerical computation of the derivative of the length variation measured by motorized lever system, which would introduce additional noise to the variable. After writing the length in its zero-mean normalized form and substituting it in the above equation, we get:

$$s = P_2 \cdot l_n + Q_2 \cdot \sqrt{1 - l_n^2} + R_2 \tag{3.4}$$

where l_n is the zero-mean normalized length, and P_2, Q_2, R_2 are new coefficients:

$$l_n = \frac{l - L_0}{A_0} \tag{3.5}$$

$$P_2 = K_p \cdot A_0 \tag{3.6}$$

$$Q_2 = K_v \cdot A_0 \cdot w \tag{3.7}$$

$$R_2 = K_p \cdot L_0 + K_r \tag{3.8}$$

3.4 Results

Regression analysis for first-order model are summarized in Table 3.1. The parameters are derived using one sine cycle for the 10 mHz stretch and 4 sine cycles for the 250 mHz stretch. Only results for the channel with the best fit out the four are given. An illustration from one of the experiments is shown on Fig. 3.9.

Table 3.1: Fit coefficients P_2, Q_2, R_2 and their corresponding RMS fit errors (RMSE) for the channel with the best fit, for both sine wave muscle stretch profiles. The rows show the results for the 10 experiments.

	10 mHz sine stretch				250 mHz sine stretch			
Rabbit	P_2	Q_2	R_2	RMSE	P_2	Q_2	R_2	RMSE
1	311	-77	514	55	320	57	471	16
2	593	-176	798	65	780	20	926	45
3	93	-25	204	40	182	-11	558	18
4	143	-66	190	23	175	-50	211	11
5	1835	268	4967	166	2176	383	4889	57
6	370	-130	566	44	721	-68	764	27
7	471	5	1076	68	658	253	791	35
8	148	-31	303	34	233	48	315	17
9	818	-228	924	79	728	-9	1121	84
10	559	159	777	66	613	406	773	36

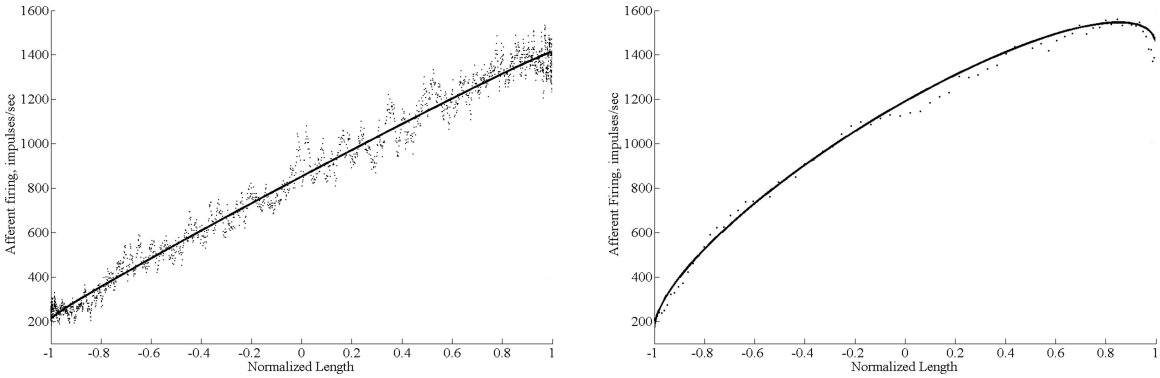

Figure 3.9: Single channel fit for stretch frequencies of 10 mHz (left) and 250 mHz (right). The abscissa shows the normalized muscle length and the ordinate shows the neural firing rate. The full lines are the fitted curves.

The RMS fit errors are larger for the slower sine wave due to the fact that for slower motion the variance of the computed firing rate is always larger, using the same length of the moving window. The difference is illustrated on Fig. 3.9 where the on the left plot the data set is noisier than the one on the right.

The relationship between firing rate and normalized length was in all cases more convex for the faster sine stretch profile. As the rate of change of muscle length increases, so does the contribution of the velocity-sensitive fibers to the aggregate firing rate. This is reflected in the increase in the fit coefficient Q_2 which quantifies the contribution of dynamic (velocity) sensitivity. The increase can be generalized between rabbits, as it appears in all 10 experiments. On the average the absolute increase in coefficient Q_2 is 124, with a standard deviation of 90 action potentials per milimeter of muscle stretch. Fit coefficients show large variability between rabbits, due to the fact that each electrode site picks up activity from a different number of units.

In a few cases with faster sine stretching the model fails to capture the non-linearity of the firing rate at the end of the muscle extension period, i.e. where the normalized sine value is +1 and movement speed is around zero (Fig. 3.10, left panel). In these cases the relative change in sensitivity from the beginning to the end of stretch is large enough to cause the failure of the model to properly capture the firing rate for the whole range of muscle stretch. In these cases the variation of fit coefficients is too large to be able to approximate them with constants. Piecewise fitting, i.e. separate curve fitting for normalized muscle length in the range from -1 to 0 and in the range from 0 to 1, produces much better fits with smaller errors (Fig. 3.10, right panel).

If the fit coefficients are known for a particular muscle, it is possible to estimate the muscle length in any given moment from the recorded ENG. When the estimation is performed on all 4 channels of the tfLIFE structure individually and then averaged, the estimated length shows a decrease of variation by about 50% compared to the estimation when only a single channel is used. An illustration is shown on Fig. 3.11. The estimation of muscle length from firing rate during the muscle stretch phase is shown on the left panel. The gray curves are the estimations from individual channels and the thick curve is the average of the single-channel estimations. The corresponding estimation errors are shown on the right panel, where the gray curves are the single-channel estimation errors and the thick curve is the multi-channel estimation error.

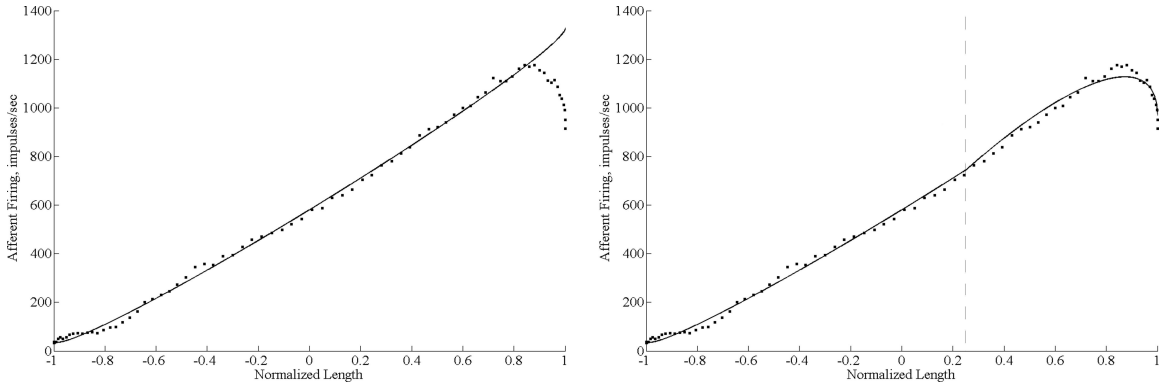

Figure 3.10: Piecewise fitting in the two regions of the normalized length separately gives better results than when fitting is performed on the whole range of motion. On the left: an example of a fit on the whole range. It fails to capture the drop in firing rate at the end of muscle extension where there is a cessation in velocity response. On the right: the same data set, but piecewise fitted using two sets of constant fit coefficients, one for each half of the normalized length range of muscle extension (from -1 to 0, and from 0 to +1). The two fit curves are joined at their intersection (at normalized muscle length of 0.253, indicated on the plot with the vertical dashed line).

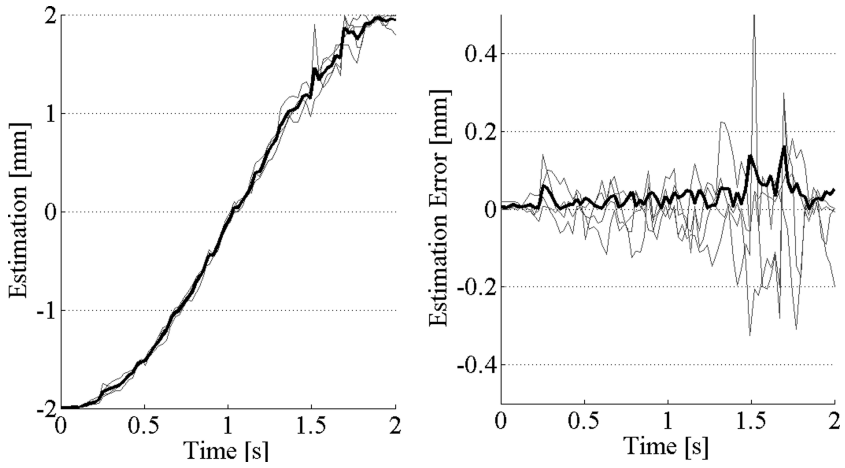

Figure 3.11: The estimations of muscle length from neural firing rate during the extension phase of the muscle. On the left panel the gray thin curves are the estimations from individual channels and the thick curve is the average of the single-channel estimations. The corresponding estimation errors are shown on the right panel. The gray thin curves are the single-channel estimation errors and the thick curve is the multi-channel estimation error.

3.5 Discussion

3.5.1 Model Parameters

Fitting the neural firing to the recorded length using the first-order model approximation shows better results compared to using a linear model. Not all muscle spindles within the muscle they reside have the same threshold of activation. Each spindle starts firing at a different muscle length. Larger afferents start firing as soon as the muscle is stretched by a small length, while smaller ones have a higher threshold and start firing only after the muscle has been more extensively stretched [Yoshida and Horch, 1996]. Therefore, the recorded aggregate afferent firing at any given muscle length is a mixture of spindles' activities, each firing at different frequencies. Furthermore, the sine amplitudes used in this study by far exceed the level under which the muscle spindles can be considered to be working in their linear region [Matthews and Stein, 1969a].

Although the fit coefficients cannot be used to directly quantify the activities of the two fiber types (a number of them is negative in sign), they do manage to capture the non-linear nature of the relationship between afferent firing rate and muscle length. For faster motion, the activity of velocity-sensitive fibers increases, which in all experiments resulted in an increase of coefficient Q_2. Whether the curve is going to be concave ($Q_2 < 0$), linear ($Q_2 = 0$) or convex ($Q_2 > 0$) depends on the interplay of two factors: the spindle recruitment curve (distribution of spindle activation thresholds as a function of muscle length) and the ratio between dynamic and static sensitivities of fibers the electrode is picking up activity from. Most of the fits for the slow sine wave tend to be either slightly concave or close to linear. On the other hand, most of the fits for the faster sine tend to be close to linear or convex.

A larger fit error with both sine frequencies can be noticed at the beginning of muscle extension (at the sine wave minimum). In the region where the stretch begins the movement velocity is around zero and the muscle is stretched the least, resulting in minimal afferent activity. As a consequence, at this point the largest percentage of neural spikes is buried under the noise gate. By removing the noise below the chosen threshold we also remove neural spikes that have their peak amplitudes below the noise gate. This is why the fit error is higher in this region.

With the faster sine wave, a considerable drop occurs in firing rate at the end of the ankle extension period. Again, like in the case before, the stretch velocity in this region is around zero and the firing rate drops rapidly. In other words, this is the region of the curve where there is a cessation of velocity response from the fibers. In a number of cases this effect is captured well only after piece-wise fitting is performed. This shows that approximating the

fit coefficients as constants throughout the entire range of motion no longer holds in these cases. Only when two sets of fit constants are adopted, the model gives satisfactory results.

3.5.2 Application in Closed-Loop FES

It is important to note that interpretation of neural firing rate from muscle spindles in a closed-loop FES system would be valid only during periods of increasing firing rate. Using only one sensor in a agonist/antagonist pair would make the detection of muscle shortening ambigous – decline of firing rate could not only be to muscle shortening, but also due to holding a fixed length, where sensory adaptation would cause a decrease in the neural firing rate.

With a real-time estimator embedded in a closed-loop control FES system it would be ideal to adapt the length of the moving window (used to compute the firing rate) to the changing stimulation parameters. With increasing stimulation levels, faster limb movements are anticipated and a smaller window length is needed. But as the window length decreases, the computed firing rate becomes more susceptible to the presence of noise spikes. In this study the same window length was used in the computation of neural firing rate for both sine wave frequencies. The results show that the range of firing rates does not vary with sine frequency. An illustration is shown on Fig. 3.9 where, in both cases, the firing rate is within the range from about 200 to 1600 impulses per second. But the shape of the curve does change with changing motion speed.

Not only can the CNS parallel-process signals from many spindles of one muscle to improve estimation of joint position, but it also has information available from multiple muscle that articulate a particular joint. Hense, information from a subset of units from one muscle (our case) cannot be expected to provide the same level of estimation accuracy. However, the tfLIFE brings with it the benefit of multi-channel recording. Estimating muscle length using more than one channel provides a more robust estimation, reducing the variance of the estimation error. Moreover, multi-channel estimation would allow having a smaller moving window than in the case of single-channel estimation, since using multiple channels provides a smaller estimation variance.

The changing of aggregate firing sensitivities to velocity of muscle stretch introduces an ambiguity in muscle length estimation from instantaneous firing rate, i.e. the relationship between muscle length and firing rate is not a one-to-one mapping. In its simplest form, an estimator based on the model described could be used in FES systems with cyclic limb movements (e.g. walking) where the estimator would estimate limb position using the same muscle stretch profiles that would be used for training. If one would like the estimator to be able to track slow and fast walking speeds, it would raise a question how would

the estimator know which curve to choose from, the one for slower or the one for faster movements. One way to deal with this issue would be to have the estimator keep a short history of previous length estimates. That way it would be able to track the change in length and choose the appropriate control curve based on the rate of the change in length. This way the estimator could know when the muscle is in extension phase (firing rate increasing).

Eventually, one would like to have a model-based estimator able be track any random limb movement with varying load. To accomplish this it would be necessary to distinguish between the afferent activities of the two fiber types and perhaps even single units. By doing so, one would be able to isolate the activity of only position-sensitive fibers and use them exclusively as input for the estimator. That way the model coefficients would be the same for all movement speeds. Separation between force- and length-sensitive fibers could also be possible by training the classifier using isometric inputs. That way the estimator would be insensitive to externally applied disturbances during limb movement. The first step towards accomplishing this task is to develop a neural spike classifier.

3.6 Summary

In the study presented in this chapter we explored the feasibility of using the new thin-film longitudinal Intra-fascicular electrode (tfLIFE) as a peripheral nerve interface. The long-term goal is to use the electrode as the neural interface in closed-loop control FES systems. Acute animal experiments were performed in which the afferent muscle spindle response to passive sinusoidal stretch was recorded with the tfLIFE. Results obtained with recorded ENG data are consistent with the results from previous studies where older generations of the LIFE were used. With its advantage of being a multi-channel electrode, the tfLIFE shows promise as a neural interface.

The proposed first-order model of muscle spindle response to passive muscle stretch manages to capture the non-linear properties of the relationship between afferent neural firing rate and muscle length. We have shown that estimation of muscle state from the recorded multi-channel ENG provides more robust results compared to using single-channel recordings.

In order for the model to be able to track muscle length variations with an a priori unknown stretch profile, classification of action potentials is needed to separate the neural activities of different fiber types. There is also room for improvement in the neural spike detection phase. Spikes detected using the simple thresholding method can also originate from noise and not from neural activity. Moreover, neural spikes with sub-threshold amplitudes are also missed. These issues are the topic of the next chapter of this report.

Chapter 4

Detection and Classification of Neural Action Potentials

4.1 Introduction

As we have seen in the previous chapter, the model of aggregate firing activity can be used to track muscle state only under the condition that the muscle stretch velocity is sufficiently low to have constant coefficients in the equation linking afferent nerve firing rate and muscle length. The ideal case would be to have a linear relationship for the whole range of motion of interest. Unfortunately, type Ia sensory fibers, that predominately encode information about the rate of change of muscle length, introduce a component in nerve response that makes the relationship non-linear and velocity-dependant.

The neuroelectric activity recorded with the tfLIFE is a mixture of signals from several adjacent neurons and noise. The experimental protocol in our animal experiments was designed in such a way to have activity from only afferent muscle spindle nerve fibers, these being type Ia and type II sensory nerve fibers. If this mixture could be decomposed into activities of these different sources, isolation of the activity of type II sensory fibers would allow for the developed model, described in the previous chapter, to be used to track muscle length variations with an a priori unknown stretch profile.

The topic of this chapter is a novel approach to neural spike detection and classification based on the continuous wavelet transform using complex wavelets. We aim at having an algorithm that would, when applied on the ENG signals recorded with the tfLIFE, have improved performance compared to the state of the art methods for real-time neural spike detection and classification, and that would be able to isolate afferent neural activity from muscle receptors having minimal dependence on muscle stretch velocity.

4.2 State of the Art in Neural Spike Sorting

Detection and classification of neural spikes are commonly referred to as spike sorting. The first step in spike sorting is the detection of neural action potentials, followed by the classification of the detected neural spike waveforms. The following is a brief overview of the state of the art in the field, with special emphasis on feasibility of using these methods with recording and interpretation of signals made using longitudinal intrafascicular electrodes in real-time conditions.

4.2.1 Neural Spike Detection

For many neurons, the most prominent feature of the action potential is its amplitude, or the height of the spike. One of the simplest ways to detect a neural spike is with a voltage threshold trigger. This method is by far the most common for measuring neural activity [Lewicki, 1998]. It is the method we used to process the data in section 3.3.2. The obvious advantage of threshold detection is that it requires minimal computing power for signal processing. It is also easy to implement with analog circuitry. The disadvantage is that it is not always possible to achieve acceptable isolation between nerve and noise spikes.

Until recently, other methods for spike detection have not been reported. In the last decade we have witnessed rapid progress in the field of neural prosthesis. Microprocessors with large computing power also became readily available, triggering a larger interest in the interpretation of multi-unit ENG using more sophisticated and power-hungry signal processing methods. In order to detect action potentials buried in noise and increase the ”contrast” between noise and neural spikes, a method using the discrete wavelet transform (DWT) for signal denoising was developed by Donoho [1995]. It involves thresholding of the detail coefficients in the wavelet decomposition. After denoising, spikes are detected by the simple voltage thresholding method. The procedure was applied on ENG signals by Diedrich et al. [2003] and recently on intraneural signals recorded using tfLIFE [Citi et al., 2008]. In both studies the Symlet 7 wavelet was used because of its similarity to the typical action potential waveform they found in their recordings. No quantitative analysis is given to justify the choice of wavelet, and the choice of denoising threshold was chosen empirically. In the latter study the authors applied the same method as in the former mentioned study, with the difference that in the latter the authors used ”cycle spinning”, a method developed by Coifman and Donoho [1995] to reduce the effects of DWT translation variance.

Signal detection can also be performed in wavelet space, without the need for reconstructing the signal using the inverse DWT. That way the required computing power is reduced, possibly an important issue if one eventually wants to have a real-time implemen-

tation of the algorithm. Only being interested in analysis and not synthesis also relaxes the constrains on wavelet choice, since not all wavelets are suitable for signal reconstruction. Kim and Kim [2003] have suggested using multi-scale wavelet analysis as an equivalent to multiple approximations of matched filters. Their method utilizes the point-wise product of wavelet transform coefficients over several selected scales. The detection method proposed does not require ”quantitative” a priori information on either the target signal or background noise, and only involves qualitative information that is common to the neural signal recordings, i.e. spike waveform shapes that are most common.

Unlike the discrete wavelet transform, the continuous wavelet transform (CWT) can operate at every scale, from that of the original signal up to some maximum scale that one determines by trading off the need for detailed analysis with available computational horsepower. The CWT is also continuous in terms of shifting. During computation, the analyzing wavelet is shifted smoothly over the full domain of the analyzed function. This eliminates the problem of translation variance when using the DWT. The stationary DWT and its equivalent methods reduce but not completely eliminate this problem [Misiti et al., 2007].

The complex wavelet transform is a complex-valued two-dimensional extension of the standard wavelet transform. It provides a suitable framework to incorporate two wavelets into one transformation, one wavelet being the real part, and the other the imaginary part of the transform. In a recent study it was demonstrated that using an approach based on the continuous complex wavelet transform for action potential detection in the auditory nerve outperforms a matched filter approach [Bourien et al., 2007].

4.2.2 Classification of Units

Neural action potentials from different neurons can be distinguished by their waveform shape in the recorded signals. These shapes depend on the neuron type, electrode construction and placement, and the tissue surrounding the electrode. Signal shapes from separate neurons can be quite similar, and high noise levels on weak nerve signals make rapid and accurate classification of spikes challenging.

If classification is to be used on-line in a closed-loop controlled FES system, it should be fast and require as little operator attention as possible. This limits the number of classification methods that can be used. In the following we give a brief overvies of the most common methods and compare their performance by looking at results reported by different authors. Performances of the different spike classification methods between different researchers are hard to compare because different data sets have been used by the various authors.

Fourier Transform

The method that shows the worst performance is based on using the Fourier Transform, as it produced the highest classification error rates. It involves computing a number of Fourier coefficients of a spike waveform and using these coefficients as features to discriminate between spikes. A number of studies report this method preforming the worst when compared to other methods [Schmidt, 1984]. A study using dual-channel intrafascicular electrodes had also shown that using the FFT is inferior to classification using time domain features [Goodall and Horch, 1992], confirming that the Fourier transform coefficients are obviously not good features for classification. As time features the authors used the minimum, the maximum, the peak-to-peak amplitude, and the rise and fall times of the action potential. A more appropriate signal basis should be used instead of the decomposition of the spike transients into a linear combination of pure sines.

Template Matching

Temporal shapes of spike waveforms can be compared to a reference template and classified into different classes based on their degree of similarity [Lewicki, 1998]. This approach is called template matching. The degree of similarity can be quantified either by computing the cross-correlation coefficient, either by computing the weighted mean square error of its samples, either by comparing amplitude histograms of waveforms samples, or by using some other distance metric. This method is also suitable for real-time applications, where the spike references are defined in a calibration phase and then subsequently used for on-line classification. Each detected spike is compared to all references and eventually classified. Then the reference for that class is updated to get a new reference.

Using a reduced feature set and not the whole spike waveform is also a possibility. Instead of using samples of the whole spike waveform, it is possible to simply use spike peak amplitudes as classification features. In cases where the noise level is not a critical issue, using this method could be sufficient for classification. In one study intrafascicular recording were made and units classified using 4 features: spike maximum, spike minimum, and timing of zero crossing in the waveform [Goodall and Horch, 1988]. In a later study by the same authors templates were constructed using the minimum, the maximum, the peak-to-peak amplitude, and the rise and fall times of the action potential [Goodall and Horch, 1992]. In their study, however, the authors only compare the performance of this method to the method using Fourier transform coefficients.

Principal Components Analysis

Using other feature sets is also possible: delay between peaks, deflection slopes, number of peaks, etc. However, choosing features based on an intuitive idea of what might be useful is an ad hoc approach and it often yields poor cluster separation. One method for choosing features automatically is with principal component analysis [Glaser and Marks, 1968], [Glaser, 1971]. The idea behind principal component analysis (PCA) is to find an ordered set of orthogonal basis vectors that capture the directions in the data of largest variation. The data are the original spikes from the recorded waveform. Real-time implementation of PCA is also possible using transversal filter structures [Schmidt, 1984]. To the best of our knowledge, there is are no results published about the use of PCA on intrafascicular ENG recordings.

Artificial Neural Networks

An artificial neural network (ANN) is a network of simple processing elements (neurons), which can exhibit complex global behavior, determined by the connections between the processing elements and element parameters. Its practical use comes with algorithms designed to alter the strength (weights) of the connections in the network to produce a desired signal flow. Using these algorithms the network is "trained" to recognize patterns which are presented at its input. After this training phase is finished, the network is ready to be used on-line to detect and classify these patterns.

McNaughton and Horch [1994] used this method for classification of spikes in recordings made with intrafascicular electrodes. They report that it was the best of all methods used in their study. Template matching came in second, and methods based on FFT and peak amplitude discrimination performed the worst. In another study the neural network approach managed to classify 6 out of a total of 10 units present in the signals. With more than 10 units present, the number of separable units dropped [Mirfakhraei and Horch, 1994]. In these studies a three-layer feedforward ANN was used.

The main drawbacks of using ANNs is that the results of classification are very sensitive to the data set used to train these networks, and obtaining a "good" training set is difficult, especially in the case with low SNR [Kim and Kim, 2003]. Moreover, there is no criteria for defining the appropriate structure nor size of the ANN. Many trials are necessary to obtain good results. At the end, whether acceptable results are obtained or not is uncertain and depends on luck.

Amplitude and shape of neural spikes change over time, due to electrode drift and fibrous encapsulation of the electrode recording sites (tissue reaction to implantation). Classifiers based on artificial neural networks would require tedious and supervised relearning

procedures which are conducted in laboratory conditions [Mirfakhraei and Horch, 1997]. This would not be very practical in real-life conditions.

4.2.3 Multiple Channels

Independent component analysis is a method that can improve source separation by taking advantage of multiple channels available. However, one restrictive assumption of this approach is that the minimum number of channels must equal the number of sources [Lewicki, 1998]. It will be shown later that the number of units picked up by one channel of the tfLIFE is greater than the number of available recording sites on the electrode.

Methods for source separation based on the relative difference between spike features recorded by different channels [McNaughton et al., 1983] are not applicable in the case of the tfLIFE either. Analysis of recorded multi-channel data recorded using tfLIFE show that the different channels need not pick up activity from the same units.

A common method for differentiating action potentials originating from different fiber type is the measurements of action potential conduction velocity. It is known that nerve fiber conduction velocity and the action potential generates is proportional to the square of fiber diameter [Burke, 1997]. In the case of muscle spindle nerve afferents, the diameters of the primary and secondary fibers is 12 and 6 μm, respectively [Boyd, 1962]. Many researchers have exploited this property to differentiate sensory fiber types using single-unit microelectrode recordings. Among others, Jansen and Matthews [1962], Renkin and Vallbo [1964], Matthews and Stein [1969b], and Poppele and Bowman [1970]. Unfortunately, since the tfLIFE electrode sites need not pick up activity from the same units, using this method is not an option for us.

4.3 Neural Spike Detection

The methodology for spike detection we develop is an expansion of idea of using complex wavelets, so it covers a range of temporal scales. As opposed to the matched filtering approach, where a priori information is necessary about action potential shapes, using the multi-scale complex wavelet approach provides multiple approximations of matched filters, which makes it a more generic approach and probably more robust when addressing the issue of changes in the spike waveforms. A training set of action potentials waveforms is therefore not necessary, which is an advantage of the wavelets approach over using artificial neural networks.

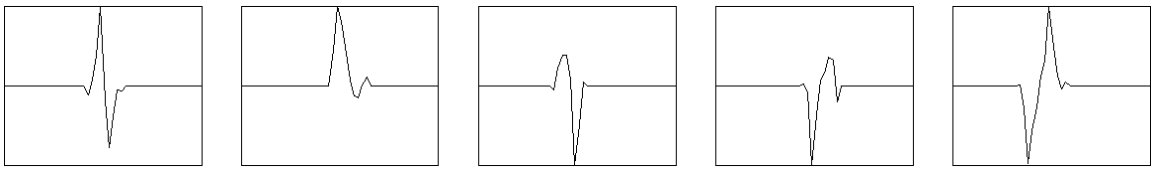

Figure 4.1: Waveforms of 5 distinctive spike shapes extracted from experimentally recorded data. The waveforms are normalized by the maximum value of the rectified waveforms. Length of each trace is 1 ms.

4.3.1 Choice of Complex Wavelet Family and Scale Factors

The following equation defines the wavelet transform:

$$W(\alpha,\tau) = \int_{-\infty}^{+\infty} x(t)\frac{1}{\sqrt{\alpha}}\Psi\left(\frac{t-\tau}{\alpha}\right)dt \tag{4.1}$$

where the real numbers α and τ denote scale and translation, respectively. The wavelet transform essentially performs a correlation analysis between the input signal $x(t)$ and the translated and dilated version of a reference signal called the mother wavelet $\Psi(t)$. Hence, it would be expected that the output would have local maxima where the input signal most closely resembles the analysis template, i.e., the wavelet function. Some wavelet basis functions are similar in shape to neural action potential. In addition, the basis function is dilated over a range of scales. If the scales are well chosen, the wavelet transform can act as a number of effective approximations of the matched filter, even though the exact action potential waveform are not known. In the case of complex wavelets the mother wavelet function $\Psi(t)$ is complex and the wavelet transform is also complex.

In order to find the optimal complex wavelet, around 30 action potentials with different waveforms were visually identified and extracted from the experimentally recorded for the modeling study (section 3.2). Five action potentials with distinctly different shapes are shown on Fig. 4.1.

The CWT was computed for all extracted waveforms using a series of complex wavelet families available in the Matlab wavelets toolbox. The computations were done using a range of scales to find the optimal scales, which produced the wavelet coefficient with the maximal magnitude. Optimal scales were selected to be the ones that produced at least one coefficient with a magnitude larger that 95% of the maximal CWT response among all scales. An example of time-scale representations of two action potentials with different shapes are shown on Fig. 4.2. In this example, the CWT was computed using the cgau1 wavelet using scales from 1 to 16. The top left plot shows coefficient magnitudes for the

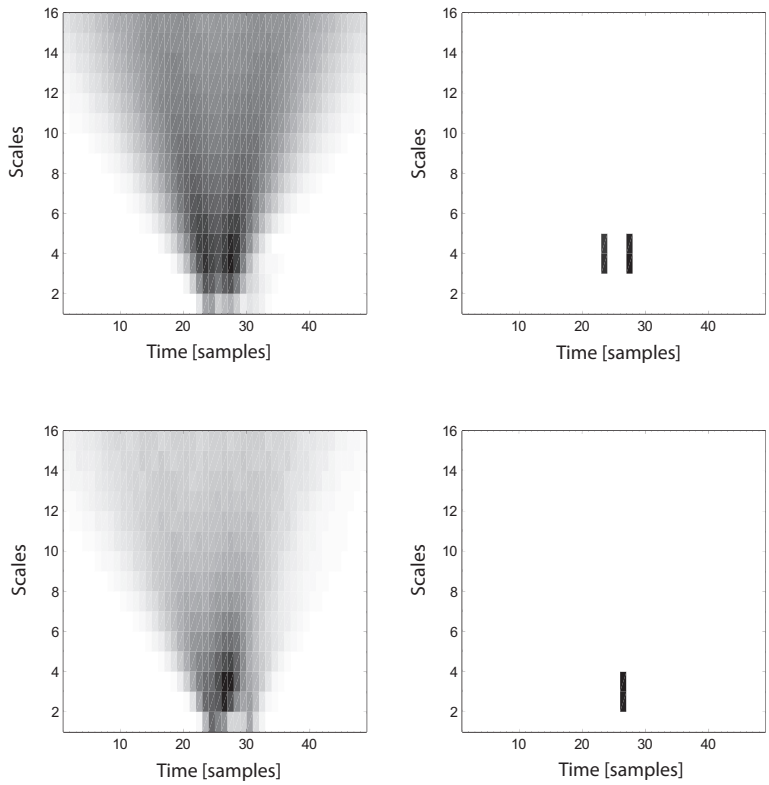

Figure 4.2: Top left: time-scale representation of one action potential waveform. Top right: the same plot but only showing wavelet coefficients larger than 95% of the maximal coefficient. Bottom: corresponding plots for another action potential with a different waveform. In both cases the CWT was computed using the cgau1 wavelet.

first action potential waveform. The top right plot is the same, but only showing the coefficients above the 95% threshold. The bottom left and right plots show the corresponding time-scale representations for another action potential, having a different shape.

The complex Gaussian family and the complex Morlet family of wavelets both produced well localized peaks in CWT space, i.e. peaks in CWT space appeared with a small or zero sample delay relative to the position of the peaks in the time time domain. In terms of the magnitude of the output coefficients, the complex Morlet family produced wavelet coefficients with a 50% lower magnitude compared to the complex Gaussian family. This was consistent for all extracted action potentials. With the complex Shannon family both the peak localization and the magnitude of the output coefficients were poor. Therefore,

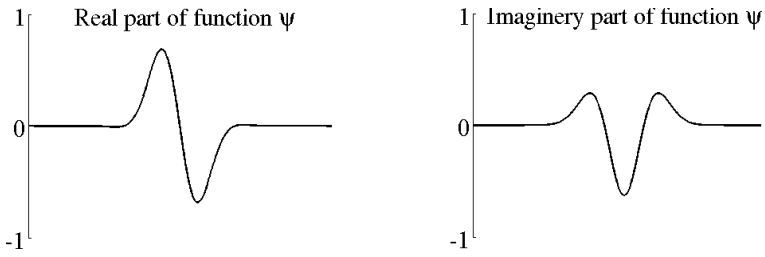

Figure 4.3: Real and imaginary parts of the ψ function for the cgau1 wavelet.

the complex Gaussian family of wavelet was the only one considered in the process of selecting the optimal wavelet to be used for spike detection, and the rest were discarded. The rabge of optimal scales for the cgau1 wavelet is from 1 to 6.

Within the complex Gaussian family, as a general rule, higher order wavelets produced wavelet coefficients with lower magnitudes, e.g. cgau1 produced a larger response than cgau2, cgau2 produced a larger response than cgau3 and so on. Consequently, the cgau1 wavelet was chosen as optimal for neural spike detection. The real part, imaginary part and modulus of the ψ function for the cgau1 wavelet are shown on Fig. 4.3.

For comparison, the above analysis was also performed using non-complex wavelets that support CWT, from which the db2 wavelet produced wavelet coefficients with maximal magnitudes. Compared to the cgau1 wavelet, the range of scales for the db2 wavelet was larger more than two times. Looking only at the inter-quartile range of the scale factors, the cgau1 wavelet requires 3 times less scale factors in order to cover all action potential waveforms (Fig. 4.7, right panel). This is important when later looking into the implementation of the algorithm. In the worst case, for the same number of scale factors, the cgau1 wavelet would require double processing time compared to using the db2 wavelet. As the number of scale factors for the db2 wavelet is more than double, it means that implementing the algorithm using the cgau1 wavelet would require less processing time.

Another benefit of having a smaller range for scale factors is the fact that it should result in better detector specificity. Using the analogy that low scale factors correspond to low frequencies in the signal spectrum and higher scale factors to higher frequency components in the signal spectrum, then a wider range of scale factors would correspond to a wider frequency bandwidth of the transforms and thus there would be more noise influence on detection performance. This will be shown to be correct later on in the report.

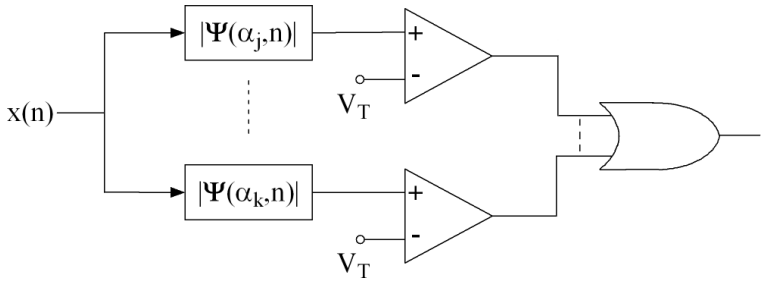

Figure 4.4: Block diagram of the proposed detection method. Wavelet coefficients for multiple scales are computed and their magnitudes compared to the a preset threshold V_T. If any of the values cross the threshold, an event is detected.

4.3.2 Algorithm Implementation

Prior to detection, signals are first band-pass filtered to remove noise and artifacts (filtering parameters are described in section 3.3.1). The detection algorithm consists of finding peaks in the signal transformed into wavelet space and searching for peaks crossing a preset threshold. Only the range of optimal scales, determined as explained earlier, are used in the computation of the multi-scale transform. In order to have the scales independent of length of the signal being processed, a windowed continuous wavelet transformed was implemented. The transform was computed using a 20 ms moving window. A block diagram of the proposed detection method is shown on Fig. 4.4

Implementing a matched filter to remove powerline noise in real-time is also a possibility. The algorithm needs to be robust enough to adapt to the changing parameters of the powerline noise. Not only does the amplitude of the harmonics change, due to multipath propagation, but so does the frequency [Olguín et al., 2005]. Fitting a sinewave of 50 Hz and a number of its harmonics on the raw data and subtracting the fit seems to give good results. Fitting and substraction of noise harmonics up until the 5th or 6th harmonic of the noise appears to be sufficient to remove slow baseline oscillations. Doing the fit on 20-ms windows (corresponding to 50 Hz) insures that the fitting algorithm locks onto the phase of the noise. This value is also suitable for real-time implementation since it is below the delay that can be tolerated in closed-loop FES control (see section 3.3.2). The sliding window length in the computation of the CWT was chosen to match this length.

Depending on the shape of an action potential, computation of its wavelet transform can result in multiple peaks from different scales to appear at different time instants – if more than one wavelet coefficient has a magnitude larger that a preset detection threshold, multiple detections of the same neural spike would occur. The effect of multiple peaks in wavelet space is illustrated on Fig. 4.2, where for one action potential the maxima are

localized at one sample (one vertical bar on the bottom right plot), while for the other waveform (top plots) the maxima appear in 2 clusters (2 vertical bars on top right plot). In the latter case there would be two events detected above the threshold for only one action potential. In order to avoid this, a refractory period[1] is introduced into the algorithm: when a spike is detected, another event can be registered only after the expiration of the preset time interval. Exploratory data analysis on all extracted action potentials showed that the scattering of these peaks is never larger than 146 μs (7 samples). Introducing the refractory period in the algorithm thus does not take into account any overlapping spikes (coming from different active units) that may occur during this period.

4.4 Classification of Action Potentials

It is important to note that our objective is not to classify all the action potentials to eventually have accurate information about single-unit activity, but rather to isolate activity from subsets of fibers that would be usable for closed-loop FES. In other words, we are interested in classes that would provide a linear relationship with muscle length and that would not change when varying the velocity of muscle motion.

In principle, there are two approaches when wavelets are used in pattern recognition problems. The first is to use one wavelet to represent all spike shape variations, and the other is to use different wavelets for each of the spike templates. In the former case one wavelet may not be sufficient if there is a large variation between the action potentials waveforms. This is very probable if a larger number of units are present in the recording. In the latter case, the best representation of different spike waveforms would be achieved by designing new wavelets for continuous wavelet transform. The procedure consists of approximating a given pattern using least squares optimization under constraints leading to an admissible wavelet. We have tried this on spike waveforms extracted from experimentally recorded ENG, and good fit could not be found for all waveforms because of the imposed constraints. Only certain biphasic action potentials produced good fits. Even if a set of wavelets could be found that represents all spike waveforms, the computational power required for real-time parallel computation of CWT coefficients and processing exceeds the available computing power available today. A compromise between the two approaches could be the representation of the full set of action potential waveforms by a reduced set of wavelets. For example, using two wavelets, i.e. using complex wavelets.

[1]Not to be confused with the nerve fiber refractory period. This refractory period implemented in the algorithm is a period during which any other peaks crossing the detector threshold will be ignored. In other words, it is the refractory period of the detector.

The multi-scale complex CWT has an advantage that it also offers a framework for classifying the detected neural spikes. Action potentials differ in their shape and amplitude and it was necessary to choose a feature set and a distance metric with which they would be distinguishable. Exploratory data analysis on the extracted neural spike waveforms indicated that the CWT coefficients computed using the same range of scale factors as in the detection algorithm could be suitable as classification features. Visual inspection of time-scale plots, like those shown on Fig. 4.2, indicate they are different for different spike waveforms. Classification could therefore be performed by creating feature vectors for the detected spikes and then clustering the data using the Euclidean distance metric. Feature vectors are created by concatenating rows of the time-scale plots for the real and imaginary part of the complex CWT transform. Each row consists of the CWT coefficients for a particular scale.

Being short transients (lasting no more than 1 ms) it is important to properly detect the onset of each detected spike. This problem is known as epoch detection. In order to compare spikes, the features vectors needed to be precisely aligned. In template matching methods spike presence is detected with thresholding and then a number of samples around that point are taken to form a spike waveform [Schmidt, 1984]. In our case, the time reference is the instant of the wavelet coefficient with the maximal magnitude.

In our context, there are two steps in the classification of detected action potentials. The first is the calibration phase, where the classification is performed off-line. The purpose of the calibration is to identify action potentials that encode relevant information for closed-loop control. In other words, we look for classes of action potentials having a linear relationship between firing rate and muscle length. Once they are identified, the second step of the classification is to recognize these particular action potentials on-line in order to estimate muscle state.

4.4.1 Calibration Procedure

One possible way for implementing the calibration is the following. Acquisition of ENG and ankle joint position are simultaneously recorded in initial signal acquisition. Action potentials are detected in the ENG and subsequently classified. One method for classifying the spike is the k-means algorithm. It is a method that is preferred over hierarchical classification methods when dealing with large data sets. The k-means method treats each wavelet signature as an object having a location in feature space. It finds a partition in which objects within each cluster are as close to each other as possible, and as far from objects in other clusters as possible. Each cluster in the partition is defined by its member objects and by its centroid, or center. The centroid for each cluster is the point to which

the sum of distances from all objects in that cluster is minimized. K-means uses an iterative algorithm that minimizes the sum of distances from each object to its cluster centroid, over all clusters. This algorithm moves objects between clusters until the sum cannot be decreased further. Like in other types of numerical minimization methods, the solution that k-means reaches often depends on the starting points. It is possible for k-means to reach a local minimum, where reassigning any one point to a new cluster would increase the total sum of point-to-centroid distances, but where a better solution does exist. In order to avoid local minima, clustering was repeated 50 times (replicates), each time using different starting points. Clustering using less replicates sometimes produced different clustering results using the same input, indicating the number of replicates was not sufficient for finding global minima in the optimization process. After the classification is complete, firing rates of each class are computed. Eventually, the linearity of the relationship between firing rates against muscle length is checked for each class.

One requirement for using k-means algorithm is to know in advance the total number of classes. In order to estimate the number of units each site of the tfLIFE picks up activity from, aggregate afferent firing rates of the post-processed ENG signals were computed by counting the number of peaks above threshold in a 1-ms moving time window with no overlap between adjacent iterations. This moving window duration matches approximately the absolute refractory period of mammalian sensory nerve fibers [von Brücke et al., 1941]. Since there cannot be two spikes originating from the same axon within this period, an estimation of the minimal number of axons can be made by counting the number of spikes in the window. Miscount can occur in cases where two or more spikes from different fibers overlap. This analysis was performed on the experimental data acquired for the modeling study, described previously (section 3.2.4). By extending the above analysis onto a number of periods of the faster sine wave, the probability of spike overlap becomes smaller, as it is unlikely that the same subset of spikes will overlap in each period at the same phase. In the analysis the highest unit count per bin that appeared at least in 3 out of 5 periods of the sine wave was taken as the estimation of the number of units.

Analysis performed on experimental data where the muscle was passively stretched, showed that the number of units being picked up by the recording electrode changes, depending on how much the muscle is stretched. The more the muscle is stretched, the more units are firing. Values in the Table 4.1 are estimates of the number of units at the time the muscle is maximally stretched. No significant differences in the numbers are found between the slower and faster sine wave data. The difference in most cases is zero or one unit. On the other hand there is a large variation when comparing between rabbits and in some cases even between different channels of one electrode. Statistically, the median number of units picked up at maximal stretch is 8, with a standard deviation of 2.7. To account for the

Table 4.1: Estimates of the number of units from which the electrode picks up activity at the point when the muscle is maximally stretched. Results are shown for each channel for both sine frequencies and for all 10 experiments.

	10 mHz sine stretch				250 mHz sine stretch			
Rabbit	Ch1	Ch2	Ch3	Ch4	Ch1	Ch2	Ch3	Ch4
1	10	9	10	8	9	9	9	6
2	13	13	10	12	12	12	9	12
3	7	8	6	6	7	7	6	7
4	7	8	5	6	7	7	4	6
5	15	15	5	3	14	14	4	3
6	8	9	8	8	7	7	8	8
7	6	4	7	10	6	3	6	8
8	5	11	8	12	6	10	10	11
9	11	9	8	8	10	9	8	8
10	9	7	7	9	8	8	7	9

changing number of classes, the total number of classes for off-line k-means clustering was set to 10, allowing the algorithm to create empty classes in order to produce best results in the optimization process.

4.4.2 On-Line Clustering

Real-time operation is not evaluated in our study. We focus only on the feasibility of finding linear classes using the wavelet-based spike sorting algorithm described in the calibration step. Nevertheless, we give here a few pointers for future realization of real-time classification.

All classes demonstrating a linear relationship are suitable to be used in the on-line clustering for estimating muscle length. Real-time operation requires a different implementation of the classification. Information about cluster centroids from the calibration step are used here as initial values for the classifier. Each new detected spike during real-time operation would be assigned to one of these initial classes, and the cluster centroid for that class updated, taking into account the signature of the new class member. The updating insures the algorithm can adapt to any slow changes in the shape of action potentials, resulting either from electrode drift or fibrous encapsulation of the electrode recording sites. Eventually, not all classes need to be used. Only classes relevant for feedback purposes are

tracked.

To give an idea of the computational requirements, off-line computation of complex wavelet coefficients at 16 scales using the cgau1 wavelet took approximately 4 seconds for 100 ms of data (update time in closed-loop control, see section 3.3.2). The computation was done using MATLAB on a desktop PC equipped with a Pentium 4 CPU running at 2.4 GHz and with 2 GB of RAM. It is expected that the processing time would be reduced approximatelly ten-fold when the algorithm is implemented using a low-level programming language, and even more if implemented using an application-specific intergrated circuit (ASIC). Therefore, it is expected that real-time implementation is possible.

4.5 Generating Synthetic ENG Data

In order to be able to evaluate the performance of the spike sorting algorithm, knowledge of the exact timing and class of each action potential in the ENG signal is needed. Because of uncertainty about this information in experimental data, artificial signals based upon recorded action potentials were synthesized.

Around 30 action potentials with different waveforms were visually identified and extracted from the experimental data recorded for the modeling study (section 3.2). From the set of extracted waveforms, 5 action potentials with distinctly different shapes were chosen to represent 5 neural spikes originating from different axons, i.e. different spike classes. These are shown on Fig. 4.1. The waveforms were normalized and used to synthesize spike trains.

Spike train firing rates were randomly chosen from within the range found in literature [Matthews and Stein, 1969a]. With the exception of burst firing, muscle spindle afferents can fire with a rate up to about 75 Hz. Burst mode firing was excluded because the amplitude of an action potential firing in burst mode can vary often as much as 50% [McNaughton et al., 1983]. This variation is due to shifts in membrane conductances during the relative refractive period of the neuron cell [Snider and Bonds, 1998] and it is only present in initial movement in primary spindle response [Proske and Gregory, 1977].

Spike amplitudes were scaled by integer values ranging from 3 to 6 standard deviations of the background noise level, which corresponds to the range of values found by visually inspecting the data recorded using tfLIFE. These 4 scaling factors represented different SNR levels for which the analysis was performed. Therefore, the SNR is defined here as the ratio of the peak amplitude of the noise-free action potential and the standard deviation of background noise. Signals were synthesized by adding the spike trains onto experimentally recorded background noise.

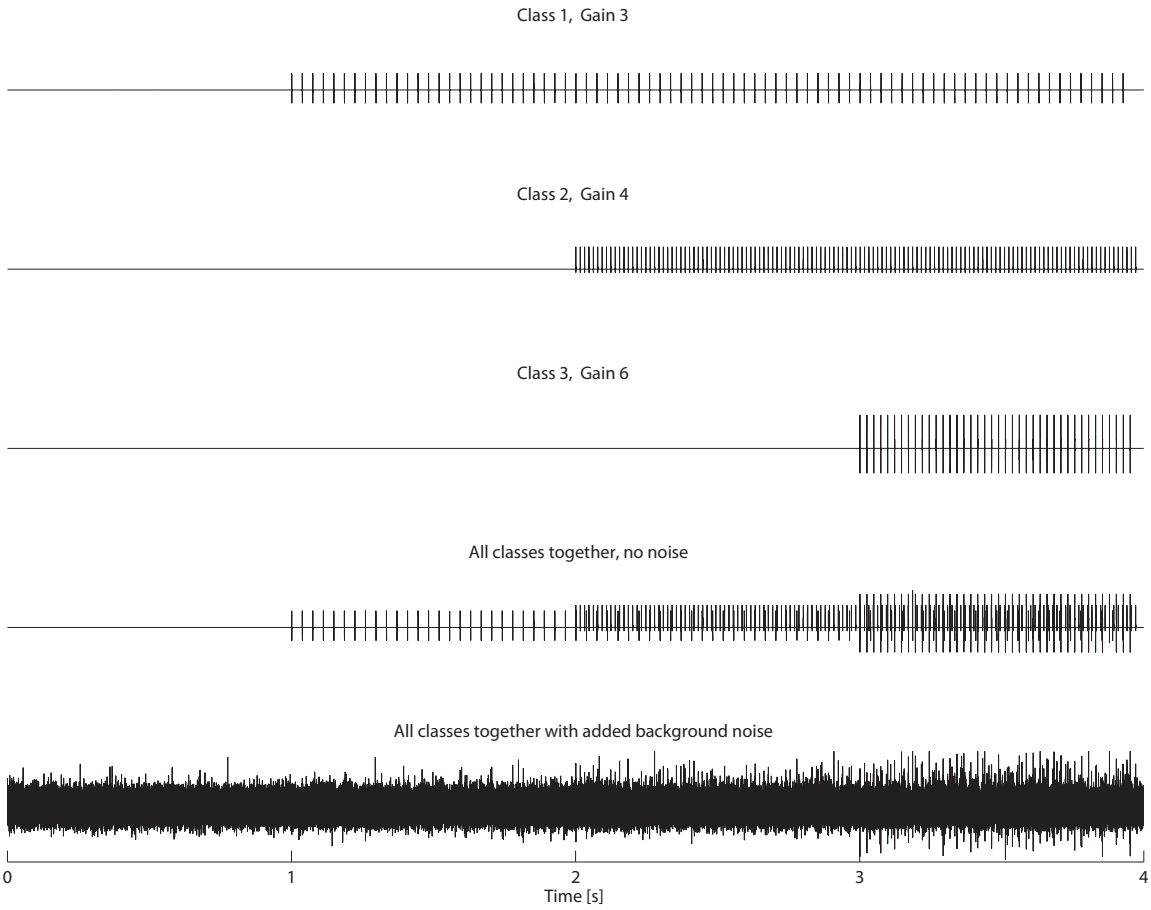

Figure 4.5: Steps in the creation of a synthetic signal with up to 3 units firing. Top 3 traces are the generated action potential trains for the 3 units. The onset of the first spike train is at $t = 1$ ms, the second train at $t = 2$ ms, and so on. The fourth trace is the superposition of traces 1-3. Eventually, background noise is added to the noise-free signal, resulting in a signal shown on the bottom trace.

Signals with up to 10 units firing simultaneously were synthesized. Spikes having the same waveform and amplitude were considered to be from the same axon (belonging to the same class). A total of 900 signals were generated: 100 signals with 2 units active, another 100 with 3 units, and so on until having 100 signals with 10 units firing simultaneously. Steps in the creation of one synthetic signal with up to 3 units active are shown on Fig. 4.5.

4.6 Results

Wavelet-based detection performance on the synthetic signals is compared to the amplitude thresholding method, being the most common used today. Detection is evaluated on a range of thresholds, starting from background noise level up to the maximal magnitude found in the transformed signal.

Classification performance is evaluated on both the synthetic ENG by comparing the wavelet-based classification to methods based on template matching and principle components analysis. These two methods, used as references in the comparison, are the most commonly used because of their relative simplicity which enables fast, real-time implementation.

Performances of the wavelet-based detector and the detector using simple amplitude thresholding are shown on Fig. 4.6 in the form of a receiver operations characteristics, or ROC curves. These curves are graphical representations of detector sensitivity vs specificity using a range of detection thresholds. On the whole range of SNR levels the wavelet-based detector outperforms the detector based on amplitude thresholding, i.e. for any given specificity, the corresponding sensitivity is greater for the wavelet-based detector. The performance gap becomes especially prominent with low SNR.

Compared to detection using the non-complex db2 wavelet, detection using the cgau1 wavelet shows better specificity in ROC space (Fig. 4.7, left). This is most probably due to the wider range of wavelet transform scale factors required for the db2 wavelet (Fig. 4.7, right). A wider scales range translates into a wider frequency bandwidth, as explained earlier. For the cgau1 wavelet the scales range was from 1 to 6, and for the db2 wavelet it was from 2 to 14.

Classification results are shown in the form of classification error rates which are ratios of the number of misclassified spikes to the total number of spikes being classified. The wavelet-based classification is compared to two other methods of classification: principal components analysis (PCA) and template matching. Results are shown on Fig. 4.8 starting from the case when only two different spike classes are present in the signal up to the case where 10 units are simultaneously firing. Classification based on template matching produced the highest classification error rates, while wavelet- and PCA-based approaches showed similar results.

The spike sorting technique was eventually applied on experimentally recorded muscle spindle afferent nerve activity. Only flexion periods of ankle joint motion (stretch periods of the MG muscle) were analyzed.

The detection threshold was chosen to be seven times the standard deviations of the background noise level (in wavelet space). Throughout all the trials, this threshold value

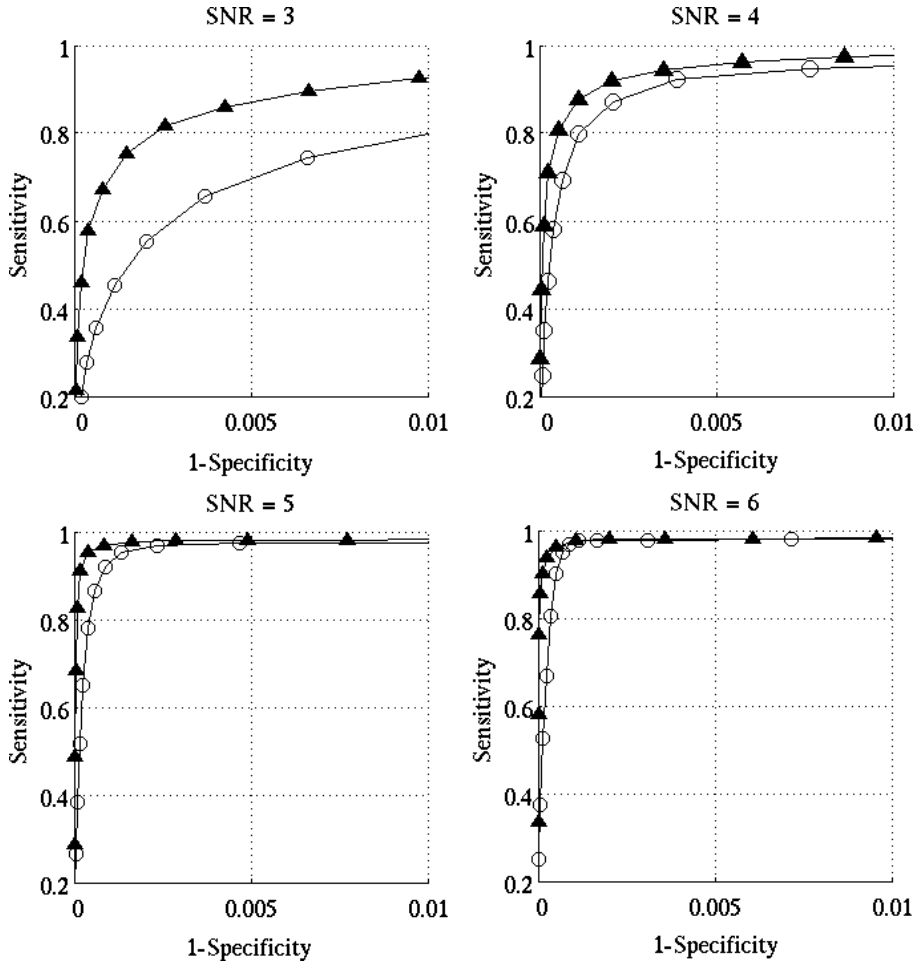

Figure 4.6: ROC curves for four SNR levels defined by the ratio of the peak amplitude of the noise-free action potentials to the standard deviation of background noise. Performances of a simple threshold detector (empty-circle line) and the wavelet-based detector (full-triangle line) are compared.

corresponded to the point on the ROC curves where the specificity starts to rapidly deteriorate while at the same time there is little improvement in sensitivity.

The detected units were classified into 10 clusters. This matches approximately the number of units being picked up by one recording site of the tfLIFE when the muscle is maximally stretched. The analysis was performed on data from all all rabbits. Results from the clustering shows that up to 2 or 3 spike classes per rabbit show a linear relationship between their computed neural firing rate and instantaneous muscle length. Since this relationship is not linear when using the aggregate afferent firing rate, the result is an indication

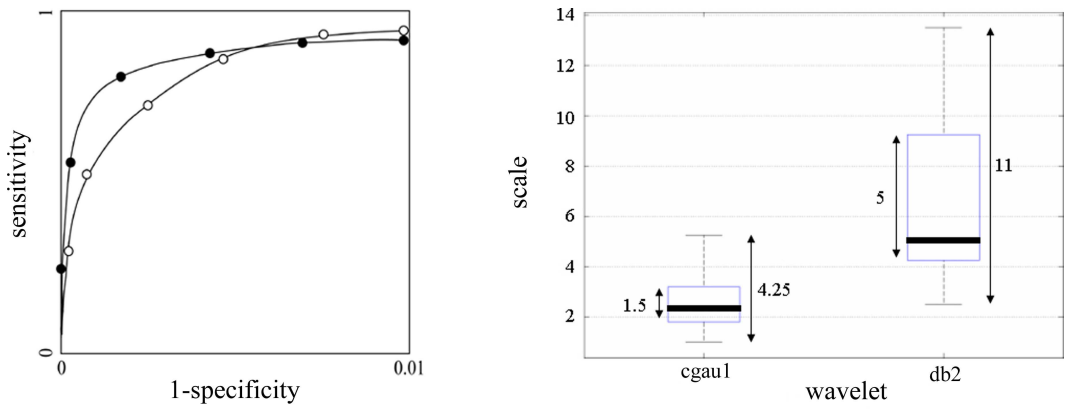

Figure 4.7: Range of detection scale factors required for the cgau1 and db2 wavelets. The increment between successive scales used was 0.25. The cgau1 wavelet has a range of optimal scales that is more than two times smaller compared to the db2 wavelet.

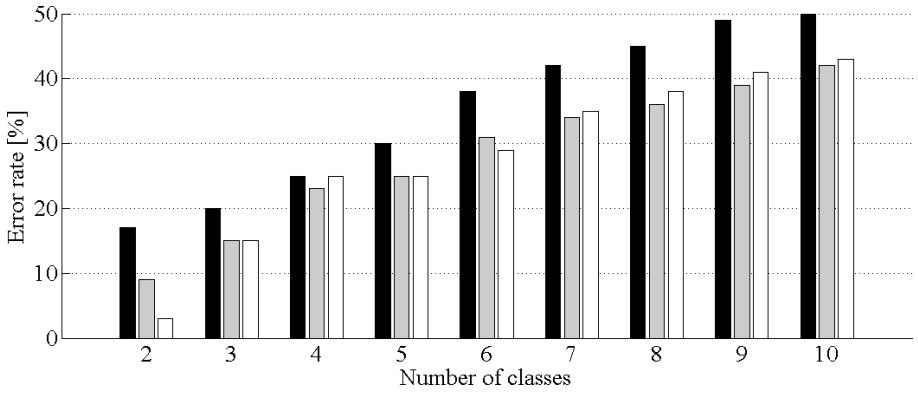

Figure 4.8: Classification error rates depending on the number of units simultaneously active. Groups of three bars represent the different classification approaches: template matching (black), principal components analysis (gray), and wavelet-based (white).

that the algorithm is capable of isolating activity of units less sensitive to muscle stretch velocity. Results from one rabbit are shown on Fig. 4.9. The left plot shows the relationship between the aggregate firing rate of all detected spikes. The relationship is clearly not linear in the region where the muscle stretch velocity slows down rapidly (region where normalized muscle length is close to 1). The right plot shows the same relationship, but this time using only the activity of the fibers insensitive to the velocity of muscle stretch. A linear regression analysis performed on both shows that the fit on the right plot is better.

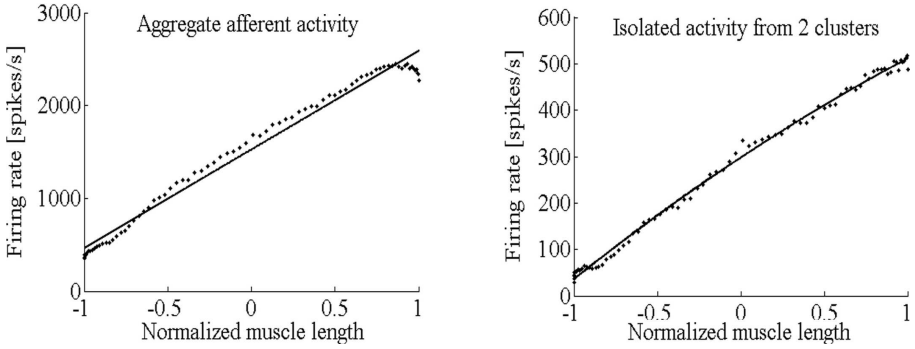

Figure 4.9: Afferent neural firing rate vs muscle length. The left plot shows the aggregate activity of all detected spikes. On the right, only activity from 2 clusters, having a good linear fit to the data, are used to compute the firing rate. Linear regression analysis was performed on both (full lines). On both plots muscle length was normalized by 4 mm.

4.7 Discussion

Results show that the continuous wavelet transform using complex wavelets is the preferred method for neural spike detection. Even though wavelet-based classification does not show improvement in error rates compared to the PCA-based algorithm, the advantage of using the wavelet-based approach is in the fact it is it provides a unique framework for both spike detection and classification, i.e. after computing the complex wavelet coefficients in the detection phase, no additional computation is required in the subsequent classification phase.

4.7.1 Cluster Centroid Comparison for Different Stretch Rates

It would be of interest to compare activities of the same units for the slow and fast muscle stretch rates in order to see if there is a change in their velocity sensitivity. However, it is difficult to identify same units in the 2 stretching conditions. Even if units have a similar shape, it is not a guarantee they are in fact from the same motor unit. As we have seen from the extracted waveforms from the experimental data, there are fewer distinctive shapes than there are units in a recording. Nevertheless, a comparison of cluster centroids from the 2 data sets can be done. In order to be able to graphically present cluster inter-distance, PCA was used to reduce the dimensionality of the time-scale signatures of cluster centroids. A comparison between cluster centroids for the slower and faster stretch rate for one rabbit are shown on Fig. 4.10, using the first two principal components. Full circles are cluster centroids from the slow muscle stretch and the empty triangles are from the faster stretch

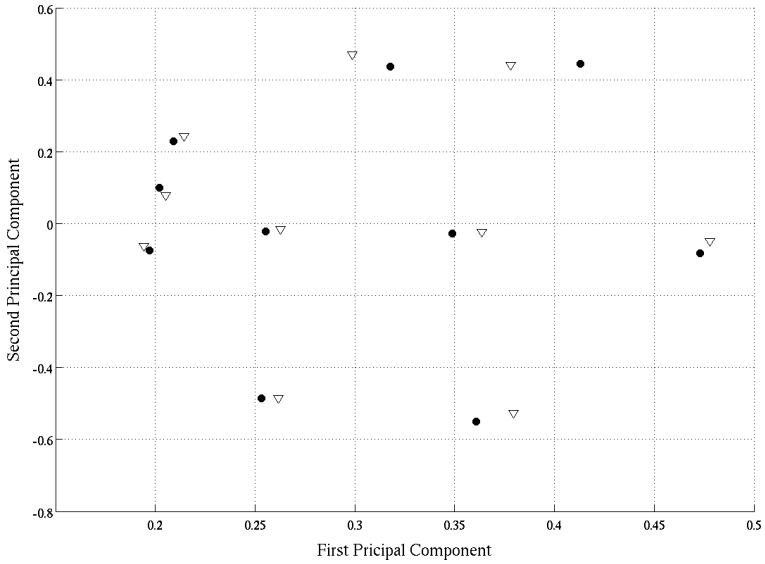

Figure 4.10: Comparison of cluster centroids for the slow (full circles) and fast (triangles) muscle stretch rates.

rate. Pairs of centroids are easily identifiable, which is a strong indication that they in fact represent the same units (or group of units having a similar shape).

All action potential classes obtained when sorting neural activity from slow muscle motion exhibit linear or very close to linear relationships between firing rate and length. On the other hand, when the same muscle is stretched with at a faster speed, a number of classes obtained from those faster stretches show obvious non-linear behavior and the rest remain linear. Under the assumption that the classes from the two cases contain action potentials from the same fibers (Fig. 4.10), one could conclude that the same class show different behaviour at different motion speeds. However, there is not enough evidence to conclude that the units that keep their linear behavior during the faster stretch rate are velocity insensitive. Even the 250 Hz muscle stretching is a very slow rate. If a definite conclusion is to be made, the behavior of there units need to be studied using faster stretch rates.

4.7.2 Aggregate Compared to Single-Cluster Activity

A difference between the aggregate firing rate and the individual class firing rates is evident. The aggregate firing rate has non-linearities where most of the units are being recruited or saturate. Single-class activity shows these distinctive onsets and saturation points. A few distinctive cases encountered in clustered data are shown on Fig. 4.11.

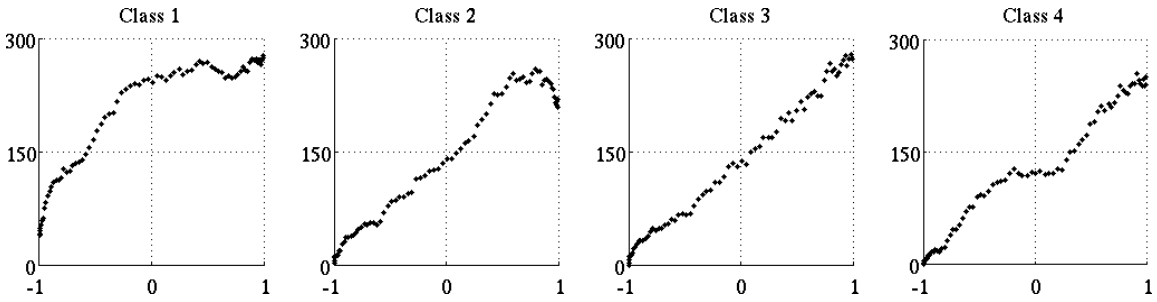

Figure 4.11: Typical profiles of firing rates vs muscle length for single clusters. On each plot the abscissa is the normalized muscle length and the ordinate is the firing rate in spikes per second.

Class 1 shows the typical behavior of a class with a low activation threshold and saturation point before the maximal muscle extension. Activity is registered even at the minimal muscle extension and saturation occurs even before the half of the muscle extension range.

The second class illustrates the difference between saturation and velocity sensitivity. Instead of maintaining a constant firing rate after saturation, with further increase in muscle length the rate starts dropping at the maximal extension, where the velocity of the stretch slows down rapidly.

The third plot is an example of a class with a linear firing rate throughout the whole range of motion. These are class behaviors we are interested in.

The fourth plot is an example of one class containing 2 units with similar shapes. The first unit starts firing with a low length threshold and quickly saturates. As the muscle is stretched further, the threshold of activation of another units is reached and it fires until maximal muscle extension. These classes can also be useful for control purposes as the activity can be modeled as a piece-wise linear function.

4.7.3 Application in Closed-Loop FES

Results show that the spike sorting algorithm could be useful in closed-loop FES systems with proprioceptive feedback from natural sensors, e.g. muscle spindles. The spike sorting scheme seems to be capable of isolating the activity of secondary sensory endings from the aggregate neural activity of muscle spindle afferents, making it possible to establish a linear relationship between muscle length and neural firing rate. This result is a step towards an on-line model-based estimator of muscle length. The more linear classes are found, the more robust the estimation of muscle state will eventually be.

The off-line calibration using sine stretch profiles, as performed in this study, can also

be done using other stretch profiles, as long as they cover the whole range of muscle motion to be tracked on-line. The criteria for finding the classes of interest is the linearity of the relationship between class firing rate and muscle length. One quantitavive criterium could be a threshold for the fit error in the linear regression analysis. Only classes having a fit error under the threshold would be selected for subsequent on-line estimation of muscle state. Whatever the stretch profile used, only the periods of increasing neural firing should be taken into account in order to avoid periods of nerve fiber adaptation, as explained earlier (first paragraph of section 3.5.2).

One of the biggest obstacles in both detecting and classifying neural spikes proves to be the low SNR of the ENG recordings. In parallel to working on the improvement of signal processing methods to minimize the effects of noise, novel recording techniques could also be used to improve signal quality [Djilas et al., 2007]. It is expected that, when signals are acquired using such techniques, the overall performance of the spike sorting algorithm should improve.

4.8 Summary

The continuous complex wavelet transform offers a convenient framework for both detection and classification of action potentials using intrafascicular electrodes. The neural spike detection outperforms the simple threshold detection, especially with signals with low SNR.

Results of classification of units into classes based on action potential waveform signatures in wavelet space indicate that the classifier is able to isolate activity having linear relationship with muscle length. This is a step towards an on-line model-based estimator of muscle length that can be used in a closed-loop FES system with natural sensory feedback.

In the case of wavelets, and all other methods for spike sorting for that matter, the major limiting factor is not in any of the processing methods, but in the recording selectivity and the signal-to-noise level in the multi-unit ENG. One way that could help improve the performance of spike sorting is to try to the improve the quality of the signal in the acquisition step of the data, even before any processing takes place. One such method, involving shielding of the implant site, will be the topic of the next chapter of this report.

Chapter 5

Improving SNR in Longitudinal Intraneural Recordings

5.1 Introduction

In FES systems simultaneous stimulation and recording are a necessity. The neural interface is located in the proximity of the neuromuscular structures of interest, leading to problems with relatively large levels of artifacts. The muscle and stimulus artifacts in tfLIFE recordings arise from the extra-neural potential gradient that drops longitudinally along the nerve. The level of muscle artifact limits the maximal gain that can be set in signal acquisition, which in turn limits the maximal signal-to-noise ratio (SNR) in the recordings. Stimulation artifact additionally corrupts the recorded signals. As we have seen in the previous chapter, the low SNR is a major issue when it comes to detecting and classifying neural action potentials. If the signal-to-noise level can be improved, the spike sorting performance would also improve.

Observations during previous work suggested that packing the implant site with carbon fiber [Yoshida and Horch, 1996] or wrapping the implant site in a small conductive wrap of metalized Teflon thin film [Yoshida et al., 1998] minimizes stimulation and EMG artifact pick-up. The conductive shield makes the extra-neural space around the implant site equipotential, which leads to the reduction of extraneural noise in the recorded signals (Fig. 5.1). On the other hand, the conductive shield also reduces ENG signal level. A possible explanation is that the conductive material of the shield provides a low-resistive pathway for the axon membrane ionic currents that generate the action potential, resulting in a lower voltage drop between the measuring electrodes. Moreover, the metallic foil can also touch the exposed indifferent site on the recording electrode, resulting in large artifacts

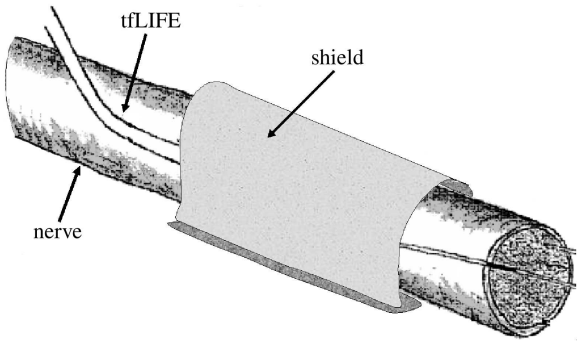

Figure 5.1: Illustration of a shield wrapped around a recording electrode implant site. If made of conductive material, the shield helps reduce stimulation artifact, but also reduces the level of ENG in the recordings.

in the recorded signal. An improvement in SNR can possibly be achieved by modifying the shield structure.

We have conducted a study with the objective to test the hypothesis that a double-layer shield improves SNR in ENG recording made using longitudinal intra-neural electrodes. Methodology for experimentally validating this hypothesis is the topic of this chapter of the report.

5.2 Shielding the Implant Site with a Double Layer

Our hypothesis was that placing a dielectric layer between the nerve and the conductive foil would prevent both the shunting effect of the action potential currents and the conductive foil touching the recording sites of the electrode. A pilot study has been conducted to experimentally evaluate this hypothesis. Instead of fabricating a double-layer foil, which would have a dielectric surface on one side and a conductive surface on the other, we opted for an ordinary cuff electrode. When placed around the nerve over the tfLIFE recording sites, with the cuff leads left unconnected, the cuff electrode should effectively act as an insulating shield. Assuming the volume inside the cuff is homogeneous and of constant resistivity, and the cuff electrode diameter is much smaller than its length, the insulating cylindrical body of the cuff electrode can be considered to linearise the external fields inside the cuff [Struijk and Thomsen, 1995]. An illustration of the field distribution inside the cuff electrode, generated by an extra-neural source, is shown on Fig. 5.2, on the right. When its its leads are left unconnected, the field distribution is as shown by the full line (OC). With its leads shorted, the field gradient becomes smaller, illustrated by the dashed line (SC).

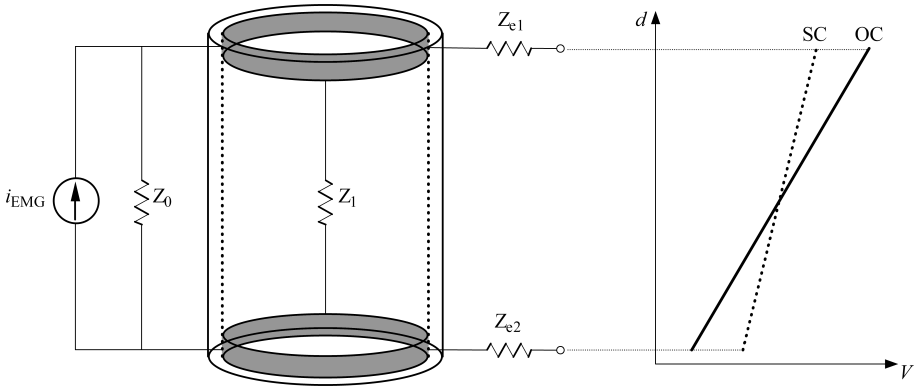

Figure 5.2: Effect of external field linearization due to the insulating cuff wall (full line OC). Shortening the outer cuff rings equalizes their potential and reduces the gradient of the artifact field distribution inside the cuff (dashed line SC). The abscissa is the electrical potential and the ordinate is the distance along the cuff.

Recording sites positioned longitudinally inside the cuff electrode should therefore register a smaller electrical potential difference in a differential recording scheme. The reduction of the slope of the artifact field distribution inside the cuff electrode when the cuff rings are connected, compared to the case when the electrode leads are left unconnected is explained in the following text.

5.2.1 Artifact Field Gradient Inside the Shield

The equivalent circuit of the recording scheme is shown on Fig. 5.2, on the left. $Z_{e1,2}$ are electrode-tissue impedances, Z_0 is the tissue impedance outside the cuff, Z_1 is the tissue impedance inside the cuff, and i_{EMG} models the artifact source. In the case the cuff leads are left unconnected, the current flowing through the tissue inside the cuff $i_{1(OC)}$ can be expressed by the following equation:

$$i_{1(OC)} = \frac{Z_0}{Z_0 + Z_1} \cdot i_{EMG} \tag{5.1}$$

Let Z_e be the equivalent series resistance of Z_{e1} and Z_{e2}. When the cuff leads are shorted, the current flowing through the tissue inside the cuff $i_{1(SC)}$ can be calculated as follows:

$$
\begin{aligned}
i_{1(SC)} &= \frac{Z_0 Z_e}{Z_0 Z_e + Z_1 Z_e + Z_0 Z_1} \cdot i_{EMG} \\
i_{1(SC)} &= \frac{Z_0}{Z_0 + Z_1} \cdot \frac{Z_e}{Z_e + \dfrac{Z_0 Z_1}{Z_0 + Z_1}} \cdot i_{EMG} \\
i_{1(SC)} &= \frac{Z_e}{Z_e + \dfrac{Z_0 Z_1}{Z_0 + Z_1}} \cdot i_{1(OC)}
\end{aligned}
$$

Assuming that Z_0 is much smaller than Z_1, the following approximation is obtained:

$$
i_{1(SC)} = \frac{1}{1 + \dfrac{Z_0}{Ze}} \cdot i_{1(OC)} \tag{5.2}
$$

Coefficients linking the currents on the left and right side of equations 5.1 and 5.2 determine the slopes of the field gradients on Fig 5.2. From equation 5.2 we see that the current flowing through the tissue inside the cuff should never be larger with the cuff leads shorted compared to the case when the leads are left unconnected. When the leads are shorted a part of the total artifact current i_{EMG} is shunted through the cuff rings and prevented to flow through the tissue inside the cuff. The percentage of the current that is shunted depends on the electrode-tissue impedance Z_e. In the theoretical case where it is zero, no current flows though the tissue inside the electrode and the field inside the cuff electrode on Fig. 5.2 is flat. On the other hand, if the impedance is large, compared to $Z_0||Z_1$, then i_1 is determined only by the equivalent parallel impedance of Z_0 and Z_1, in which case there is no difference between $i_{1(OC)}$ and $i_{1(SC)}$.

5.2.2 Experimental Evaluation

Additional experiments needed to be run in order to experimentally evaluate the effect of shielding on the levels of recorded ENG and on the levels of stimulation and EMG artifact. Acute animal experiments were conducted on 5 anesthetized New Zealand white rabbits. Animal preparation was similar to that used in the modeling and spike sorting studies (section 3.2.1), except for the differences described in the following text. The motorized lever system in this study was used merely to insure the muscle length remains constant throughout the experiment. Muscle stretching was not required. The implanted tfLIFE was used to record compound nerve action potential response to electrical stimulation. The sciatic nerve was not crushed, as single-unit activity was of no interest to us in this study. Stimulation and recording were conducted using the same equipment and setup as in the modeling

study, except for the fact that here the simulation trigger was also also recorded on one additional channel on the digital tape recorder. It was used later in data analysis for trigger averaging the nerve twitch response.

Nerve activity was elicited by electrical stimulation delivered through a bipolar circumferential cuff electrode implanted around the tibial nerve. In further text this electrode will be referred to as the *stimulation cuff*. The resulting ENG, EMG, and stimulus artifacts were recorded through the 4 channels of the tfLIFE. Another bipolar cuff electrode was used as the shield. In further text this electrode will be referred to as the *shielding cuff*. Both cuff electrodes were 10 mm long with a 2 mm inner diameter. Measurements consisted of recording the neural response to electrical stimulation using pulse trains (pulse duration 100 μs and pulse repetition frequency 1 Hz). With increasing stimulation intensity the number of activated motor units increases leading to an increase in recorded nerve and muscle response. The recruitment curve was experimentally obtained by starting with stimulation intensities below nerve threshold and increasing the stimulation intensity in increments until there was no more change in the response (maximal neural response and maximal EMG artifact). The motor unit recruitment curve from one experiment is shown on Fig. 5.3. It can be seen that with stimulation below threshold (normalized intensity 0.2 in this example) there is no nerve response. The nerve response then appears and grows with increasing stimulation intensity until it reaches saturation (at normalized stimulation intensity 0.5). At this point all motor units are recruited and there is no effect of any further increase in stimulation intensity.

Four shielding configurations were tested:

1. no shield (baseline recording);
2. conductive shield only (aluminum foil wrapped around the LIFE implant site);
3. open-circuit shielding cuff (shielding cuff electrode placed around the LIFE implant site with its leads left unconnected);
4. short-circuited shielding cuff (shielding cuff electrode placed around the LIFE implant site with the leads from the end rings shorted).

After the signals for the first configuration were recorded, the metallic foil was carefully placed around the nerve. Care was taken not to move the recording electrode or injure the nerve. The same goes for the case when the metallic foil was removed and the shielding cuff subsequently implanted around the tfLIFE. Between the two configurations with the shielding cuff no animal handling was necessary since the electrode leads were left outside the animal which enabled their easy connection.

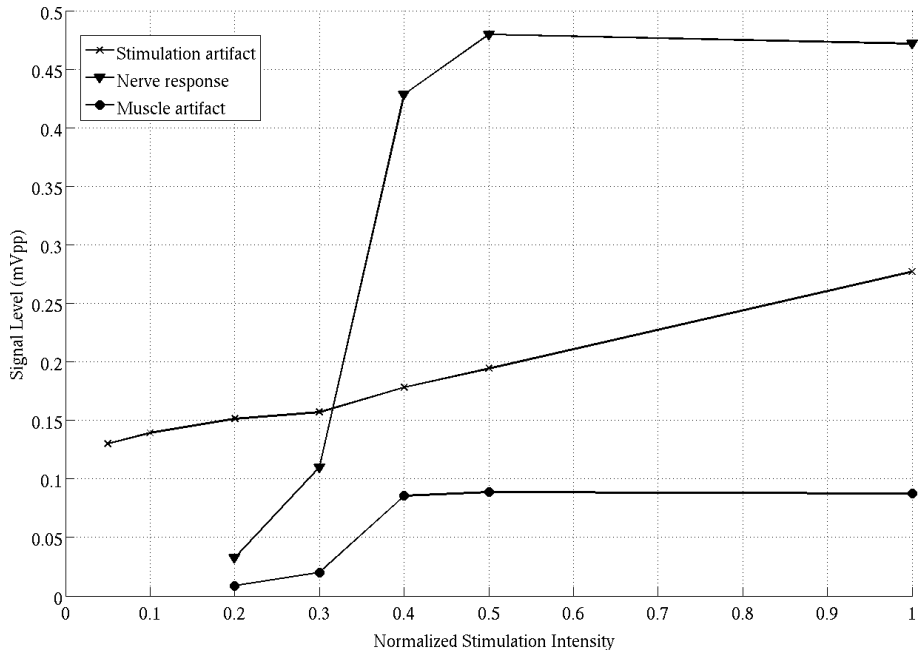

Figure 5.3: Levels of stimulation artifact, nerve response and muscle artifact from one experiment. The stimulation artifact increase linearly with stimulation intensity. Nerve and muscle response becomes visible above the activation threshold 0.2. After all motor units are recruited at stimulus intensity 0.5, there is no further increase and nerve and muscle response. Values on the abscissa are normalized by the maximal intensity used.

Minimal electrode movement can result in moving one or more recording sites completely outside the target fascicle. Even if an electrode slips only slightly, remaining in the fascicle of interest, the recording sites may pick up activity from a completely different subset of units within the same fascicle. Moreover, there is a possibility of the tfLIFE being displaced during electrical stimulation, due to mechanical forces produced by the contracting muscles. In all cases where there was evidence of electrode movement, recorded data were excluded from the analysis. Even with precautions taken, in two rabbits we could not register a nerve response to electrical stimulation, but stimulation and muscle artifact were still present in these rabbits. Eventually, artifact data from all recordings was processed from all 5 rabbits, while ENG data only from 3 rabbits was available.

5.2.3 Nerve and Artifact Signal Components

Electronic noise was removed by stimulation triggered averaging. Duration of recordings for each incrementing step of the stimulation intensity was 30 seconds. This provided a

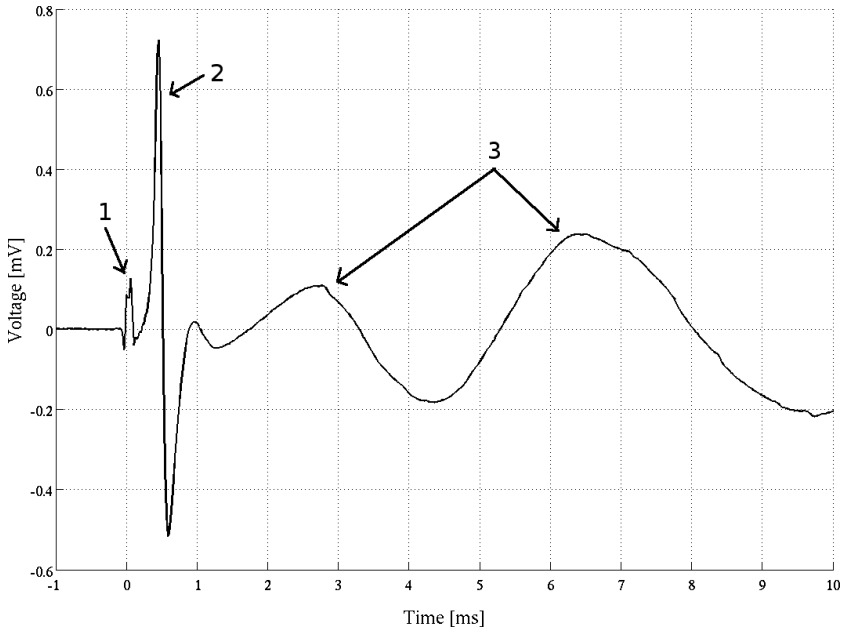

Figure 5.4: Trigger-averaged response to electrical stimulation with twitches. Three distinctive components can be identified, appearing one after another: 1) stimulation artifact, synchronous with stimulus pulse, activity from 0 to about 100 μs; 2) compound nerve action potential, the biphasic waveform just after the stimulus artifact; and 3) muscle artifact, activity starting from around 1 ms post stimulus until the end of the trace.

sufficient number of one-second bins to be used in the averaging. Three signal components can be distinguished on the averaged traces: the stimulus artifact appears first, immediately followed by the compound action potential, and eventually the EMG artifact appears (Fig. 5.4).

Levels of each signal component in the twitch response were quantified in the following way. The level of the stimulation artifact was taken to be the peak-to-peak amplitude of the averaged signal in a time range from the beginning of the stimulation pulse (t=0) until approximately 200 μs post stimulus. The estimate of the nerve response component was the peak-to-peak amplitude of the averaged trace approximately between 0.2 ms and 1 ms. Finally, the EMG artifact level was the peak-to-peak amplitude of the averaged trace starting approximately from 1 ms post stimulus until the response settled back to baseline. Time intervals were visually identified and manually selected for each rabbit because of the slight variability between experiments – nerve and muscle artifacts had different onsets because of the different distances between the stimulating and recording electrodes in each preparation. Signal component levels as a function of stimulation intensity from one

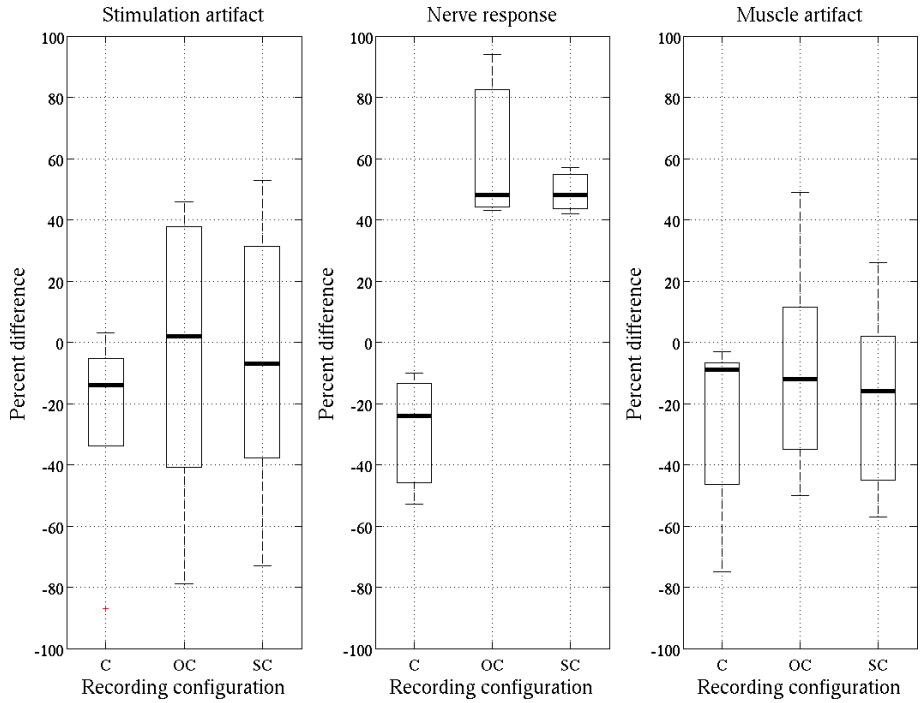

Figure 5.5: Percent differences for the 3 recording configurations: C – conductive foil wrapped around the implant site, OC – cuff electrode around the implant site with its leads left unconnected, and OS – cuff electrode around tfLIFE implant site with its end rings shorted. The box plots show levels for stimulus artifact (left), neural response (center) and EMG artifact (right), relative to the case where no shielding is used.

experiment is shown on Fig. 5.3.

5.3 Results

The shielding strategies (no shielding, conductive shield, open-circuit shielding cuff, and shorted shielding cuff) were compared in terms of three parameters: level of nerve response, level of stimulus artifact, and level of EMG artifact. The results in form of statistical box plots are shown in Fig. 5.5. Each box has lines at the lower quartile, median (thick horizontal line), and upper quartile values. Whiskers extend from each end of the box to the adjacent values in the data. Outliers are displayed with a + sign. The results compare shielding performances using data from all rabbits (3 rabbits for ENG data, and 5 for artifacts data).

The recording configuration with no shielding was the reference in the evaluation of the

Table 5.1: Percent differences of nerve signal levels for the 3 recording configurations: C – conductive foil wrapped around the implant site, OC – cuff electrode around the implant site with its leads left unconnected, and OS – cuff electrode around tfLIFE implant site with its end rings shorted. Values in bold text are medians.

	Rabbit 1	Rabbit 2	Rabbit 3	Mean	Std
C	-10	**-24**	-53	-29	22
OC	94	43	**48**	62	28
SC	57	42	**48**	49	8

three cases where shields were used, i.e. neural and artifact levels from the recordings with different shields were compared relatively to the levels from the recording with no shield.

Results for the levels of neural response are summed in Table 5.1. Recording with the open cuff shield produced the highest ENG levels. Compared to the no shielding case, the ENG level was higher in the worst case by 43% and in the best case by 94%. Using the shorted shielding cuff gave slightly lower ENG levels than with the open shielding cuff. In the worst case the improvement was by 42% and in the best case by 57%. Using the conductive shield reduced the ENG level for all three rabbits, in the worst case by 53% and in the best case by 10%.

Results for stimulation artifact levels are summed in Table 5.2. The results for shielding configurations with cuffs (OC and SC) compared between rabbits show no trend when compared between rabbits. In 2 rabbits there is a reduction in artifact, in another 2 there is an increase in artifact. When compared between the two shielding configurations for the same rabbit, the results are the same for the OC and SC configurations. In the case of the recording configuration with the conductive shield there is a trend of decrease in stimulation artifact, the average drop being 24%.

Results for EMG artifact levels are summed in Table 5.3. For all rabbits the conductive shield decreased muscle artifact. Results for the cuff shields are mixed as in the case with stimulus artifact, but to a lesser extent. A drop in EMG artifact is present in 4 rabbits (in 3 the drop is above 10%) and in one case an increase of artifact level is registered. As in the case with both stimulus artifact and ENG signal level, no significant difference is observed between the OC and CS recording configurations.

Table 5.2: Percent differences of stimulus artifact levels for the 3 recording configurations: C – conductive foil wrapped around the implant site, OC – cuff electrode around the implant site with its leads left unconnected, and OS – cuff electrode around tfLIFE implant site with its end rings shorted. Values in bold text are medians.

	Rabbit 1	Rabbit 2	Rabbit 3	Rabbit 4	Rabbit 5	Mean	Std
C	-87	-16	3	-8	**-14**	-24	36
OC	-79	35	46	**2**	-28	-5	51
SC	-73	24	53	**-7**	-26	-6	48

Table 5.3: Percent differences of muscle artifact levels for the 3 recording configurations: C – conductive foil wrapped around the implant site, OC – cuff electrode around the implant site with its leads left unconnected, and OS – cuff electrode around tfLIFE implant site with its end rings shorted. Values in bold text are medians.

	Rabbit 1	Rabbit 2	Rabbit 3	Rabbit 4	Rabbit 5	Mean	Std
C	-3	-37	-75	**-9**	-8	-26	30
OC	49	-30	-50	**-12**	-1	-9	37
SC	26	-41	-57	**-16**	-6	-19	32

5.4 Discussion

The conductive shield (Aluminum foil) around the nerve reduced both the ENG levels and artifacts, most probably due to the shunting effect described earlier. These observations confirm the results from previous work by Yoshida and Horch [1996] and Yoshida et al. [1998]. We will focus our discussion here on the effect of shielding using cuff electrodes.

5.4.1 Increased Neural Signal Level with an Insulating Shield

As predicted, an insulating shield between the nerve and a conductive shield prevented the shunting effect of the action potential ionic currents. Not only has it not reduced the ENG level in the recordings, but increased it, in all three rabbits (Table 5.1). One possible explanation is that this is due to the fact that the ionic currents were confounded in a smaller extra-cellular volume around the nerve, producing a larger voltage drop along the increased resistance of its path.

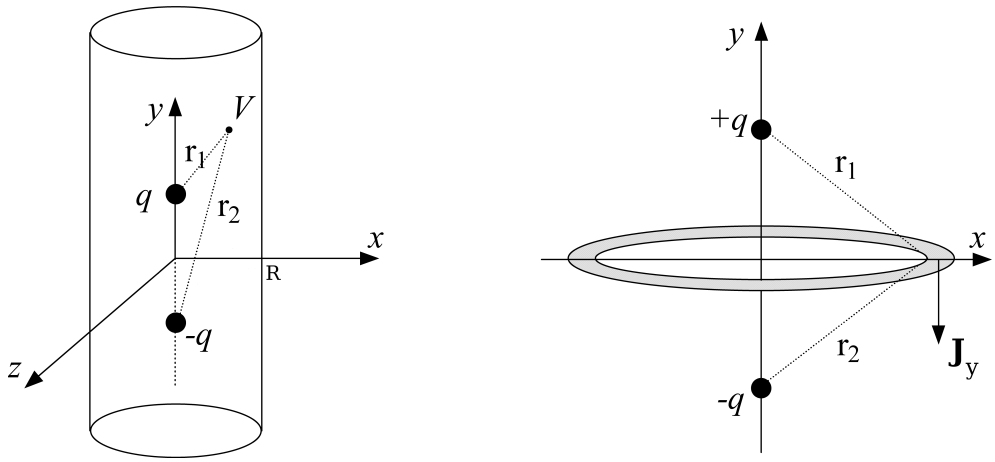

Figure 5.6: On the left, an illustration of a electric dipole inside a cuff electrode. The cuff electrode is the cylinder. The dipole is placed concentrically with the y-axis, inside the cylinder. On the right, integration of the electric field J_y over the transverse plane x0z produces the current intensity through the plane. The shaded area is the infinitesimal surface dS of the integration domain.

This phenomenon can be explained using an electric dipole as a model of a neural action potential generator. Each pole of the dipole carries the same electrical charge q, but of opposite polarity. The distance between the poles is the dipole length d. The dipole is placed inside the cuff electrode which is modeled as an infinitely long cylindrical body with specific conductivity σ, permittivity ε, and radius R. The surface of the cylinder bounds the current from the dipole inside the volume of the cylinder (Fig. 5.6). The potential V at any point in space created by the dipole is given by:

$$V = \frac{q}{4\pi\varepsilon r_1} + \frac{-q}{4\pi\varepsilon r_2} = \frac{q}{4\pi\varepsilon}\left(\frac{1}{r_1} - \frac{1}{r_2}\right) \tag{5.3}$$

where r_1 and r_2 are the distances from point with coordinates (x,y,z) to each of the electric charges:

$$r_1 = \sqrt{x^2 + (y - d/2)^2 + z^2} \tag{5.4}$$

$$r_2 = \sqrt{x^2 + (y + d/2)^2 + z^2} \tag{5.5}$$

where d is the distance between the two opposite electric charges of the dipole. Since the dipole is used as a model of the generator of the nerve action potential, the distance d is the spacing between the nodes of Ranvier of the axon generating the action potential. The

components of the electric field E_x, E_y and E_z are equal to the components of the negative gradient of the potential V:

$$E_x = -\frac{dV}{dx} = -\frac{qx}{4\pi\varepsilon}\left(\frac{1}{r_1^3} - \frac{1}{r_2^3}\right) \tag{5.6}$$

$$E_y = -\frac{dV}{dy} = -\frac{q}{4\pi\varepsilon}\left(\frac{y-d/2}{r_1^3} - \frac{y+d/2}{r_2^3}\right) \tag{5.7}$$

$$E_z = -\frac{dV}{dz} = -\frac{qz}{4\pi\varepsilon}\left(\frac{1}{r_1^3} - \frac{1}{r_2^3}\right) \tag{5.8}$$

In our particular case we are interested in calculating the current I flowing through the transverse cross-section of the cuff electrode. Therefore, only the y-axis component of the electrical field vector is of interest. Knowing that the current density J_y is proportional to the electric field E_y, we can obtain the current intensity I. To simplify calculus we will calculate the current through the cross section at $y = 0$:

$$I = \int_S J_y\, dS = \sigma \int_S E_y dS \tag{5.9}$$

$$I = -\frac{q\sigma}{2\pi\varepsilon} \int_S \frac{(d/2)dS}{(x^2 + (d/2)^2)^{3/2}} \tag{5.10}$$

$$I = -\frac{q\sigma}{\varepsilon} \int_0^R \frac{(d/2)x\,dx}{(x^2 + (d/2)^2)^{3/2}} \tag{5.11}$$

where $dS = 2\pi x dx$ is the infinitesimal surface of the integration domain S, and R is inner radius of the cuff electrode (see illustration on the right on Fig. 5.6). Solving the upper integral leads to the following equation for the total current flowing through the transverse section of the cuff electrode at $y = 0$:

$$I = \frac{q\sigma}{\varepsilon}\left(1 - \frac{d/2}{\sqrt{R^2 + (d/2)^2}}\right) \tag{5.12}$$

If we let $R \to \infty$, which is the case when there is no boundary around the dipole, the fraction in the above equation becomes zero. The ratio between currents for $R = 1$ mm (radius of our cuff electrode in experiments) and for $R \to \infty$ gives us the effective increase in resistance between the cases with and without the isolating cylindrical shield around the dipole, respectively. The graph on Fig. 5.7 shows the dependency of this ratio on the spacing between the nodes of Ranvier.

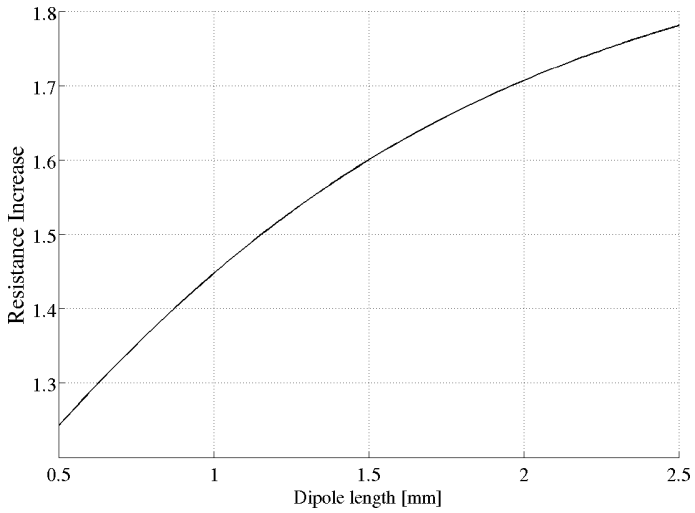

Figure 5.7: Resistance increase when the cuff electrode is put around the dipole.

From the experimental data in Table 5.1 we see that the median increase in resistance of medium would be around 50%. The corresponding resistance increase in that case is 1.5, estimating the dipole length to be a just a little over 1 mm. This value matches very well with the spacing between the nodes of Ranvier for real axons. The literature reports that the spacing between the nodes are between 1 and 2 mm [Kandel et al., 2000]. The presented model can therefore be used to explain the phenomenon that results in a larger ENG level pickup when putting the cuff electrode around the recording electrode implant site.

The same shielding cuff electrode was used in all experiments. In some preparations it fitted around the nerve better and in other preparations the nerve diameter was smaller and the cuff didn't provide a good fit around the nerve, leaving the electrode loose. Using a shielding cuff electrode with a diameter that would provide a better fit to the nerve would have probably resulted in a smaller standard deviation of results between rabbits.

5.4.2 Electrode-Tissue Impedance and Level of Muscle Artifact

An interesting observation in the case of EMG is that where is no significant difference between the OC and SC recording configurations, indicating that the impedance Z_e was much higher compared to the impedance Z_0 (see Fig. 5.2). Nevertheless, some shunting of the artifact current can be noticed in all rabbits, since the artifact is always lower for the SC configuration. Percent differences of the peak-to-peak amplitudes of artifact for the SC and OC recording configurations are shown in Fig. 5.8 in the form of statistical box plots.

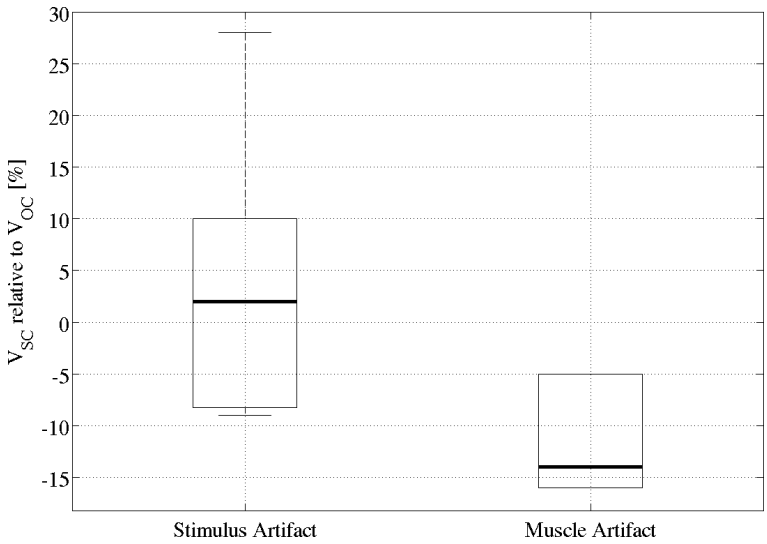

Figure 5.8: Percent difference of peak-to-peak amplitudes of the artifact signal components between the SC and OC recording configurations.

Triantis et al. [2003] report that the typical values for $Z_{e1,2}$ are 1 kΩ, for Z_0 it is 200 Ω, and for Z_1 it is 5 kΩ. Substituting these values in equation 5.2, we get a reduction of 10% in artifact level when the cuff rings are shorted. This values correlates well with the experimental results for both stimulus and muscle artifact. Only in the case of the first rabbit the stimulus artifact is greater for the OC compared to SC case. The value of +28% here suggests this is an outlier, as it is clearly not in the order of magnitude of the other data. One also has to note that the authors in the above study did not report at which frequency were the above values measured impedance. It was most probably for the frequency band between 1 and 2 kHz, matching the spectral components of interest when analyzing the ENG. For lower frequencies (EMG signal spectral peak power is around 250 Hz), the impedance magnitudes are probably even higher.

To reach any final conclusion about effect of shielding on the different signal components additional experiments need to be carried out. Results presented here can only be considered preliminary, as this is still an ongoing study. Assuming that the electrode-tissue impedance between the cuff rings and their surrounding tissue plays a crucial role is the effectiveness of artifact reduction, the standard cuff electrode can be modified so that its metallic rings are made wider. This way the contact area between the electrode and tissue would be increased, leading to a reduction in contact impedance. An illustration of the modified cuff is shown on Fig. 5.9. On top is a standard cuff with its rings of width L', and below is the modified cuff with its cuff rings made wider, $L'' > L'$. Fabrication of the

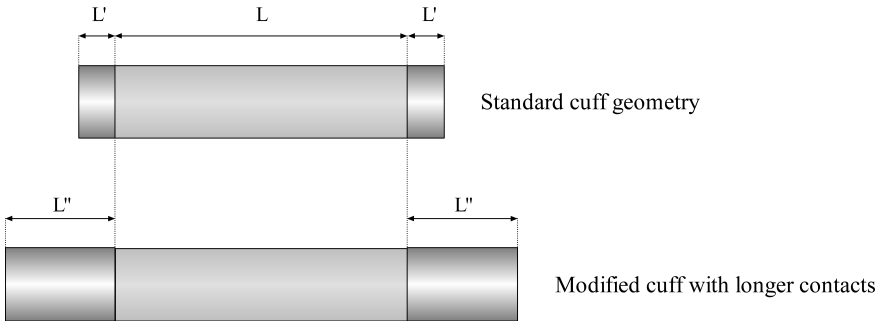

Figure 5.9: The cuff electrode on the top has the standard geometry. Typical electrode length, including the metallic contact widths is around 10 mm, with each ring having a width up to 1 mm (shown to scale). The bottom electrode has increased contact ring width to provide lower electrode-tissue impedance.

modified cuff would not be any more complex compared to making a standard cuff. The same fabrication procedure, described in section 3.2.2, can be used to make a cuff electrode with wider rings.

5.5 Summary

In the study presented in this chapter we looked into the possibility of shielding the implant site of a recording LIFE electrode as a means to improve the signal-to-noise ratio in our recordings with the tfLIFE. A cuff electrode was used for this purpose. Three shields were compared to the case where no shielding was used: 1) conductive shield, 2) open circuit shielding cuff and 3) shorted shielding cuff electrode. They were compared in terms of their effect on the levels of nerve response, stimulation artifact and EMG artifact.

Preliminary results show that the conductive shield placed around the recording site reduces the recorded ENG signal level. A cuff electrode placed around the tfLIFE implantation site increases the recorded ENG levels in both the case where the cuff leads are left unconnected and in the case where the leads are shorted. One possible explanation is that the boost in ENG signal is a result of an increase in resistance of the path along which the ionic currents, generating the nerve action potential, are flowing. The increase can be predicted by a simple model using an electric dipole as the source of axonal membrane currents. The amount of increase predicted by the model correlates well with the experimental data.

A conductive foil placed around the tfLIFE implant site decreased both the stimulus and muscle artifact levels in the recorded signals. In all experiments but one, the two cuff

shielding configurations helped reduce the muscle artifact pickup. An equivalent circuit model of the artifact source and its interaction with the electode and surrounding tissues predicted a 10% difference between the open and shorted cuff shielding configurations, which is in agreement with the experimental data. For stimulus artifact, results show no trend. This is still an ongoing study and more experiments are needed to draw definite conclusions.

Chapter 6

Conclusion and Final Remarks

6.1 Conclusion

There are several outcomes from the work on this thesis. Firstly, the new tfLIFE was experimentally tested and it appears to be usable as a neural interface for recording muscle receptors activity from afferent sensory fibers. Secondly, the developed model of muscle spindle neural response to passive muscle stretch, in combination with the developed spike sorting algorithm, provides a basis for an on-line estimator of muscle state in a closed-loop FES system, where the estimator would feed back to the controller the information about the length of the muscle in which the spindles reside in. We have also shown that using multiple channels of ENG, now available with the tfLIFE, provides a more robust estimation of muscle length compared to estimation based on a single channel of ENG.

The novel neural spike detection scheme, based on the multi-scale continuous wavelet transform using complex wavelets shows better performance compared to the classical detection based on thresholding; the novel method for classification based on spike signatures in wavelet space performs equally well as the best state of the art methods, but, unlike other methods, requires no additional computation time because it uses data obtained directly from the detection step of the algorithm. Classification of muscle receptor action potentials manages to produce classes having firing rates that are less dependant on muscle motion velocity compared to the aggregate firing of all fibers, which provides a larger range of muscle motion in which the developed model could be used as a basis for a future on-line estimator of muscle state in a closed-loop FES system.

Finally, the novel shielding technique, where a cuff electrode is placed around the tfLIFE implant site, shows improvement of the signal-to-noise level in recordings made using intraneural longitudinally placed electrodes. Using this shielding technique in signal acquisition would therefore also result in the overall improvement of a model-based muscle

state estimator, since the performance of the spike sorting algorithm depends on the level of SNR in the recordings.

6.2 Remaining Challenges

The next logical step, following this study, is to design, implement and experimentally validate an on-line estimator of muscle state. It would be designed on the basis of the model defined is chapter 3 using only clusters of data obtained using the methods presented in chapter 4. It is expected that using the shielding technique, presented in chapter 5 would improve the performance of the system. Eventually, the estimator is to be integrated inside a closed-loop control system. Work on the model on which the estimator would be based will also complement the muscle model that is currently being developed in the DEMAR laboratory [Makssoud et al., 2004], [Guiraud et al., 2008].

6.2.1 Reflex Regulation of Muscle Spindle Sensitivity

In real situations, however, the neural activity recorded with the tfLIFE is not purely afferent sensory activity from muscle spindles. Muscle spindles also have descending neural pathways that regulate the sensitivity of these sensors. In this thesis we have focused on de-efferented animal preparations, where the sciatic nerve was crushed proximal to the implant site and where there was only afferent nerve activity present in the recordings. It was a starting point for the experimental validation of the new LIFE and for exploring the possibilities of interpreting the recording with the electrode. It is now a question whether or not the developed spike sorting scheme would be able to differentiate the accenting from the descending nerve activity. This is also the case with SCI, where spinal reflex pathways are still present.

Once the spike sorting algorithm is able to separate afferent from efferent information flow, further work on the model should be directed toward modeling the effect of gamma motor neuron activity on afferent nerve response. Only then the FES system based on the methodology developed would be applicable in real-life situations. The developed model can be used as a starting point in further studies. It has been shown by Jansen and Matthews [1962] that the difference in firing rate vs length response of secondary ending, before and after removing reflex control of spindle sensitivity, is only a shift in the curve, i.e. its shape remains the same. On the other hand, the firing rate of the primary endings also increase with the drive intact, but its not a simple shift, the curve also changes shape. Moreover, the change of shape was different between different primary fibers. This behavior, also taking into account the known differences in distinctive patterns of static and dynamic gamma

fibers [Taylor et al., 2000], could be the exploited in the identification of different sources in the signal decomposition. Work on these issues requires modifying the experimental protocol to include intact instead of de-efferented animal preparations. The approach we propose could lead to a solution to monitor reflexes and maybe control spasticity which remains an issue in some patients.

6.2.2 Muscle Fatigue

Another topic of interest is muscle fatigue. With artificial electrical stimulation, muscle fibers are not recruited in a natural way [Gandevia et al., 1995]. In natural control of movement small muscle fibers are activated first and larger fibers are activated with increased contraction intensity. Moreover, with high contraction levels, not all muscle fibers are active at one time; while a subset of muscle fibers within a muscle is contracting, the rest are inactive and resting. During prolonged contraction, sets of muscle fibers switch on and off asynchronously, producing a smooth whole muscle contraction.

During artificial electrical stimulation the order of recruitment of muscle fibers is reversed and always the same, contrary to natural recruitment. Large fibers are activated first. More importantly, during high stimulation levels, all muscle fibers are recruited and the muscle fatigues more quickly compared to the case were the muscles are activated by the central nervous system. The problem is even more pronounced in the muscles below the injury level in paraplegic individuals who will utilize FES systems, who's muscles atrophy due to disuse.

It is presently largely unknown what is the effect of fatigue of afferent muscle spindle nerve activity. If there is any affect, it would be of great importance to be able to decode information about the level of muscle fatigue in a FES system. With the developed spike sorting algorithm it is possible to investigate the effects of fatigue on individual classes and not only on the aggregate neural firing. However, to investigate the effect of fatigue of different sensory fiber types requires precise knowledge of the type of sensory fibers. As explained earlier, there is not sufficient evidence that the classes obtained with the spike sorting algorithm truly correspond to different fibers. A proved method for accurately classifying fiber types is by the used of microelectrode recordings from individual fibers and classification by fiber conduction velocity, such as in studies during the 1960s by Jansen and Matthews [1962], Renkin and Vallbo [1964], Matthews and Stein [1969b], Poppele and Bowman [1970] and others. In either case, experimental evaluation would require designing specific experimental protocols.

Another way to monitor the level of muscle fatigue is tracking shifts in the power spectrum of the electrical activity of the muscle fibers [Gandevia et al., 1995], i.e. by recording

the electromyogram (EMG) of the muscle using an EMG electrode. This would, of course, require using an additional electode and an EMG signal processing unit in the FES system.

6.3 Perspectives

Eventually, when the technology advances sufficiently to allow for the separation of activities from different sensory modalities, such as activity from skin stretch receptors, one can envisage implanting more distally to the muscle. Activity from these natural sensors could also be useful for feedback in FES, since they also play a part in the sensing of limb position in the CNS, called cutaneous proprioception [Kandel et al., 2000]. Moreover, recording of afferent activity from these and other sensors in awake and moving animals is unavoidable. Therefore, separation of these sources is a necessity if a FES system is to be useful in practice.

The experimental work during animal experiments had revealed some issues regarding the fixation of the LIFE connector close to the implantation site. In acute experiments it is sufficient to suture the connector to any surrounding tissue, or simply letting it lie loose during the experiment. However, for chronic preparation, the electrode contact must be firmly fixed. One solution for this problem would be the redesign of the connector in form of a cuff electrode. This way the electrode could be easily fixed onto the peripheral nerve and it would at the same time allow for having the shielding structure around the LIFE active sites. This could also reduce electrode migration and slippage during movement. Furthermore, the area on the shield could be used to host amplification electronic circuitry. The active electronics could receive power by connecting it to a nearly implanted device, such as the BION, a microstimulator device that has already been evaluated in clinical trials [Baker et al., 2005]. When in recording mode this device could acquire ENG from the LIFE; and when in stimulation mode it could act as an electronic stimulator. That way the LIFE would act as a bidirectional neural interface.

The knowledge acquired from monitoring muscle receptor responses could be integrated into the muscle model developed by DEMAR [Makssoud et al., 2004], [Guiraud et al., 2008], together with the information one could obtain about muscle fatigue and reflexes.

Chapter 7

Resumé en Français

7.1 Introduction

Les fuseaux neuro-musculaires sont de petits récepteurs sensoriels encapsulés qui se présentent sous une forme apparentée à un fuseau ou fusiforme. Leur principale fonction consiste à signaler les modifications de la longueur du muscle dans lequel ils se trouvent. Les modifications de la longueur d'un muscle sont associées à des modifications des angles des articulations que le muscle croise, de sorte que l'activité des fuseaux neuro-musculaires puisse être utilisée par le système nerveux central pour détecter les positions relatives de segments corporels. Ces capteurs demeurent intacts et actifs en dessous du niveau de lésion de patients souffrant d'une lésion de la moelle épinière. Avec l'apparition des interfaces neuroprothétiques, l'activité nerveuse afférente des fuseaux neuro-musculaires peut être envisagée comme une source potentielle d'information rétroactive dans les systèmes de Stimulation Electrique Fonctionnelle en boucle fermée (FES).

Dans une étude antérieure, un dispositif de commande en boucle fermée simple a été mis en oeuvre pour effectuer le suivi d'une trajectoire désirée pour l'angle de l'articulation en présence de perturbations appliquées depuis l'environnement extérieur [Yoshida and Horch, 1996]. Les auteurs ont adopté un schéma de commande dans lequel ils ont implanté une paire d'électrodes intrafasciculaires longitudinales à canal unique (LIFE) dans les nerfs innervant la paire de muscles agoniste/antagoniste de l'articulation. Le but était de faire fonctionner les deux électrodes en modes opposés, par exemple, une électrode stimulant l'agoniste, l'autre enregistrant l'activité du fuseau neuro-musculaire de l'antagoniste, et vice versa. De cette manière, l'électrode d'enregistrement détecte toujours l'activité neurale d'un muscle étiré passivement. Les auteurs ont montré que cette approche était applicable dans des conditions restrictives (vitesse et plage de mouvements limitées) en raison de la non prise en compte de la variation de la sensibilité dynamique des

terminaisons sensorielles des fuseaux neuro-musculaires.

7.2 Modèle d'Activité Nerveuse Afférente Pour Estimer l'Etat d'un Muscle

Si l'on pouvait développer un modèle permettant de relier l'activité nerveuse afférente des fuseaux neuro-musculaires à la longueur d'un muscle pour la plage du mouvement de la cheville lors de la locomotion, cela représenterait une avancée pour obtenir un système d'estimation en ligne, basé sur le modèle, de la longueur du muscle. Définir un tel modèle a été le premier objectif de la présente thèse.

Peu avant de commencer le travail de cette thèse, une nouvelle génération d'interface neurale intrafasciculaire, l'électrode intrafasciculaire à film mince (tfLIFE), a été conçue et fabriquée, mais n'a pas encore été testée complètement dans des conditions expérimentales. Des expériences pratiquées d'emblée sur des lapins, qui sont nécessaires pour acquérir les données de validation de tout modèle proposé, se sont également avérées une occasion de tester la nouvelle électrode in vivo. L'électrode elle-même a été conçue pour être implantée de manière longitudinale dans le nerf périphérique, et elle permet d'enregistrer jusqu'à 8 canaux d'un ENG provenant de sous-ensembles d'axones au sein d'un fascicule nerveux (Fig.7.1).

Un modèle prenant en compte les différentes sensibilités des fibres afférentes des fuseaux neuro-musculaires a été proposé et validé expérimentalement. Des expériences ont été réalisées sur dix lapins blancs de Nouvelle Zélande. L'anesthésie est induite et maintenue tout au long des expériences. Une électrode tripolaire à manchon (gouttière) est implantée autour du nerf sciatique (Fig.7.2, partie gauche). Elle est utilisée pour obtenir la courbe force-longueur pour le muscle gastrocnémien. Une stimulation électrique est appliquée en utilisant une unité de stimulation couplée à une unité d'isolation photoélectrique. Une structure de type tfLIFE est implantée dans la ramification tibiale du nerf sciatique innervant le muscle gastrocnémien de la patte postérieure gauche du lapin (Fig. 7.2, partie droite). Celui-ci se situe à 3 cm du site d'implantation de la tfLIFE. L'électrode permet de mesurer l'activité électroneurographique (ENG) provenant du fascicule dans lequel la structure a été implantée. Pour obtenir une activité afférente purement musculaire dans les enregistrements, le nerf sciatique a été écrasé à proximité du manchon et des sites d'implantation de la tfLIFE à l'aide d'une paire de forceps.

Pour immobiliser la patte gauche du lapin, on fixe celle-ci via les articulations du genou et de la cheville à un châssis mécanique immobilisé en utilisant des broches pour os placées à travers les épiphyses distales du fémur et du tibia. Le tendon calcanéen commun est at-

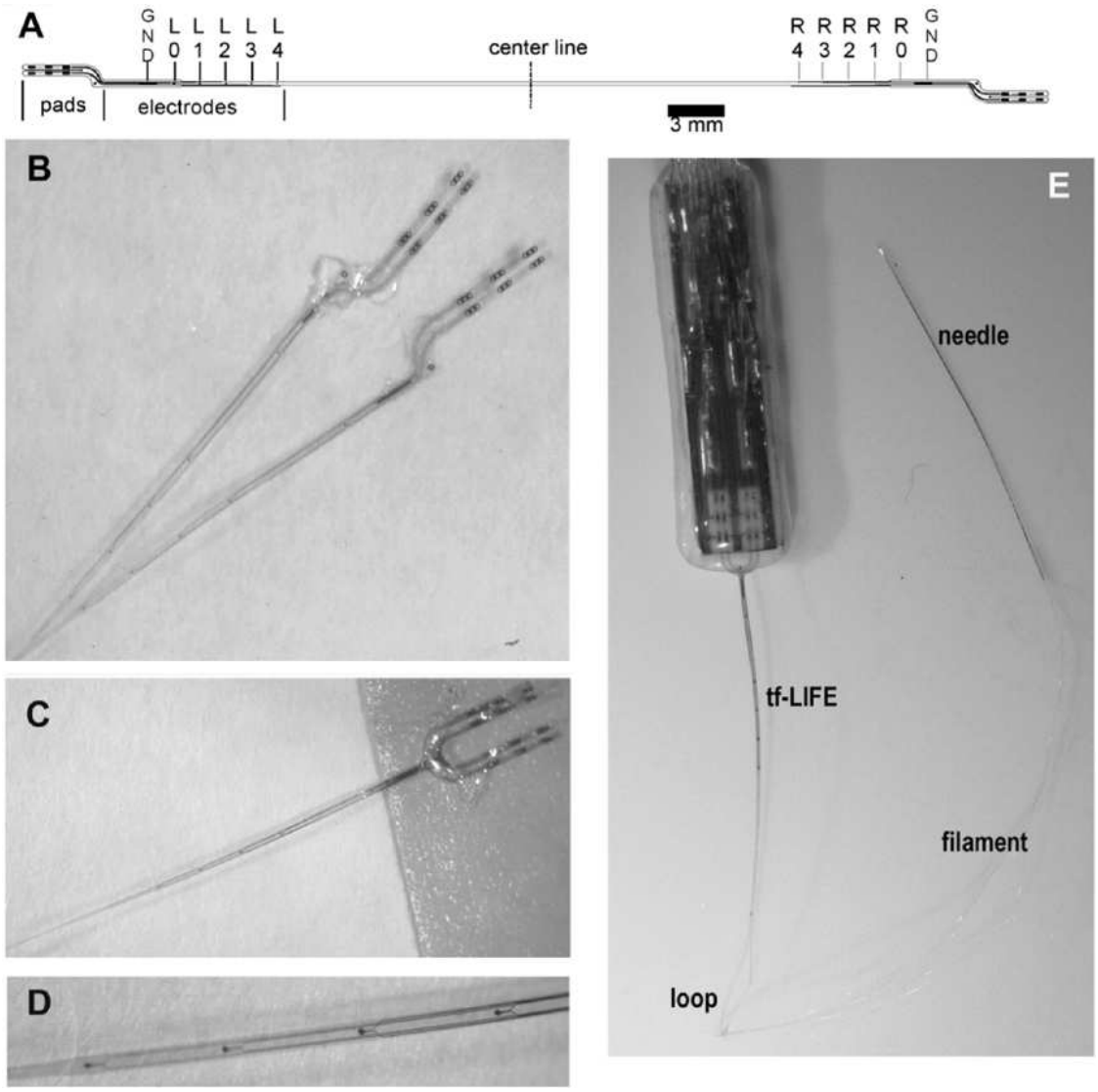

Figure 7.1: (A) Schéma de la tfLIFE. Chaque moitié de la structure dispose d'une électrode de terre (GND), d'une électrode indifférente (L0, R0) et de quatre sites d'enregistrement (L1-4, R1-4). (B) La tfLIFE est pliée via la ligne centrale, de sorte que les deux branches puissent être étroitement apposées. (C) Vue de la partie proximale de l'électrode. (D) Vue agrandie, représentant les quatre sites actifs, obtenue par pulvérisation de Pt. (E) Photographie de l'ensemble du système. La tfLIFE est fixée à la partie d'extrémité à un connecteur en céramique pour permettre les opérations d'enregistrement/stimulation du nerf. La boucle située entre les deux branches de la tfLIFE est connectée à un filament en Kevlar, qui est lui-même collé à une aiguille en tungstène pour l'insertion dans le nerf. Adaptation de Lago et al. [2007].

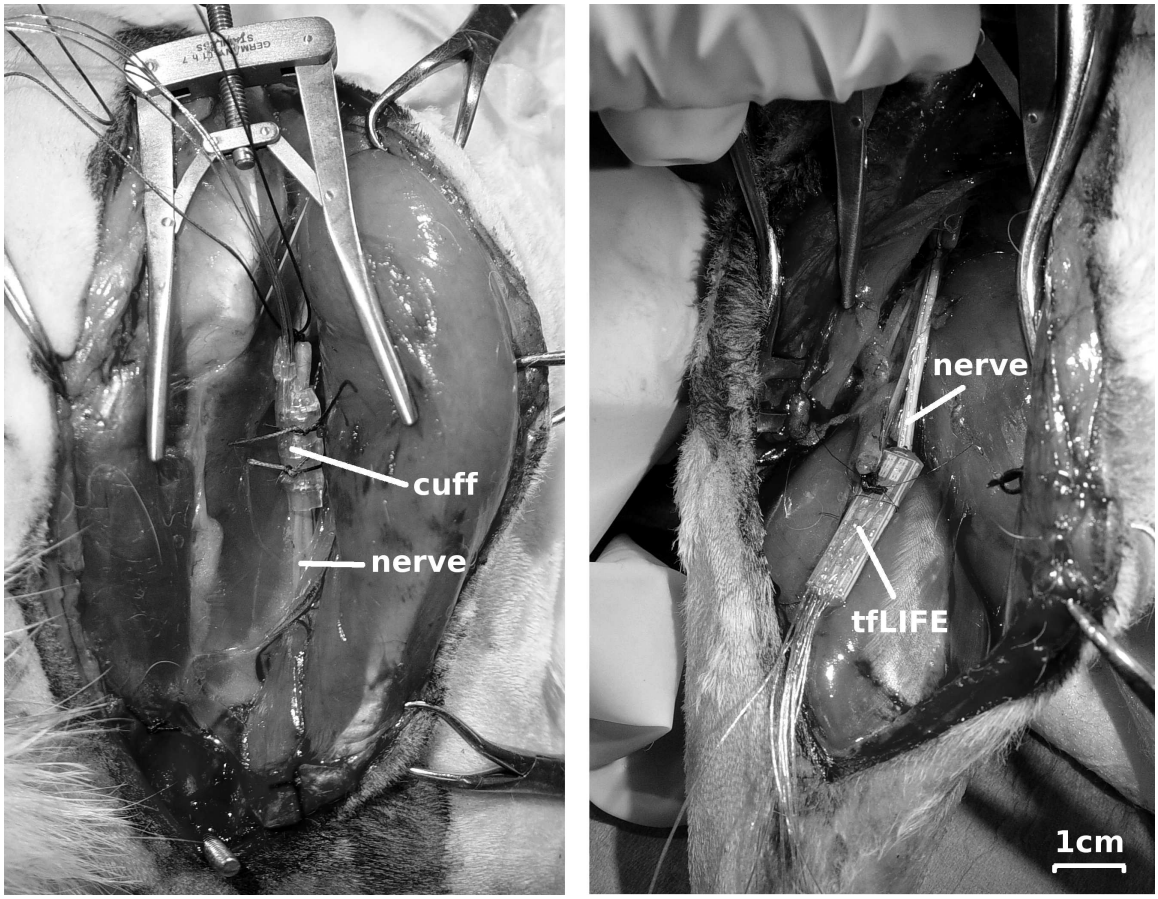

Figure 7.2: Electrodes utilisées dans les expériences. *Partie gauche*: électrode tripolaire à manchon implantée autour du nerf sciatique. *Partie droite*: tfLIFE implantée à l'intérieur du fascicule du nerf sciatique innervant le muscle MG. La structure à film mince est trop petite pour être vue, on ne distingue que le connecteur de l'électrode. L'échelle est la même pour les deux images. Elle est indiquée dans l'angle inférieur droit de l'image de droite.

taché au bras d'un système à levier motorisé en utilisant un fil composé de fibres de Kevlar. Le système à levier motorisé sert à la fois de mécanisme d'actionnement et de mesure. Le fait de tirer les fibres de Kevlar produit une extension de la cheville, et le relâchement des fibres de Kevlar provoque une flexion de la cheville (le muscle étiré retournant à l'état de repos en raison de son élasticité intrinsèque). La fixation au châssis mécanique garantit l'élimination de vibrations mécaniques, que pourrait provoquer un pied oscillant librement (Fig.7.3).

On soumet le muscle à des étirements de type sinusoïdal à 2 fréquences: 10 mHz et 250 mHz. Les deux profils d'étirement présentent une amplitude de pic à pic de 4 mm. Des

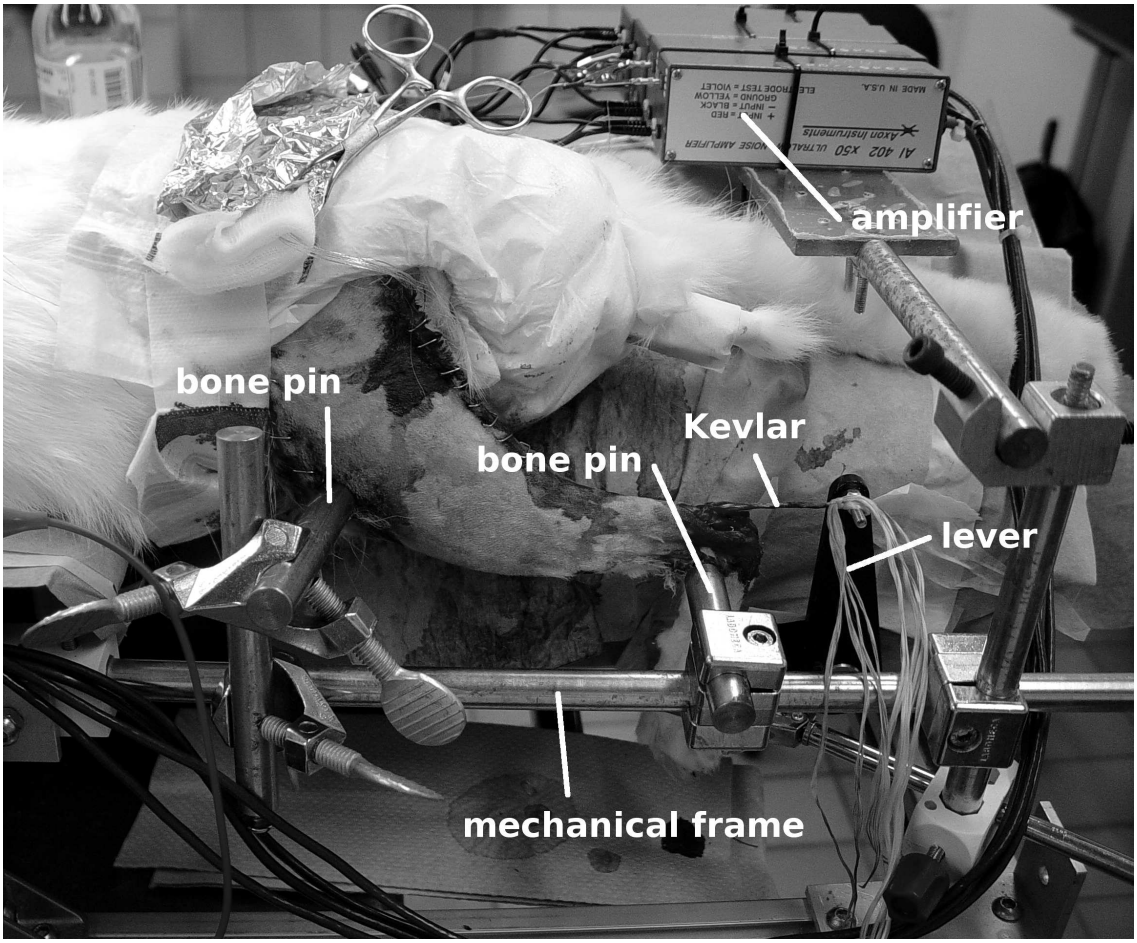

Figure 7.3: Montage expérimental. La patte gauche du lapin est fixée au niveau des articulations du genou et de la cheville à un châssis mécanique immobilisé en utilisant des broches pour os placées à travers les épiphyses distales du fémur et du tibia. Le tendon calcanéen commun est attaché au bras d'un système à levier motorisé en utilisant un fil constitué de fibres de Kevlar.

enregistrements simultanés sont réalisés à partir de quatre sites de l'électrodes intrafasciculaire. Les durées des enregistrements sont de 2 minutes pour l'étirement le plus lent (de manière à permettre l'achèvement d'un cycle complet de la sinusoïde) et d'à peine plus d'une minute pour l'étirement plus rapide (4 cycles de la sinusoïde). Un exemple de relation entre la vitesse de réaction du nerf afférant de fuseaux neuro-musculaires et la longueur du muscle est donné sur la Fig.7.4.

Nous avons proposé un modèle du premier ordre pour exprimer la relation entre le taux de décharge neurale et la longueur musculaire. Seules les périodes de flexion de la cheville

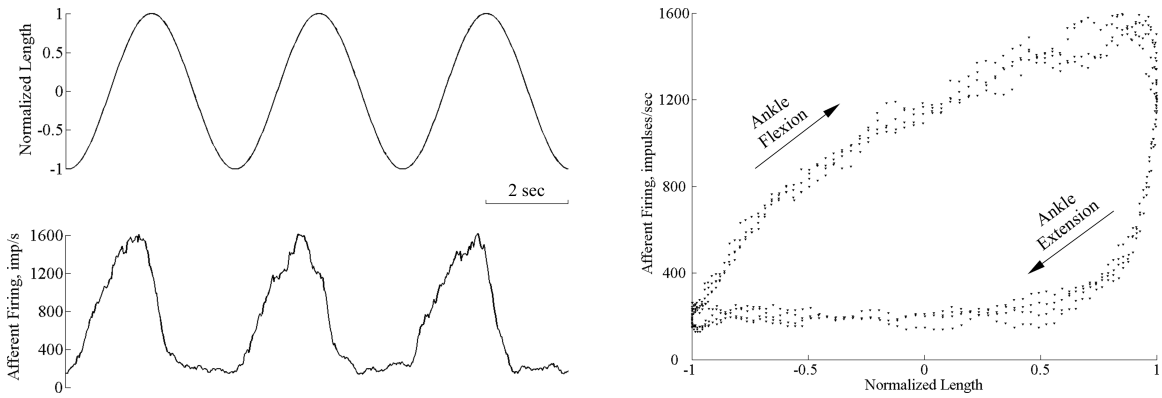

Figure 7.4: *Partie supérieure gauche*: Trois périodes d'une onde sinusoïdale normalisée, utilisées comme profil d'étirement passif du muscle avec une amplitude de 4 mm de pic à pic et une fréquence de 250 mHz. *Partie inférieure gauche*: Vitesse de réaction cumulée calculée en utilisant une fenêtre mobile à 100 ms sur un canal de l'ENG post-traité. *Partie droite*: Relation entre la vitesse de réaction et la longueur musculaire normalisée pour les 3 périodes de la sinusoïde représentées sous forme superposée dans le tracé. Le muscle est étiré pendant la flexion de la cheville et contracté pendant l'extension de la cheville.

sont modélisées car le muscle n'est étiré passivement qu'au cours de ces périodes, selon le schéma de commande de FES adopté. Les résultats issus de la validation expérimentale du modèle ont montré que le modèle parvient à capturer les propriétés non linéaires de la relation entre la taux de décharge neurale afférente et la longueur du muscle. Un exemple d'analyse de l'ajustement des sonnées expérimentales par un modèle de régression est représenté sur la Fig.7.5. En outre, l'estimation de l'état du muscle effectuée à partir de l'ENG multi-canaux enregistré donne des résultats plus précis et plus solides en comparaison de l'utilisation d'enregistrements d'ENG à canal unique.

7.3 Détection et Classification des Potentiels d'Action Neurale

L'activité neuroélectrique enregistrée avec la tfLIFE est un mélange de signaux provenant de plusieurs neurones adjacents et de bruit. Si l'on pouvait décomposer ce mélange en activités de ces différentes sources, les activités d'unités individuelles pourraient être analysées pour interpréter le codage d'informations complexe, qui n'est pas évident dans le cadre d'une activité d'unités multiples cumulées. Dans notre cas particulier, lorsque l'on enregistre l'activité de fibres de fuseaux neuro-musculaires, l'objectif est de parvenir

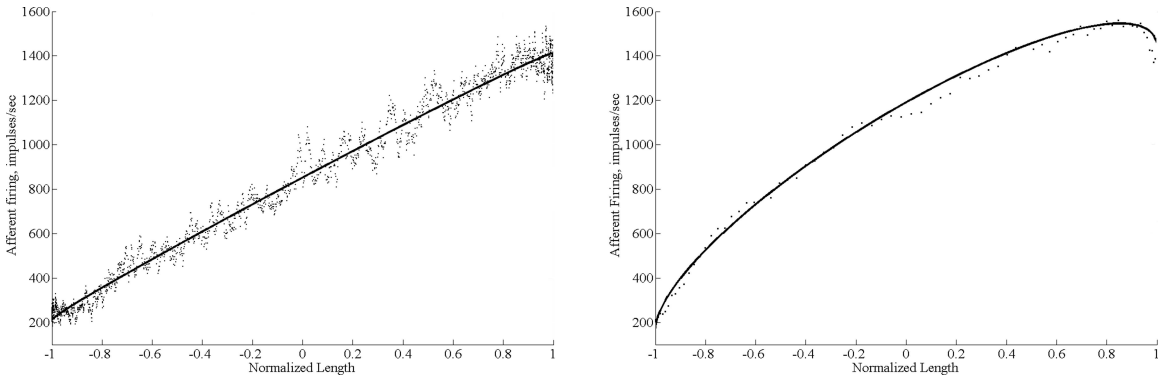

Figure 7.5: Réglage à un seul canal pour des fréquences d'étirement de 10 mHz (à gauche) et de 250 mHz (à droite). L'abscisse représente la longueur musculaire normalisée et l'ordonnée représente la vitesse de réaction neurale. Les lignes en trait continu sont les courbes modélisées.

à classer les potentiels d'action détectés en fonction du type de fibre nerveuse sensorielle. Si l'on pouvait isoler l'activité de fibres sensorielles insensibles à la vitesse d'étirement (fibres sensorielles de type II), le modèle développé de réaction afférente de fuseaux neuro-musculaires pourrait être utilisé pour suivre les variations de longueur musculaire avec un profil d'étirement à priori inconnu.

On propose une approche pour détecter et classer une impulsion neurale basée sur la transformée en ondelettes continues (CWT) à partir d'ondelettes complexes. Les coefficients d'ondelettes complexes sont utilisés comme mesure du degré de similarité de profils dans le signal à la forme d'onde de type ondelettes. La détection d'impulsions consiste à établir une valeur de seuil pour l'amplitude de ces coefficients, et on utilise les "signatures" de CWT complexes, à échelles multiples, des impulsions détectées pour la classification.

La performance de détection basée sur les ondelettes des signaux synthétiques est comparée au procédé d'établissement d'une valeur de seuil de l'amplitude. La détection est évaluée sur une plage de valeurs de seuil, en commençant par un niveau de bruit de fond jusqu'à l'amplitude maximale observée dans le signal transformé. La performance de classification est évaluée à la fois sur l'ENG synthétique en comparant la classification basée sur les ondelettes à des procédés basés sur la correspondance entre matrices et sur l'analyse en composantes principales. Ces deux procédés, utilisés comme références dans la comparaison, sont les plus couramment utilisés en raison de leur relative simplicité, qui permet une mise en oeuvre rapide en temps réel.

Les performances du détecteur basées sur les ondelettes et utilisant le simple établissement d'une valeur de seuil d'amplitude sont représentées sur la Fig.7.6 sous la

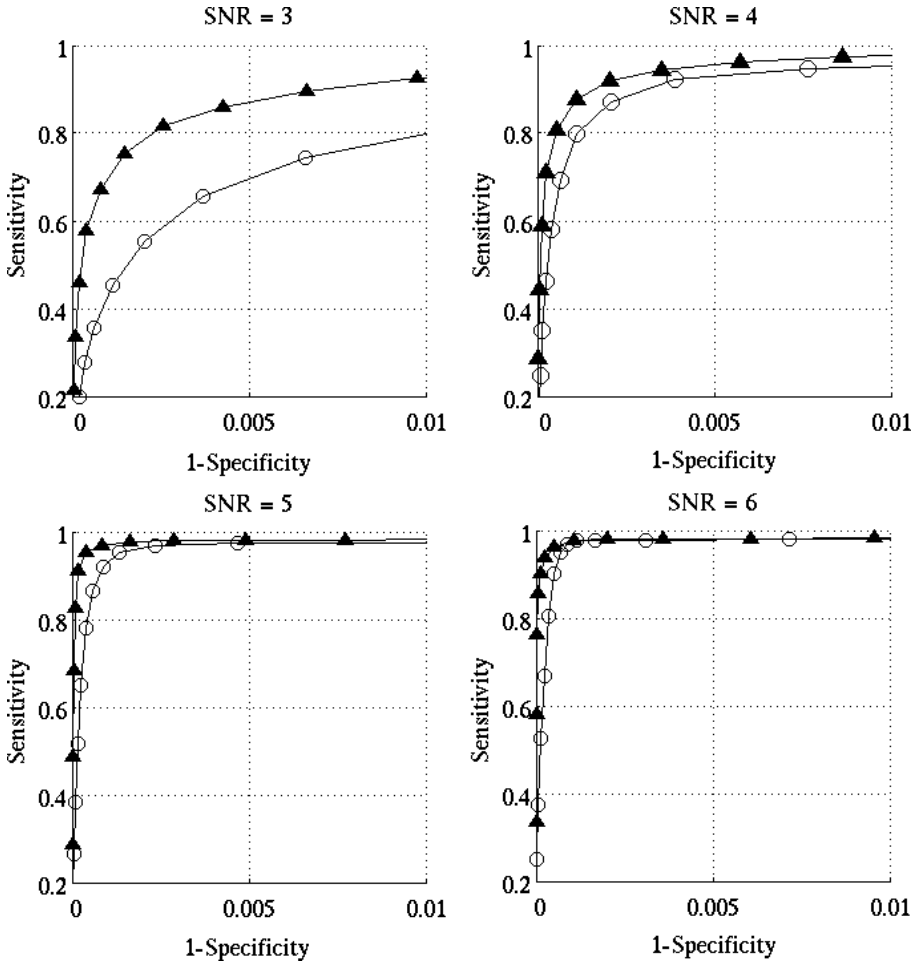

Figure 7.6: Courbes ROC pour quatre niveaux de SNR définis par le rapport de l'amplitude du pic des potentiels d'action exempts de bruit à l'écart type du bruit de fond. Les performances d'un simple détecteur de seuil (courbe formée par les cercles vides) et du détecteur basé sur les ondelettes (courbe formée par les triangles pleins) sont comparées.

forme de courbes de caractéristiques d'opérations de récepteur ou courbes ROC. Ces courbes sont des représentations graphiques de la sensibilité du détecteur en fonction de la spécificité utilisant une plage de valeurs de seuils de détection. Sur la plage complète des niveaux de SNR, le détecteur basé sur les ondelettes présente de meilleures performances que le détecteur basé sur l'établissement de valeurs de seuil de l'amplitude, c'est-à-dire que pour une spécificité donnée quelconque, la sensibilité correspondante est supérieure pour le détecteur basé sur les ondelettes. L'intervalle de performances devient particulièrement important avec un SNR faible.

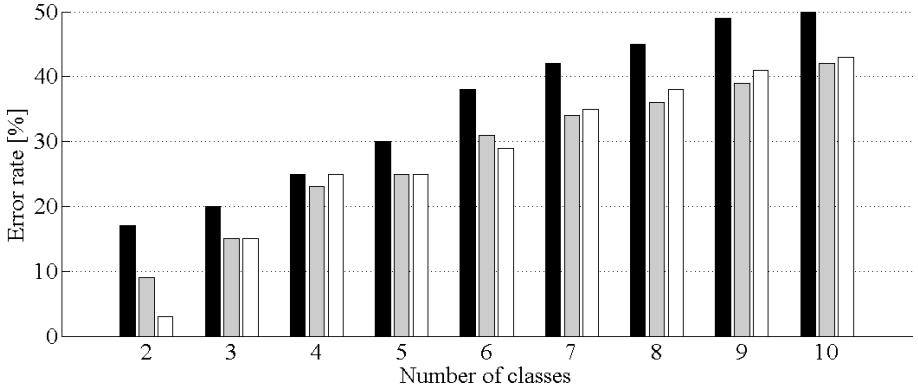

Figure 7.7: Taux d'erreurs de classification dépendant du nombre d'unités actives simultanément. Des groupes de trois barres (histogrammes) représentent les différentes approches de classification: la correspondance entre matrices (en noir), l'analyse des composantes principales (en gris) et l'analyse basée sur les ondelettes (en blanc).

Les résultats de classification sont représentés sur la Fig.7.7 sous la forme de taux d'erreurs de classification qui représentent des rapports du nombre d'impulsions mal classées au nombre total d'impulsions classées. La classification basée sur les ondelettes est comparée à deux autres procédés de classification: l'analyse des composantes principales (PCA) et la correspondance entre matrices. Les résultats sont représentés en commençant par le cas dans lequel seulement deux classes d'impulsions différentes sont présentes dans le signal jusqu'au cas dans lequel 10 unités réagissent simultanément. La classification basée sur la correspondance entre matrices donne les taux d'erreurs de classification les plus élevés, tandis que les approches basées sur les ondelettes et sur la PCA présentent des résultats similaires.

La technique de tri d'impulsions est éventuellement appliquée à l'activité nerveuse afférente de fuseaux neuro-musculaires enregistrée expérimentalement. Seules des périodes de flexion de l'articulation de la cheville (périodes d'étirement du muscle MG) sont analysées. La valeur de seuil de détection est choisie de manière à représenter sept fois les écarts types du niveau de bruit de fond (dans l'espace des ondelettes). Sur l'ensemble des essais, cette valeur de seuil correspond, sur les courbes ROC, au point auquel la spécificité commence à se détériorer rapidement, tandis que l'on observe, dans le même temps, une légère amélioration de la sensibilité.

Les unités détectées sont classées en 10 groupes. Ceci correspond à peu près au nombre d'unités prises par un site d'enregistrement de la tfLIFE lorsque le muscle est étiré au maximum. L'analyse est effectuée sur des données provenant de tous les lapins. Les résultats du regroupement des données montrent que jusqu'à 2 ou 3 classes d'impulsions

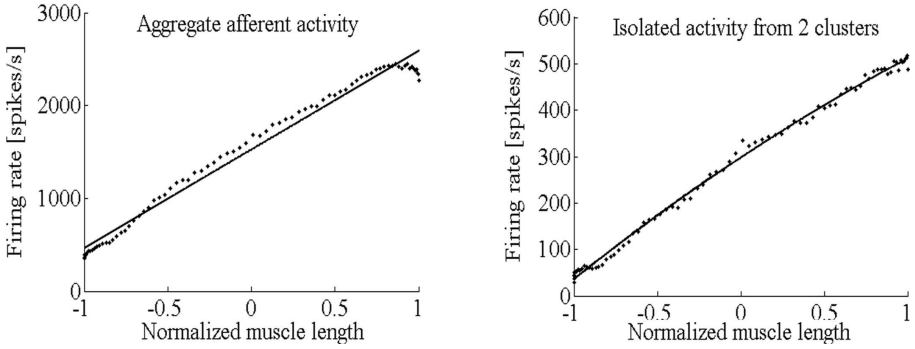

Figure 7.8: Vitesse de réaction neurale afférente par rapport à la longueur musculaire. Le tracé de gauche montre l'activité cumulée de toutes les impulsions détectées. Sur la partie droite, seule l'activité de 2 groupes, présentant un bon ajustement linéaire avec les données, est utilisée pour calculer la vitesse de réaction. On effectue une analyse de régression linéaire sur les deux tracés (lignes pleines). Sur les deux tracés, la longueur musculaire est normalisée par 4 mm.

par lapin on obtient une relation linéaire entre leur taux de décharge neurale calculée et la longueur musculaire instantanée. Les résultats pour un lapin sont présentés sur la Fig.7.8. Le tracé de gauche représente la relation entre la longueur et le taux de décharge cumulé de toutes les impulsions détectées. A l'évidence, la relation n'est pas linéaire dans la région o la vitesse d'étirement du muscle ralentit rapidement (région o la longueur musculaire normalisée est proche de 1). Le tracé de droite montre la même relation, mais en utilisant cette fois uniquement l'activité des fibres insensibles à la vitesse d'étirement musculaire. Une analyse de régression linéaire effectuée sur les deux tracés montre que la modélisation est meilleure sur le tracé droit.

Les résultats de la classification d'unités en classes basées sur les signatures de la forme d'onde de potentiel d'action dans un espace d'ondelettes indiquent que le système de classement est capable d'isoler une activité présentant une relation linéaire avec la longueur musculaire. Ceci représente une avancée pour un dispositif d'estimation en ligne de la longueur musculaire, basé sur un modèle, que l'on peut employer dans un système de FES en boucle fermé avec rétroaction sensorielle naturelle.

L'un des principaux facteurs limitatifs d'un procédé quelconque de tri d'impulsions est le faible niveau de signal-au-bruit (SNR) dans l'ENG enregistré. Une manière qui pourrait permettre d'améliorer la qualité de l'acquisition du signal, même avant que ne s'effectue un quelconque traitement, implique de protéger le site de l'implant.

7.4 Amélioration du SNR Dans des Enregistrements Intra-Neuraux

Parallèlement au travail sur la modélisation et le tri d'impulsions de l'activité neurale, nous avons proposé un nouveau schéma d'enregistrement susceptible d'améliorer le SNR dans des enregistrements intra-neuraux, que l'on a validé au plan expérimental. Dans les systèmes de FES, la stimulation et l'enregistrement simultanés sont nécessaires et l'interface neurale se situe habituellement à proximité des structures neuro-musculaires intéressantes, ce qui se traduit par des problèmes en matière de niveaux relativement importants d'artéfacts dans l'ENG. Les artéfacts de muscle et de stimulation dans l'ENG proviennent du gradient de potentiel extra-neural qui chute longitudinalement le long du nerf. Le niveau d'artéfact du muscle limite le gain maximal qui peut être réglé dans l'acquisition du signal, ce qui limite, en retour, le rapport signal-au-bruit maximal (SNR) dans les enregistrements. L'artéfact de stimulation corrompt, en outre, les signaux enregistrés. Le faible SNR est un problème majeur lorsqu'il s'agit de détecter et de classer des potentiels d'action neurale. Si le SNR peut être amélioré, les performances de tri d'impulsions s'amélioreront également.

Les observations faites au cours de travaux antérieurs suggèrent que le fait d'enrouler le site d'implant dans une petite enveloppe conductrice constituée d'un film mince de Téflon métallisé ou de remplir le site d'implant avec des fibres de carbone, minimisait la stimulation et la prise d'artéfact d'EMG. La protection confère à l'espace extra-neural environnant le site d'implant un caractère équipotentiel, ce qui entraîne la diminution du bruit extra-neural dans les signaux enregistrés. Malheureusement, la protection conductrice réduit également le niveau de signal de l'ENG. Une explication possible est que le matériau conducteur de la protection fournit une voie de faible résistivité pour les courants ioniques de potentiels d'action; ce qui provoque une chute de tension plus faible entre les électrodes de mesure. De plus, la feuille métallique peut également entrer en contact avec l'électrode de référence, ce qui produit d'importants artéfacts dans le signal enregistré, avant que l'électrode ne soit finalement encapsulée par le tissu conjonctif formant une gaine. Notre hypothèse est que la mise en place d'une couche diélectrique entre le nerf et la feuille conductrice empêchera à la fois l'effet de court-circuit sur les courants de potentiels d'action et le contact de la feuille conductrice avec les sites d'enregistrement de l'électrode (Fig.7.9).

Une étude pilote a été réalisée pour évaluer expérimentalement cette hypothèse. Au lieu de fabriquer une feuille à deux couches, qui présenterait une surface diélectrique sur un cté et une surface conductrice sur l'autre, nous avons opté pour une électrode ordinaire à manchon (gouttière). Une fois placée autour du nerf sur les sites d'enregistrement de la LIFE avec ses fils conducteurs non connectés, l'électrode à manchon agit effective-

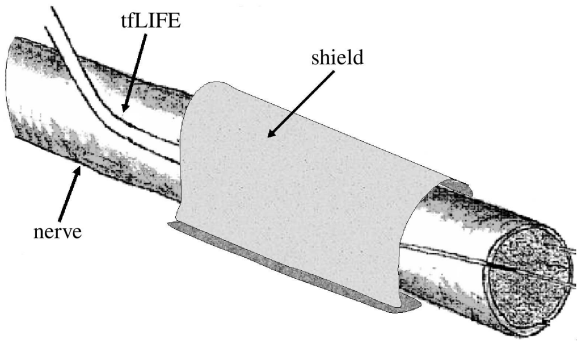

Figure 7.9: Illustration d'une protection enveloppée autour d'un site d'implant d'électrode d'enregistrement. Si celle-ci se est constituée d'un matériau conducteur, la protection contribue à diminuer l'artéfact de stimulation, mais réduit également le niveau d'ENG dans les enregistrements. Avec une protection du type double couche, la couche conductrice externe est censée diminuer la prise de champ électrique extraneural (artéfacts de stimulation et d'EMG) et la couche diélectrique interne sert à éviter le contact entre le nerf et la couche conductrice.

ment comme une protection isolante. En connectant ses fils conducteurs, le potentiel des bagues du manchon devrait représenter la moyenne des potentiels observés entre les bagues lorsque les conducteurs du manchon sont laissés ouverts. Cette configuration devrait avoir à peu près le même effet sur la distribution du champ électrique (artéfact) extra-neural à l'intérieur du manchon qu'une protection de type double couche (une couche conductrice sur une couche isolante) enveloppée autour de l'électrode d'enregistrement.

D'autres expériences doivent être effectuées, afin d'évaluer expérimentalement l'effet de la protection. Des expériences ont été pratiquées sur 5 lapins blancs de Nouvelle Zélande anesthésiés. La préparation des animaux est similaire à celle pratiquée pour les études de modélisation et de tri d'impulsions, excepté les différences décrites dans le texte ci-après. Le système à levier motorisé est utilisé dans cette étude pour garantir que la longueur du muscle reste constante sur l'ensemble de l'expérience. La tfLIFE implantée a été utilisée pour enregistrer le potentiel d'action nerveux composé en réponse à une stimulation électrique. Le nerf sciatique n'a pas été écrasé, dans la mesure o l'activité d'une unité unique ne présente pas d'intérêt dans cette étude. La stimulation et l'enregistrement sont effectués en utilisant le même équipement et le même montage que dans l'étude de modélisation, excepté que l'on a également enregistré, ici, le déclenchement de la simulation sur un canal supplémentaire sur l'enregistreur à bande numérique. On l'a utilisé ultérieurement dans une analyse de données comme signal de synchronisation en vue de calculer la moyenne, synchronisée avec la stimulation, de la réponse twitch du nerf.

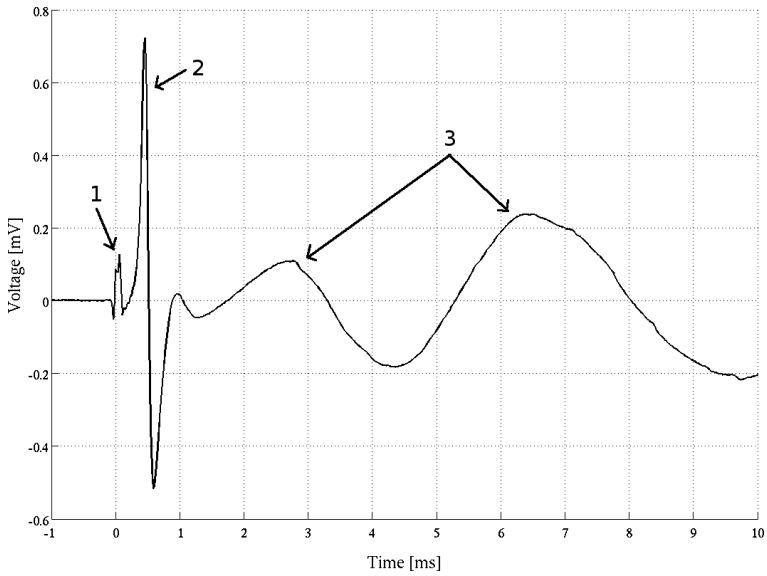

Figure 7.10: Réaction moyenne, synchronisée sur la stimulation, en réponse à une stimulation électrique par secousses nerveuses. Trois composantes distinctes apparaissant successivement peuvent être identifiées: 1)l'artéfact de stimulation, synchrone avec l'impulsion de stimulation, dont l'activité s'étend de 0 à environ 100 μs; 2)le potentiel d'action composé du nerf, soit la forme d'onde biphasique située juste après l'artéfact de stimulation et 3)l'artéfact du muscle, dont l'activité démarre environ 1 ms après la stimulation et se poursuit jusqu'à la fin du tracé.

L'activité nerveuse est déclenchée par le biais d'une stimulation électrique délivrée via une électrode circonférentielle tripolaire à manchon implantée autour du nerf tibial. Les signaux sont enregistrés via les 4 canaux de la tfLIFE. Une autre électrode tripolaire à manchon est utilisée comme protection. Les manchons de stimulation et de protection ont les mêmes dimensions. Les mesures consistent à enregistrer la réaction neurale répondant à une stimulation électrique utilisant des trains d'impulsions (durée d'impulsion de 100 ms et fréquence de répétition des impulsions de 1 Hz). Les courbes de recrutement sont obtenues en commençant avec des intensités de stimulation inférieures à la valeur de seuil du nerf, puis en augmentant l'intensité de stimulation par incréments jusqu'à ce qu'il n'y ait plus de variation de la réaction (réaction neurale maximale et artéfact d'EMG maximal). Une illustration des composantes du signal dans la réponse moyenne, synchronisée avec la stimulation, de la réaction de secousses du nerf est représentée sur la Fig.7.10.

Trois stratégies de protection (protection conductrice, manchon protecteur en circuit ouvert et manchon de protection en court-circuit) ont été comparées en termes de trois paramètres: le niveau de réaction du nerf, le niveau d'artéfact de la stimulation et le niveau

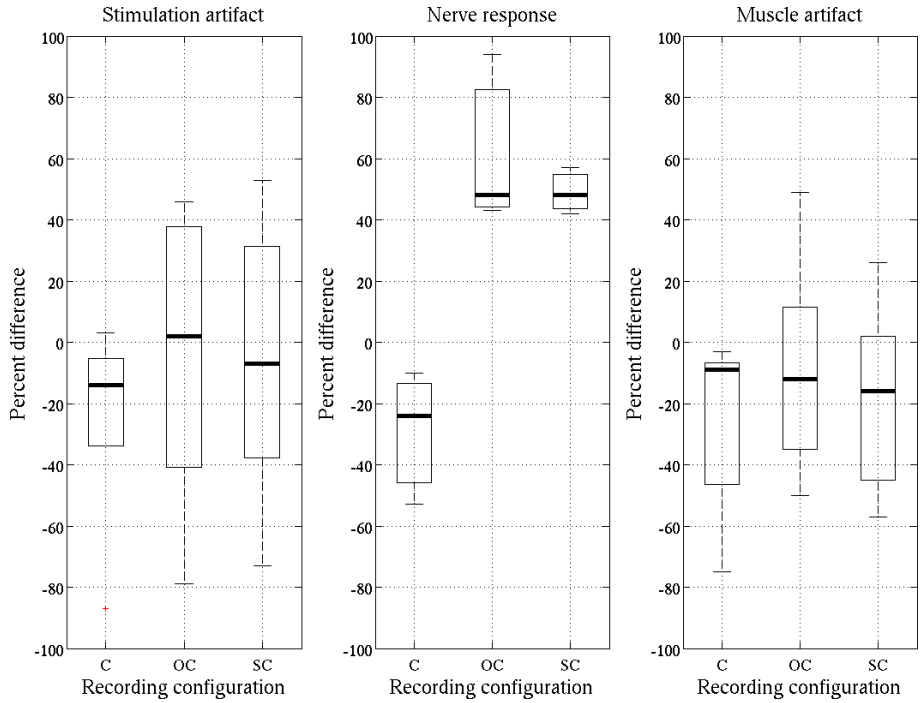

Figure 7.11: Pourcentage des différences pour les 3 configurations d'enregistrement: C – feuille conductrice enveloppée autour du site d'implant, OC – électrode à manchon disposée autour du site d'implant, ses conducteurs étant laissés en mode non connecté et OS – électrode à manchon située autour du site d'implant de la tfLIFE, ses bagues d'extrémité étant en mode court-circuit. Les tracés en boîte (à moustaches) montrent les niveaux pour un artéfact de stimulation (à gauche), pour la réaction neurale (au centre) et pour l'artéfact d'EMG (à droite) en comparaison du cas dans lequel aucune protection n'est utilisée.

d'artéfact de l'EMG. Les résultats représentés sous la forme de diagrammes statistiques en boîte à moustaches sont représentés sur la Fig.7.11. On compare les niveaux de signaux au cas réalisé en l'absence de protection lors de l'enregistrement. Chaque boîte présente des lignes au niveau des quartiles inférieur, médian (ligne horizontale épaisse) et au niveau du quartile supérieur. Des moustaches s'étendent à partir de chaque extrémité de la boîte aux valeurs adjacentes dans les données. Les points atypiques sont affichés avec un signe +. Les résultats comparent les performances de protection en utilisant les données tirées de tous les lapins (3 lapins pour les données d'ENG et 5 pour les données d'artéfacts).

Les résultats préliminaires montrent que la protection conductrice disposée autour du site d'enregistrement diminue le niveau de signal d'ENG enregistré. Une électrode à manchon placée autour du site d'implantation de la tfLIFE augmente les niveaux d'ENG enreg-

istrés à la fois dans le cas o les conducteurs du manchon demeurent non connectés et dans le cas o les conducteurs sont en court-circuit. Une explication possible est que la poussée de tension dans le signal d'ENG résulte d'une augmentation de la résistance du trajet le long duquel circulent les courants ioniques qui génèrent le potentiel d'action du nerf. Cette augmentation peut être prédite par un modèle simple en utilisant un diple électrique comme source de courants membranaires axonaux. Le taux d'augmentation prédit par le modèle est en bonne corrélation avec les données expérimentales.

Une feuille conductrice placée autour du site d'implant de la tfLIFE diminue les niveaux d'artéfacts issus tant de la stimulation que du muscle dans les signaux enregistrés. Dans toutes les expériences, à l'exception d'une, les deux configurations de protection à manchon contribuent à réduire la prise d'artéfact du muscle. Un modèle de circuit équivalent de la source d'artéfact et de son interaction avec l'électrode et les tissus environnants prédit une différence de 10% entre les configurations de protection à manchon en circuit ouvert et fermé, ce qui corrobore les données expérimentales. Pour l'artéfact de stimulation, les résultats ne présentent pas de tendance. Cette étude est encore en cours et il est nécessaire d'effectuer davantage d'expériences pour tirer des conclusions définitives.

7.5 Conclusions

Les résultats des études effectuées au cours de cette thèse sont: 1)un modèle de réaction neurale de fuseaux neuro-musculaires en réponse à un étirement passif des muscles; ce modèle pourra être mis en oeuvre dans un dispositif d'estimation en ligne de l'état du muscle au sein d'un système de FES en boucle fermée, le dispositif d'estimation restituant de manière rétroactive au dispositif de commande l'information concernant l'état du muscle o se trouvent les fuseaux neuro-musculaires; 2)un algorithme pour décomposer le mélange de signaux provenant de multiples fibres nerveuses en sources séparées. Cela permet d'utiliser le modèle défini pour suivre l'état du muscle avec, à priori, un mouvement musculaire inconnu; 3)une technique d'isolation pour améliorer le niveau signal-au-bruit dans des enregistrements effectués en utilisant des électrodes intraneurales disposées longitudinalement. Le renforcement du niveau de signal neural permettra l'amélioration des performances de l'algorithme pour la séparation des sources.

Ce travail étant achevé, il est à présent possible de procéder au développement d'un dispositif d'estimation de la longueur musculaire en ligne, basé sur un modèle, qui peut être utilisé dans un système de stimulation électrique fonctionnelle commandé en boucle fermé.

Bibliography

E. D. Adrian and Y. Zotterman. The impulses produced by sensory nerve-endings. Part II. The response of a single end-organ. *Journal of Physiology*, 61(2):151–171, May 1926.

L. N. S. Andreasen and J. J. Struijk. Signal strength versus cuff length in nerve cuff electrode recordings. *IEEE Transactions on Biomedical Engineering*, 49(9):1045–1050, 2002.

C. Azevedo and K. Yoshida. Towards a model-based estimator of muscle length and force using muscle afferent signals for real-time FES control. In *Proceedings of the International Conference on Computer as a Tool (EUROCON)*, Belgrade, Serbia and Montenegro, November 2005.

L. Baker, R. Waters, C. Winstein, H. Kaplan, W. Tran, F. J. R. Richmond, and G. E. Loeb. Clinical applications of BION microstimulators. In *Proceedings of the First International Conference on Neural Interface and Control*, pages 185–188, Wuhan, China, May 2005.

D. Barker, M. J. Stacey, and M. N. Adal. Fusimotor innervation in the cat. *Proceedings of the Royal Society of London. Series B, Biological Sciences*, 258(825):315–348, 1970.

J. Bourien, J. Ruel, L. Senhadji, and J. L. Puel. Comparison of three spike detectors dedicated to single unit action potentials of the auditory nerve. In *Proceedings of the 29th Annual International Conference of the IEEE EMBS*, Lyon, France, August 2007.

I. A. Boyd. The structure and innervation of the nuclear bag muscle fibre system and the nuclear chain muscle fibre system in mammalian muscle spindles. *Philosophical transactions of the Royal Society of London. Series B, Biological Sciences*, 245(720): 81–136, 1962.

B. S. Bregman, E. Kunkel-Bagden, L. Schnell, H. N. Dai, D. Gao, and M. E. Schwab. Recovery from spinal cord injury mediated by antibodies to neurite growth inhibitors. *Nature*, 378:498–501, 1995.

Joseph D. Bronzino, editor. *The Biomedical Engineering Handbook*. CRC Press, second edition, 2000.

C. Brosamle, A. B. Huber, M. Fiedler, A. Skerra, and M. E. Schwab. Regeneration of lesioned corticospinal tract fibers in the adult rat induced by a recombinant, humanized IN-1 antibody fragment. *Journal of Neuroscience*, 20:8061–8068, 2000.

D. Burke. Unit identification, sampling bias and technical issues in microneurographic recordings from muscle spindle afferents. *Journal of Neuroscience Methods*, 74(2):137–144, 1997.

E. T. Chemineau, V. Schnabel, and K. Yoshida. A modeling study of the recording selectivity of longitudinal intrafascicular electrodes. In *Proceedings of the 9th Annual Conference of the International Functional Electrical Stimulation Society*, Bournemouth, UK, September 2004.

H. Cheng, Y. Cao, and L. Olson. Spinal cord repair in adult paraplegic rats: partial restoration of hind limb function. *Science*, 273:510–513, 1996.

L. Citi, J. Carpaneto, K. Yoshida, K. P. Hoffmann, K. P. Koch, P. Dario, and S. Micera. On the use of wavelet denoising and spike sorting techniques to process electroneurographic signals recorded using intraneural electrodes. *Journal of Neuroscience Methods*, 172(2): 294–302, 2008.

R. R. Coifman and D. L. Donoho. Translation-invariant de-noising. Technical report, Yale University and Stanford University, 1995.

G. S. Dhillon and K. Horch. Direct neural sensory feedback and control of a prosthetic arm. *IEEE Trans Neural Syst Rehabil Eng.*, 13(4):468–472, 2005.

G. S. Dhillon, S. M. Lawrence, D. T. Hutchinson, and K. Horch. Residual function in peripheral nerve stumps of amputees: Implications for neural control of artificial limbs. *Journal of Hand Surgery*, 29(4):605–615, 2004.

A. Diedrich, W. Charoensuk, R. J. Brychta, A. C. Ertl, and R. Shiavi. Analysis of raw microneurographic recordings based on wavelet de-noising technique and classification algorithm: Wavelet analysis in microneurography. *IEEE Transactions on Biomedical Engineering*, 50(3):41–50, 2003.

M. Djilas, K. Yoshida, M. Kurstjens, and C. Azevedo-Coste. Improving the signal-to-noise ratio in recordings with thin-film longitudinal intra-fascicular electrodes using shielding cuffs. In *Proceedings of the 3rd International IEEE EMBS Conference on Neural Engineering*, Cohala Coast, Hawaii, USA, May 2007.

D. L. Donoho. De-noising by soft-thresholding. *IEEE Transactions on Information Theory*, 41(3):613–627, 1995.

S. C. Gandevia, R. M. Enoka, A. J. McComas, D. G. Stuart, and C. K. Thomas, editors. *Fatigue: Neural and muscular mechanisms*. Springer, first edition, 1995.

E. M. Glaser. Separation of neuronal activity by waveform analysis. *Advances in Biomedical Engineering*, 1:77–136, 1971.

E. M. Glaser and W. B. Marks. On-line separation of interleaved neuronal pulse sequences. *Data Acquisition and Processing in Biology and Medicine*, 5:137–156, 1968.

E. V. Goodall and K. W. Horch. Identification of single units in multi-unit recordings from peripheral nerves. In *Proceedings of the Annual International Conference of the IEEE EMBS*, volume 3, pages 1166–1167, November 1988.

E. V. Goodall and K. W. Horch. Separation of action potentials in multiunit intrafascicular recordings. *IEEE Transactions on Biomedical Engineering*, 39(3):289–295, 1992.

E. V. Goodall, T. M. Lefurge, and K. W. Horch. Information contained in sensory nerve recordings made with intrafascicular electrodes. *IEEE Transactions on Biomedical Engineering*, 38(9):846–850, 1991.

J. A. Goodall, K. W. Horch, T. G. McNaughton, and C. M. Lybbert. Analysis of single-unit firing patterns in multi-unit intrafascicular recordings. *Medical & Biological Engineering & Computing*, 31(3):257–267, 1993.

G. M. Goodwin, D. I. McCloskey, and P. B. C. Matthews. Proprioceptive illisions induced by muscle vibration: Contribution by muscle spindles to perception? *Science*, 175 (4028):1382–1384, 1972.

W. M. Grill and J. T. Mortimer. Quantification of recruitment properties of multiple contact cuffelectrodes. *IEEE Transactions on Rehabilitation Engineering*, 4(2):49–62, 1996.

D. Guiraud, T. Stieglitz, K. Koch, J. Divoux, and P. Rabischong. An implantable neuroprosthesis for standing and walking in paraplegia: 5-year patient follow-up. *Journal of Neural Engineering*, 3:268–275, 2006.

D. Guiraud, H. E. Makssoud, P. Poignet, and P. Wieber. A physiology based skeletal muscle model for functional electrical stimulation applications. Submitted to Biological Cybernetics, March 2008.

M. Hansen, M. K. Haugland, and F. Sepulveda. Feasibility of using peroneal nerve recordings for deriving stimulation timing in a foot drop correction system. *Neuromodulation*, 6(1):68–77, 2003.

M. Hansen, M. K. Haugland, and T. Sinkjær. Evaluating robustness of gait event detection based on machine learning and natural sensors. *IEEE Transactions on Neural Systems and Rehabilitation Engineering*, 12(1):81–88, 2004.

M. Haugland. A flexible method for fabrication of nerve cuff electrodes. volume 1, pages 359–360, 1996.

M. Haugland, A. Lickel, J. Haase, and T. Sinkjær. Control of FES thumb force using slip information obtained from the cutaneous electroneurogram in quadriplegic man. *IEEE Transactions on Rehabilitation Engineering*, 7:215–227, 1999.

M. K. Haugland and J. A. Hoffer. Slip information provided by nerve cuff signals: Application in closed-loop control of functional electrical stimulation. 2:29–36, 1994.

M. K. Haugland and T. Sinkjær. Cutaneous whole nerve recordings used for correction of footdrop in hemiplegic man. *IEEE Trans. Rehab. Eng.*, 3:307–317, 1995.

A. Hoffer, M. Haugland, and T. Li. Obtaining skin contact force from implanted nerve cuff recording electrodes. In *Proceedings of the Annual International Conference of the IEEE Engineering in Engineering in Medicine and Biology Society*, volume 3, pages 928–929, November 1989.

A. Hoffer, R. B. Stein, M Haugland, T. Sinkjær, W. Durfee, A. B. Schwartz, G. E. Loeb, and C. Kantor. Neural signals for command control and feedback in functional neuromuscular stimulation: A review. *Journal of rehabilitation research and development*, 33 (2):145–157, 1996.

J. A. Hoffer. *Long term peripheral nerve activity during behaviour in the rabbit; the control of locomotion*. PhD thesis, Johns Hopkins University, 1975.

J. A. Hoffer and K. Kallesøe. Nerve cuff electrodes for prosthetic and research applications. In *Proceedings of the 4th Annual Conference of the International Functional Electrical Stimulation Society*, Sendai, Japan, August 1999.

J. A. Hoffer, M. Haugland, and T. Sinkjær. Functional restoration of precision grip using slip information obtained from peripheral nerve recordings. In *Proceedings of the Annual International Conference of the IEEE Engineering in Engineering in Medicine and Biology Society*, volume 13, pages 896–897, November 1991.

K. P. Hoffmann and K. P. Koch. Final report on design consideration of tLIFE2. Technical report, IBMT, 2005.

K. W. Horch and G. S. Dhillon, editors. *Neuroprosthetics: Theory and Practice*. World Scientific Publishing Company, 2004.

J. Houk and W. Simon. Responses of golgi tendon organs to forces applied to muscle tendon. *Journal of Neurophysiology*, 30(6):1466–1481, 1967.

A. Inmann and M. Haugland. Functional evaluation of natural sensory feedback incorporated in a hand grasp neuroprosthesis. *Medical Engineering & Physics*, 26:439–447, 2004.

J. K. S. Jansen and P. B. C. Matthews. The central control of the dynamic response of muscle spindle receptors. *Journal of Physiology*, 161:357–378, 1962.

J. A. D. Jensen, P. Pocwiardowski, P. O. Persson, L. Hultman, and P. Moller. Acoustic streaming enhanced electrodeposition of nickel. *Chemical Physics Letters*, 368(5):732–737, 2002a.

W. Jensen, T. Sinkjær, and F. Sepulveda. Improving signal reliability for on-line joint angle estimation from nerve cuff recordings of muscle afferents. *Annals of Biomedical Engineering*, 10(3):133–139, 2002b.

S. Jezernik and T. Sinkjær. Detecting sudden bladder pressure increases from the pelvic nerve afferent activity. In *Proc. 20th IEEE Int. Conf Eng. Med. Biol. Soc.*, volume 5, pages 2532–2535, Hong Kong, China, September 1998.

T. E. Johnston, R. R. Betz, B. T. Smith, B. J. Benda, M. J. Mulcahey, R. Davis, T. P. Houdayer, M. A. Pontari, A. Barriskill, and G. H. Creasey. Implantable FES system for upright mobility and bladder and bowel function for individuals with spinal cord injury. *Spinal Cord*, 43:713–723, 2005.

L. L. Jones, M. Oudega, M. Barlett Bunge, and M. H. Tuszynski. Neurotrophic factors, cellular bridges and gene therapy for spinal cord injury. *Journal of Physiology*, 533: 83–89, 2001.

E. R. Kandel, J. H. Schwartz, and T. M. Jessell. *Principles of neural science*. McGraw-Hill, fourth edition, 2000.

D. Kim, V. Adipudi, M. Shibayama, S. Giszter, A. Tessler, M. Murray, and K. J. Simansky. Direct agonists for serotonin receptors enhance locomotor function in rats that received neural transplants after neonatal spinal transection. *Journal of Neuroscience*, 19:6213–6214, 1999.

K. H. Kim and S. J. Kim. A wavelet-based method for action potential detection from extracellular neural signal recording with low signal-to-noise ratio. *IEEE Transactions on Biomedical Engineering*, 50(8):9991011, 2003.

N. Lago, K. Yoshida, K. P. Koch, and X. Navarro. Assessment of biocompatibility of chronically implanted polyimide and platinum intrafascicular electrodes. *IEEE Transactions on Biomedical Engineering*, 54(2):281–290, 2007.

S. M. Lawrence, G. S. Dhillon, and K. W. Horch. Fabrication and characteristics of an implantable, polymer-based, intrafascicular electrode. *Journal of Neuroscience Methods*, 131:9–26, 2003.

S. M. Lawrence, G. S. Dhillon, W. Jensen, K. Yoshida, and K. W. Horch. Acute peripheral nerve recording characteristics of polymer-based longitudinal intrafascicular electrodes. *IEEE Transactions on Neural Systems and Rehabilitation Engineering*, 12(3):345–348, 2004.

T. Lefurge, E. Goodall, K. Horch, L. Stensaas, and A. Schoenberg. Chronically implanted intrafascicular recording electrodes. *Annals of Biomedical Engineering*, 19:197–207, 1991.

M. S. Lewicki. A review of methods for spike sorting: The detection and classification of neural action potentials. *Network: Computation in Neural Systems*, 9(4):53–78, 1998.

G. E. Loeb, F. J. R. Richmond, W. J. Moore, and R. A. Peck. Design fabrication hermetic microelectronic and of implants. In *Proceedings of the 1st Annual International IEEE-EMBS Special Topic Conference on Microtechnologies in Medicine & Biology*, pages 455–460, Lyon, France, October 2000.

G. E. Loeb, R. Davoodi, M. Mileusnić, R. Ananthl, A. Inmann, and I. E. Brown. Strategic development of sensorimotor prosthetic technology. In *Proceedings of the 25th Annual International Conference of the IEEE EMBS*, pages 218–243, Cancun, Mexico, September 2003.

G. M. Lyons, T. Sinkjær, J. H. Burridge, and D. J. Wilcox. A review of portable FES-based neural orthoses for the correction of drop foot. *IEEE Transactions on Neural Systems and Rehabilitation Engineering*, 10(4):260–279, 2002.

H. E. Makssoud, D. Guiraud, and P. Poignet. Mathematical muscle model for functional electrical stimulation control strategies. In *Proceedings of the IEEE International Conference on Robotics and Automation*, volume 2, pages 1282–1287, New Orleans, LA, USA, April 2004.

M. Malagodi, K. W. Horch, and A. A. Schoenberg. An intrafascicular electrode for recording of action potentials in peripheral nerves. *Annals of Biomedical Engineering*, 17: 397–410, 1989.

J. A. Malmstorm, T. G. McNaughton, and K. Horch. Recording properties and biocompatibility of chronically implanted polymer-based intrafascicular electrodes. *Annals of Biomedical Engineering*, 26:1055–1064, 1998.

J. Marcoux and S. Rossignol. Initiating or blocking locomotion in spinal cats by applying noradrenergic drugs to restricted lumbar spinal segments. *Journal of Neuroscience*, 20: 8577–8585, 2000.

F. H. Martini. *Fundamentals of Anatomy and Physiology*. Benjamin Cummings, seventh edition, 2005.

P. B. C. Matthews and R. B. Stein. The sensitivity of muscle spindle afferents to small sinusoidal changes of length. *Journal of Physiology*, 200(3):723–743, 1969a.

P. B. C. Matthews and R. B. Stein. The regularity of primary and secondary muscle spindle afferent discharges. *Journal of Physiology*, 202(1):59–82, 1969b.

B. L. McNaughton, J. O'Keefe, and C. A. Barnes. The stereotrode: A new technique for simultaneous isolation of several single units in the central nervous system from multiple unit records. *Journal of Neuroscience Methods*, 8(4):391–397, 1983.

T. G. McNaughton and K. W. Horch. A dual-channel intrafascicular electrode for tracking single cell activities in peripheral nerves. In *Proceedings of the Annual International Conference of the IEEE EMBS*, volume 11, pages 1326–1327, November 1992.

T. G. McNaughton and K. W. Horch. Action potential classification with dual channel intrafascicular electrodes. *IEEE Transactions on Biomedical Engineering*, 41(7):609–616, 1994.

S. Micera, W. Jensen, F. Sepulveda, R. R. Riso, and T. Sinkjær. Neuro-fuzzy extraction of angular information from muscle afferents for ankle control during standing in paraplegic subjects: An animal model. *IEEE Transactions on Biomedical Engineering*, 48(7):787–794, 2001.

K. Mirfakhraei and K. Horch. Classification of action potentials in multi-unit intrafascicular recordings using neural networks pattern-recognition techniques. *IEEE Transactions on Biomedical Engineering*, 41(1):89–91, 1994.

K. Mirfakhraei and K. Horch. Recognition of temporally changing action potentials in multiunit neural recordings. *IEEE Transactions on Biomedical Engineering*, 44(2):123–131, 1997.

M. Misiti, Y. Misiti, G. Oppenheim, and J.-M. Poggi, editors. *Wavelets and their applications*. ISTE Publishing Company, first edition, 2007.

N. Nannini and K. Horch. Muscle recruitment with intrafascicular electrodes. *IEEE Transactions on Biomedical Engineering*, 38(8):769–776, 1991.

G. G. Naples, J. T. Mortimer, A. Scheiner, and J. D. Sweeney. A spiral nerve cuff electrode for peripheral nerve stimulation. *IEEE Transactions on Biomedical Engineering*, 35(11): 905–916, 1988.

X. Navarro, T. B. Krueger, N. Lago, S. Micera, T. Stieglitz, and P. Dario. A critical review of interfaces with the peripheral nervous system for the control of neuroprostheses and hybrid bionic systems. *Journal of the Peripheral Nervous System*, 10:229258, 2005.

D. O. Olguín, F. Bouchereau, and S. Martínez. Adaptive notch filter for EEG signals based on the LMS algorithm with variable step-size parameter. March 2005.

L. Olson. Regeneration in the adult central nervous system: Experimental repair strategies. *Nature Medicine*, 3:1329–1335, 1997.

Henry W. Ott. *Noise Reduction Techniques in Electronic Systems*. John Wiley & Sons, second edition, 1988.

B. Pagès and U. Proske. Effect of halothane anesthesia on responses from primary endings of muscle spindles in the cat. *Experimental Neurology*, 28(3):393–402, 1970.

K. G. Pearson. Could enhanced reflex function contribute to improving locomotion after spinal cord repair? *Journal of Physiology*, 533:75–81, 2001.

P. Popesko, V. Rajtová, and J. Horák. *A color atlas of anatomy of small laboratory animals*, volume 1. Saunders Ltd, 2002.

D. Popović and S. Sinkjær. *Control of movement for the physically disabled*. Springer, first edition, 2000.

R. E. Poppele and R. J. Bowman. Quantitative description of linear behavior of mammalian muscle spindles. *Journal of Neurophysiology*, 33(1):59–72, 1970.

A. Prochazka, V. K. Mushahwar, and D. B. McCreery. Neural prostheses. *Journal of Physiology*, 533(1):99–109, 2001.

U. Proske and J. E. Gregory. The time-course of recovery of the initial burst of primary endings of muscle spindles. *Brain Research*, 121(2):358–361, 1977.

A. Ramon-Cueto, M. I. Cordero, F. F. Santos-Benito, and J. Avila. Functional recovery of paraplegic rats and motor axon regeneration in their spinal cords by olfactory ensheathing glia. *Neuron*, 25:425–435, 2000.

B. Z. Renkin and Å. K. Vallbo. Simultaneous responses of groups I and II cat muscle spindle afferents to muscle position and movement. *Journal of Neurophysiology*, 27: 429–450, 1964.

M. G. Ribotta, J. Provencher, D. Feraboli-Lonherr, S. Rossignol, A. Privat, and D. Orsal. Activation of locomotion in adult chronic spinal rats is achieved by transplantation of embryonic raphe cells reinnervating a precise lumbar level. *Journal of Neuroscience*, 20:5144–5152, 2000.

P. M. Richardson, U. M. McGuinness, and A. J. Aguayo. Axons from CNS neurons regenerate into PNS grafts. *Nature*, 284:264–265, 1980.

R. R. Riso, F. K. Mosallaie, W. Jensen, and T. Sinkjær. Nerve cuff recordings of muscle afferent activity from tibial and peroneal nerve in rabbit during passive ankle motion. *IEEE Transactions on Rehabilitation Engineering*, 8:244–248, 2000.

D. Roetenberg, C. T. M. Baten, and P. H. Veltink. Estimating body segment orientation by applying inertial and magnetic sensing near ferromagnetic materials. *Journal of Neurophysiology*, 15(3):469–471, 2007.

E. Schmidt. Computer separation of multi-unit neuroelectric data: A review. *Journal of Neuroscience Methods*, 12:95–111, 1984.

A. A. Schoenberg, M. Malagodi, and K. Horch. Extraction of somatosensory information from peripheral nerves for fns applications. In *Proceedings of the IX International Symposium on External Control of Human Extremities*, pages 363–373, Belgrade, Serbia, 1987.

C. S. Sherrington and E. H. Hering. On reciprocal innervation of antagonist muscles. Fourth note. *Proceedings of the Royal Society of London. Series B, Biological Sciences*, 62:183–187, 1897-1898.

T. Sinkjær. Integrating sensory nerve signals into neural prosthesis devices. *Neuromodulation*, 3(1):35–41, 2000.

T. Sinkjær, B. Hinge, A. Jorgensen, M. L. Jensen, and M. Haugland. Whole sensory nerve recordings in human – Application for neural prostheses. In *Proceedings of the Annual International Conference of the IEEE EMBS*, volume 13, pages 900–901, November 1991.

U. Slawinska, H. Majczynski, and R. Djavadian. Recovery of hindlimb motor functions after spinal cord transection is enhanced by grafts of the embryonic raphe nuclei. *Experimental Brain Research*, 132:27–38, 2000.

R. K. Snider and A. B. Bonds. Classification of non-stationary neural signals. *Journal of neuroscience methods*, 84(1-2):155–66, 1998.

R. B. Stein, D. Charles, T. Gordon, J. A. Hoffer, and J. Jhamandas. Impedance properties of metal electrodes for chronic recording from mammalian nerves. *IEEE Transactions on Biomedical Engineering*, 25(6):532–537, 1978.

R. B. Stein, D. J. Weber, Y. Aoyagi, A. Prochazka, J. B. M. Wagenaar, S. Shoham, and R. A. Normann. Coding of position by simultaneously recorded sensory neurones in the cat dorsal root ganglion. *Journal of Physiology*, 580(3):883–896, 2004.

T. Stieglitz, M. Schuettler, A. Schneider, E. Valderrama, and X. Navarro. Noninvasive measurement of torque development in the rat foot: Measurement setup and results from stimulation of the sciatic nerve with polyimide-based cuff electrodes. *IEEE Transactions on Neural Systems and Rehabilitation Engineering*, 11(4):427–436, 2003.

K. Strange and J. A. Hoffer. Restoration of use of paralyzed limb muscles using sensory nerve signals for state control of FES-assisted walking. *IEEE Trans. Rehab. Eng.*, 7: 289–300, 1999.

J. J. Struijk and M. Thomsen. Tripolar nerve cuff recording: Stimulus artifact, EMG and the recorded nerve signal. In *IEEE 17th Annual Conference of the Engineering in Medicine and Biology Society*, volume 2, pages 1105–1106, Montreal, Canada, September 1995.

J. J. Struijk, M. Thomsen, J. O. Larsen, and T. Sinkjær. Cuff electrodes for long-term recording of natural sensory information. *IEEE Engineering in Medicine and Biology*, 18(3):91–98, 1999.

A. Taylor, P. H. Ellaway, R. Durbaba, and S. Rawlinson. Distinctive patterns of static and dynamic gamma motor activity during locomotion in the decerebrate cat. *Journal of Physiology*, 529(3):825–836, 2000.

I. F. Triantis, A. Demosthenous, N. Donaldson, and J. J. Struijk. Experimental assessment of imbalance conditions in a tripolar cuff for ENG recordings. In *Proceedings of the 1st International IEEE EMBS Conference on Neural Engineering*, Capri Island, Italy, March 2003.

B. Upshaw and T. Sinkjær. Digital signal processing algorithms for the detection of afferent nerve activity recorded from cuff electrodes. *IEEE Transactions on Rehabilitation Engineering*, 6:172–181, 1998.

L. Vodovnik, C. D. Long, J. B. Reswick, A. Lippay, and D. Starbuck. Myo-electric control of paralyzed muscles. *IEEE Transactions on Biomedical Engineering*, 12:169–172, 1965.

L. Vodovnik, W. J. Crochetiere, and J. B. Reswick. Control of a skeletal joint by electrical stimulation of antagonists. *Medical & Biological Engineering*, 5:97–109, 1967.

E. T. von Brücke, M. Early, and A. Forbes. Recovery of responsiveness in motor and sensory fibers during the relative refractory period. *Journal of Neurophysiology*, 4:80–91, 1941.

J. Y. Wei, J. Simon, M. Randić, and P. R. Burgess. Joint angle signaling by muscle spindle receptors. *Brain Research*, (370):119–126, 1986.

J. J. Whalen III, J. D. Weiland, and P. C. Searsona. Electrochemical deposition of platinum from aqueous ammonium hexachloroplatinate solution. *Journal of the Electrochemical Society*, 152(11):738–743, 2005.

P. B. Yoo and D. M. Durand. Selective recording of the canine hypoglossal nerve using a multicontact flat interface nerve electrode. *IEEE Transactions on Biomedical Engineering*, 52(8):1461–1469, 2005.

K. Yoshida and K. Horch. Selective stimulation of peripheral nerve fibers using dual intrafascicular electrodes. *IEEE Transactions on Biomedical Engineering*, 40(5):492–494, 1993.

K. Yoshida and K. Horch. Closed-loop control of ankle position using muscle afferent feedback with functional neuromuscular stimulation. *IEEE Transactions on Biomedical Engineering*, 43(2):167–176, 1996.

K. Yoshida and R. B. Stein. Characterization of signals and noise rejection with bipolar longitudinal intrafascicular electrodes. *IEEE Transactions on Biomedical Engineering*, 46(2):226–234, 1999.

K. Yoshida, K. Jovanović, and R. B. Stein. Developments in longitudinal intra-fascicular electrodes for peripheral nerve recording and stimulation. In *Proceedings of the 28th Annual Meeting of the Society for Neuroscience*, Los Angeles, USA, November 1998.

K. Yoshida, D. Pellinen, D. Pivin, P. Rousche, and D. Kipke. Development of the thin-film longitudinal intra-fascicular electrode. In *Proceedings of the 5th Annual Conference of the International Functional Electrical Stimulation Society*, Aalborg, Denmark, June 2000.

K. Yoshida, I. Lewinsky, M. Nielsen, and M. Hylleberg. Implantation mechanics of tungsten microneedles into peripheral nerve trunks. *Medical and Biological Engineering and Computing*, 45(4):413–420, 2007.

T. Zigova, E. Y. Snyder, and P. R. Sanberg, editors. *Neural stem cells for brain and spinal cord repair*. Humana Press, 2002.

O. Zou, W. Tan, E. S. Kim, and G. E. Loeb. Implantable bimorph piezoelectric accelerometer for feedback control of functional neuromuscular stimulation. In *Proceedings of the 12th International Conference on Solid State Sensors, Actuators and Microsystems*, pages 413–420, Boston, USA, June 2003.

Appendix A

Biopotential Amplifier

During the course of this thesis, the DEMAR team was in the process of setting up its own animal lab for conducting future animal experiments. There was a need for having a neural signal amplifer that would be used for multi-channel ENG signal acquisition, using the tfLIFE and possibly also cuff nerve electrodes. This chapter describes the process of building such an amplifier.

A.1 Amplifier Design

The amplification circuitry configuration is based on an amplifer designed by Dr. Ken Yoshida at Bioectronics laboratory at the Center for Sensory-Motor Interaction at Aalborg University in Denmark. The amplifier configuration has already been tested and used in a number of animal experiments where it provided satisfactory ENG recordings. Hence, there was no need to design an amplifier from scratch.

Schematic capture was done using the CadSoft EAGLE software package. The schematic circuit diagram of one channel of the amplifer is shown on Fig. A.1. Component values for the parts on the schematic are listed in Table A.1.

The power supply circuitry was designed to provide ± 10 V output according to the recommendations from the LM317 and LM337 voltage regulators application notes, given in the component data sheets provided by the manufacturer. The schematic circuit diagram of the power supply is shown on Fig. A.2. Component values for the parts on the schematic are also listed in the above table.

A double-sided printed circuit board (PCB), dimensions 107 by 68 mm, was designed to hold 8 amplification channels and the power supply circuitry. Two 3 mm vias were included to provide later fixation of the board in an enclosure. The final artwork of top and

Table A.1: Components listing for one channel of the amplifier and for the power supply.

Part	**Value**	**Device**	**Package**	**Library**	**Layer**
C1	10n	C-EU050-050X075	C050-050X075	rcl	Top
C2	10n	C-EU050-050X075	C050-050X075	rcl	Top
C3	4.7u	C-EU150-084X183	C150-084X183	rcl	Top
C25	10u	CPOL-EUE5-5	E5-5	rcl	Top
C26	10u	CPOL-EUE5-5	E5-5	rcl	Top
C27	1u	CPOL-EUE5-5	E5-5	rcl	Top
C28	1u	CPOL-EUE5-5	E5-5	rcl	Top
C29	100n	C-EU050-025X075	C050-025X075	rcl	Top
C30	100n	C-EU050-025X075	C050-025X075	rcl	Top
D1	1N4004	1N4004	DO41-10	diode	Top
D2	1N4004	1N4004	DO41-10	diode	Top
IC1	INA118P	INA118P	DIL08	burr-brown	Top
IC2	AD797N	AD797N	DIL08	linear	Top
IC17	-	LM317L	317L	v-reg	Top
IC18	-	LM337L	337L	v-reg	Top
JP1	-	JP1E	JP1	jumper	Bottom
JP2	-	JP1E	JP1	jumper	Bottom
JP3	-	JP1E	JP1	jumper	Bottom
R1	10M	R-EU-0207/10	0207/10	rcl	Top
R2	10M	R-EU-0207/10	0207/10	rcl	Top
R3	10M	R-EU-0207/10	0207/10	rcl	Top
R4	10M	R-EU-0207/10	0207/10	rcl	Top
R5	1K	R-EU-0207/10	0207/10	rcl	Bottom
R6	10k	R-EU-0207/10	0207/10	rcl	Bottom
R7	10R	R-EU-0207/10	0207/10	rcl	Top
R8	190R	R-EU-0207/10	0207/10	rcl	Top
R9	100R	R-EU-0207/10	0207/10	rcl	Top
R73	240E	R-EU-0207/10	0207/10	rcl	Top
R74	1K68	R-EU-0207/10	0207/10	rcl	Top
R75	240E	R-EU-0207/10	0207/10	rcl	Top
R76	1K68	R-EU-0207/10	0207/10	rcl	Top
V	-	SLR-2-012	SLR-2-012	con-LIFE	Bottom
S	-	22-23-2031	22-23-2031	con-molex	Top
VOUT	-	22-23-2031	22-23-2031	con-molex	Top

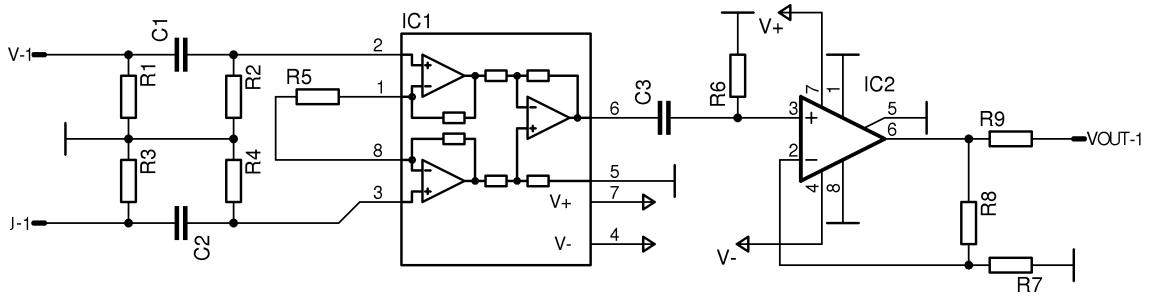

Figure A.1: Schematic circuit diagram of one channel of the amplifer.

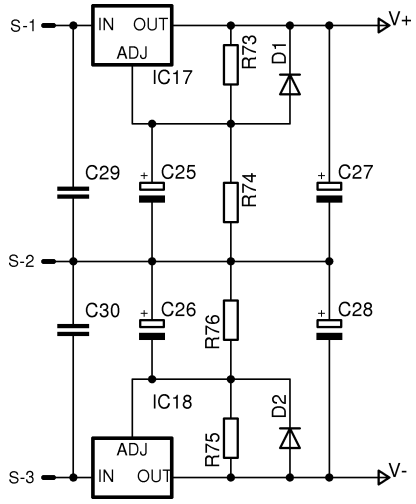

Figure A.2: Schematic circuit diagram of the power supply.

bottom layers of the PCB are shown on Figure A.3 and A.4, respectively. The parts layout is shown on Fig. A.5.

Resistors that set the gain (R5) and high-pass filter corner frequencies (R6) are mounted on the bottom side of the PCB so they can be easily accessed and changed if needed.

Jumpers near the input tfLIFE connector are there to provide selection of the tfLIFE sites to be used as the differential input: pin J-1 (Fig. A.1) can be connected either to ground or indifferent tfLIFE sites either to the signal ground. Independent setting of the reference for the left and right side of the tfLIFE loop is also provided. Pin V-1 is connected directly to the corresponding site of the tfLIFE input connector, i.e. to tfLIFE sites R1-4 and L1-4 (Fig. 2.18, panel A). The tfLIFE connector used was a high-density two-row SLR-2-050 connector from Fischer Elektronik. Only 12 pins on the connector are used. Connector device definition (symbol, gates and package) was created separatelly, since it was not available in the standard libraries.

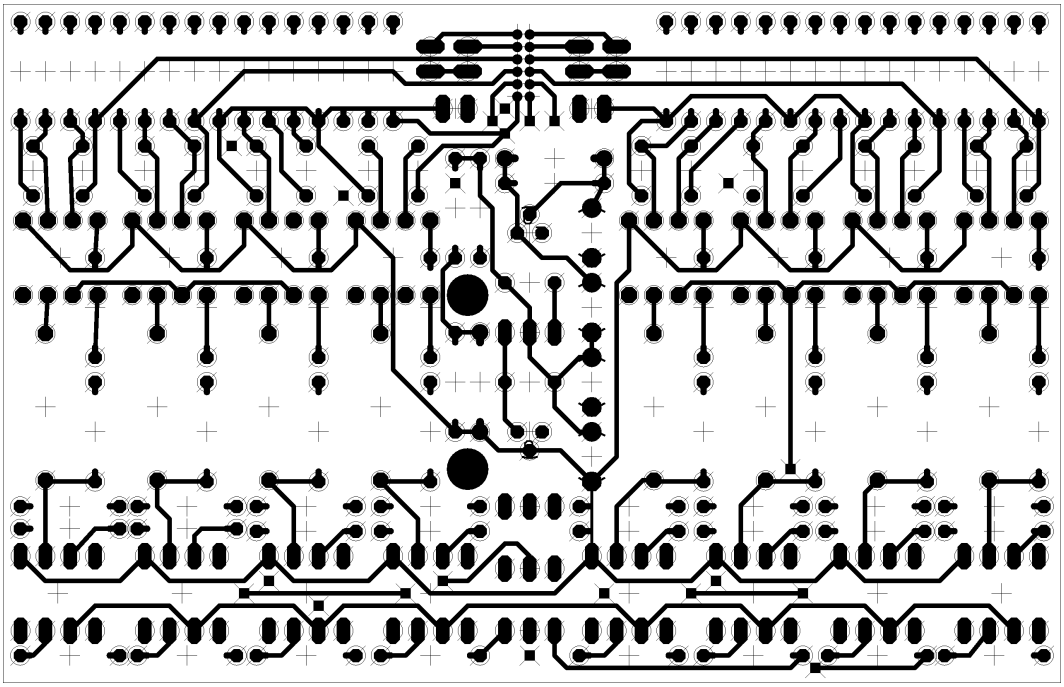

Figure A.3: Printed circuit board. Top layer artwork.

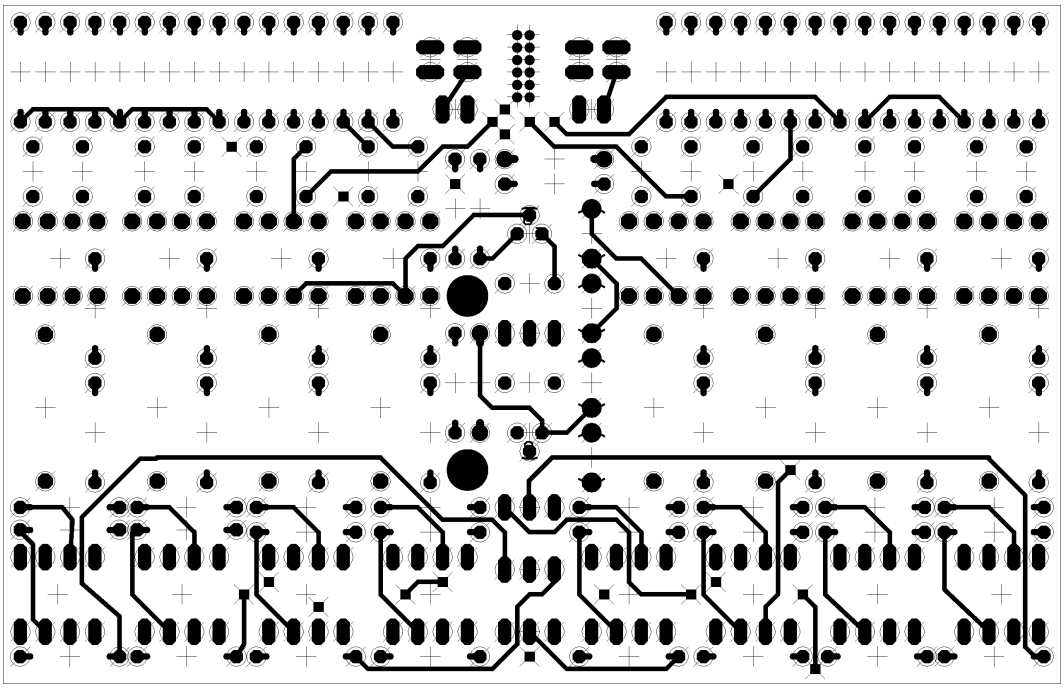

Figure A.4: Printed circuit board. Bottom layer artwork.

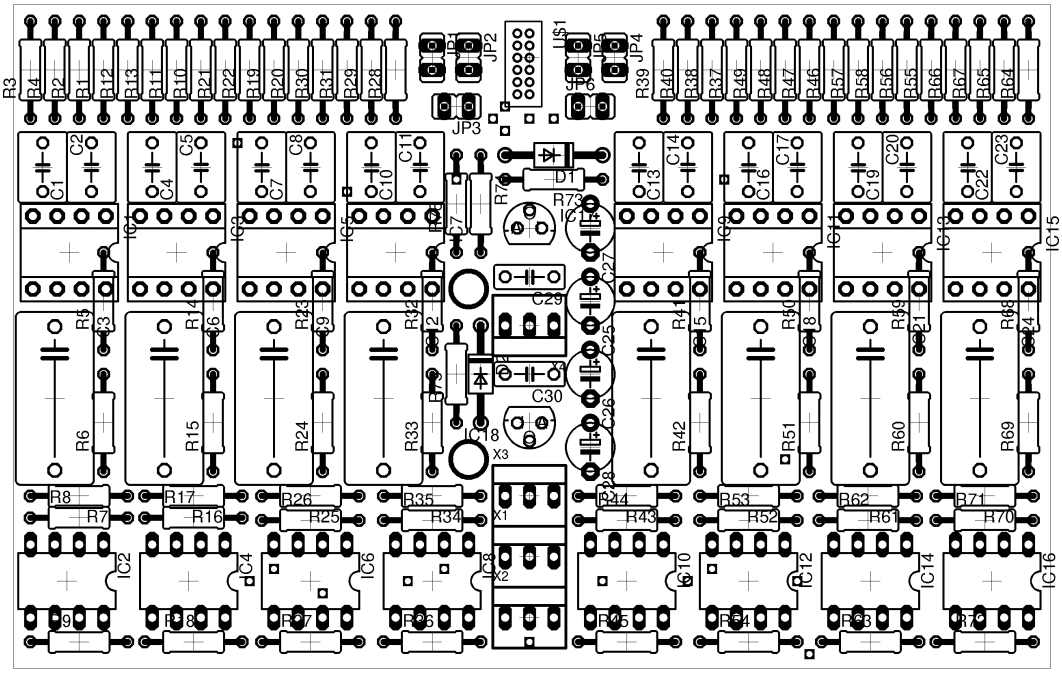

Figure A.5: Printed circuit board. On-board component layout.

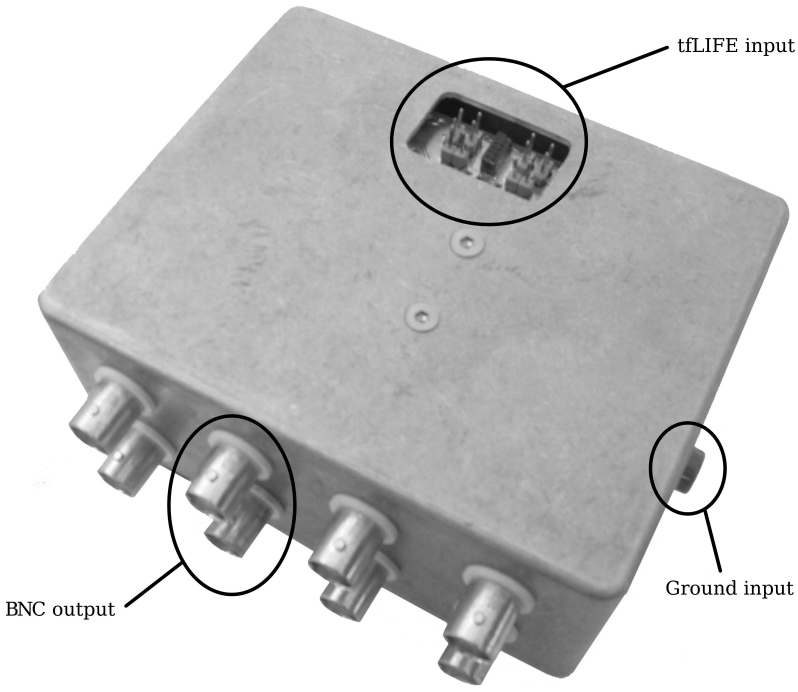

Figure A.6: Photograph of assembled amplifier. Power supply connectors (obscured) are on the opposite side of the ground connector.

A.2 Fabrication and Assembly

After manufacturing the printed circuit board and mounting on-board components, the PCB was placed into its housing and off-board connectors were mounted. A metal box was chosen as an enclosure. Properly grounding such an enclosure acts as a Faraday cage, protecting the PCB from capacitively coupled noise sources. Wiring together the power, signal and hardware ground at only one point close to the power supply provided a practical grounding system at low frequencies [Ott, 1988]. The signal ground provides the reference potential for the circuitry, set with the reference input electrode connected using a 2 mm connector on the side of the box. The enclosure also holds 8 BNC output connectors and 2 standard power connectors. Separate connectors for the power supply (one for each polarity) were chosen to facilitate easy use of external laptop batteries for powering the amplifier. On top of the box there an exposure provides access to the area of the bottom side of the PCB where the on-board tfLIFE input is located (Fig. A.6).

Appendix B

List of Publications

M. Djilas, K. Yoshida, and C. Azevedo-Coste. Interpretation of ENG signal for FES closed-loop control. In *Proceedings of the 11th Annual Conference of the International Functional Electrical Stimulation Society*, Miyagi-Zao, Japan, September 2006.

M. Djilas, K. Yoshida, M. Kurstjens, and C. Azevedo-Coste. Improving the signal-to-noise ratio in recordings with thin-film longitudinal intra-fascicular electrodes using shielding cuffs. In *Proceedings of the 3rd International IEEE EMBS Conference on Neural Engineering*, Cohala Coast, Hawaii, USA, May 2007.

M. Djilas, C. Azevedo-Coste, D. Guiraud, J. Bourien, and K. Yoshida. Wavelet-based spike sorting of muscle spindle afferent nerve activity recorded with thin-film intrafascicular electrodes. In *Proceedings of the 13th Annual Conference of the International Functional Electrical Stimulation Society*, Freiburg, Germany, September 2008.

M. Djilas, K. Yoshida, and C. Azevedo-Coste. Interpretation of ENG signals recorded using thin-film longitudinal intrafascicular electrodes for FES closed-loop control. *Submitted for publication in journal*.

RESUME en français: Le sujet de cette thèse se situe dans le cadre général de la restauration du mouvement de membres paralysés à travers la stimulation électrique fonctionnelle (FES) implantée. L'objectif du projet était d'explorer la faisabilité d'utiliser les informations issues des fibres nerveuses sensorielles des récepteurs musculaires comme information de retour d'une commande en boucle fermée d'un système FES à travers des électrodes nerveuses périphériques intra fasciculaires. Des expérimentations animales aigues ont été réalisées pour mesurer les réponses afférentes des fuseaux neuromusculaires à des étirements passifs du muscle. Les enregistrements ont été réalisés en utilisant une nouvelle électrode Intra-fasciculaire (tfLIFE), développées par le Dr. Ken Yoshida à l'université d'Aalborg au Danemark. Un modèle du premier ordre de la réponse des fuseaux neuromusculaires à des étirements passifs a été proposé. Ce modèle prend en compte les propriétés non linéaires des activités neurales afférentes. De plus, l'estimation de l'état du muscle à partir d'un enregistrement ENG multicanaux a fourni des résultats plus robustes comparés à un enregistrement monocanal.
Pour que le modèle ci-dessus puisse être utilisé pour l'estimation de l'état du muscle, le taux de variation de la longueur du muscle pendant le mouvement doit avoir un effet négligeable sur les paramètres du modèle. Nous avons proposé dans cette thèse une approche pour la détection et la classification de pics dans l'enregisrement neural dans l'objectif d'isoler les activités neurales sensorielles des récepteurs musculaires ayant une sensibilité minimale à la vitesse de l'élongation musculaire. L'algorithme est basé sur la transformée en ondelettes continue multi-échelle utilisant des ondelettes complexes. Le système de détection utilise une simple détection par seuillage, couramment utilisée, particulièrement avec les enregistrements ayant un faible rapport signal sur bruit. Les résultats de classification des unités montrent que la classification développée est capable d'isoler l'activité ayant une relation linéaire avec la longueur du muscle. Ceci constitue une étape vers une estimation, en ligne basée modèle, de la longueur du muscle qui pourra être utilisée dans un système FES en boucle fermée utilisant des informations sensorielles naturelles.
Un des principaux problèmes limitant l'interprétation des données ENG est le faible niveau du signal neural par rapport à celui du bruit dans l'enregistrement. Nos hypothèses ont été que le blindage de l'implant aiderait à améliorer le rapport signal sur bruit. Des résultats expérimentaux, issus d'une étude préliminaire que nous avons réalisée, montrent que le placement d'électrodes standards à manchon placées autour du site d'implantation de la tfLIFE augmentait le niveau du signal ENG dans les enregistrements.

RESUME en anglais: The topic of this thesis was the rehabilitation of movement of paralyzed limbs through functional electrical stimulation (FES). The objective of the project was to explore the possibility of using information from sensory nerve fibers of muscle receptors as feedback of the closed-loop control of FES systems using intrafascicular peripheral nerve electrodes.
Acute animal experiments were performed to record afferent muscle spindle responses to passive stretch. The recordings were performed using the new thin-film Longitudinal Intra-Fascicular Electrode (tfLIFE), developed by Dr. Ken Yoshida at Aalborg University in Denmark. A first-order model of muscle spindle response to passive muscle stretch was proposed that manages to capture the non-linear properties of the afferent neural activity. Moreover, estimation of muscle state from the recorded multi-channel ENG provided more robust results compared to using single-channel recordings.
For the abovementioned model to be usable in a estimator of muscle state, the rate of change of muscle length during movement must have negligible effect on model parameters. A neural spike detection and classification scheme was developed for the purpose of isolating sensory neural activity of muscle receptors having minimal sensitivity to the velocity of muscle motion. The algorithm was based on the multi-scale continuous wavelet transform using complex wavelets. The detection scheme outperforms the commonly used simple threshold detection, especially with recordings having low SNR. Results of classification of units indicate that the developed classifier is able to isolate activity having linear relationship with muscle length, which is a step towards on-line model-based estimation of muscle length that can be used in a closed-loop FES system with natural sensory feedback.
One of the main issues limiting the interpretation of ENG data is the low level of the neural signal compared to the level of noise in the recordings. Our hypothesis was that shielding the implant site would help improve signal-to-noise level. Experimental results from a preliminary study indicate that placing a standard cuff electrode around the tfLIFE active sites increases the level of ENG signal in the recordings.

DISCIPLINE: Physiologie, Traitement du signal, Automatique et Electronique

MOTS-CLES : Bioingénierie, prothèses neurales, traitement du signal biologique, stimulation électrique fonctionnelle, boucle rétroactive sensorielle naturelle, stratégies de commande

INTITULE ET ADRESSE DE L'U.F.R. OU DU LABORATOIRE: Le Laboratoire d'Informatique, de Robotique et de Microélectronique de Montpellier (LIRMM), 161 rue Ada, 34392 Montpellier Cedex 5 – France